

A Full-Scale, Single-Column Bridge Bent Tested by Shake-Table Excitation

Matthew J. Schoettler
José I. Restrepo
Gabriele Guerrini
David E. Duck
Francesco Carrea

Center for Civil Engineering Earthquake Research
Department of Civil Engineering/258
University of Nevada
Reno, NV 89557

August 2012

ABSTRACT

A landmark test of a reinforced concrete bridge column was conducted on the George E. Brown, Jr. Network for Earthquake Engineering Simulation's shake table at U.C. San Diego. This was the first full-scale shake table test of a bridge column designed to current US seismic design provisions and tested under dynamic conditions. Caltrans seismic design guidelines were followed for the design and detailing of the 1.2-m (4-ft) diameter column. The flexurally dominant test specimen was subjected to ten significant ground motions and tested to impending collapse. The results provide the basis for comparison with a small scale shake table test to evaluate the reliability of small scale testing and significance of scale effects under dynamic conditions. The column exhibited a ductile response with a well formed plastic hinge within one column diameter from the base. Concrete spalling was observed after a simulated design level earthquake. Longitudinal bar buckling, longitudinal bar fractures, and concrete core crushing were mechanisms for deteriorating strength and stiffness, but were induced in the later stages of testing after stable response to repeated demands beyond the design level event.

Keywords: Reinforced concrete, bridge column, shake table test.

ACKNOWLEDGMENTS

This project was sponsored by the Federal Highway Administration contract DTFH61-07-C- 00031. Additional support was provided from California Department of Transportation, Missouri State DOT, Oregon State DOT, Montana State DOT (Through the Transportation Pooled-fund Study Project TPF 5(180)), the Pacific Earthquake Engineering Research Center's Program of Applied Earthquake Engineering Research of Lifelines Systems supported by the California Energy Commission, and the Pacific Gas and Electric Company.

This work made use of the Earthquake Engineering Research Centers Shared Facilities supported by the National Science Foundation, under award number EEC-9701568 through the Pacific Earthquake Engineering Research Center (PEER).

Any opinions, findings, and conclusions or recommendations expressed in this material are those of the authors and do not necessarily reflect those of the Federal Highway Administration or the National Science Foundation.

CONTENTS

ABSTRACT	III
ACKNOWLEDGMENTS	V
CONTENTS.....	VII
LIST OF FIGURES.....	X
LIST OF TABLES	XV
1 INTRODUCTION.....	1
2 LITERATURE REVIEW	2
3 DESIGN OF THE EXPERIMENT	3
4 TEST SETUP	5
4.1 Column	7
4.2 Footing.....	7
4.3 Superstructure mass.....	8
5 MATERIAL PROPERTIES	9
5.1 Concrete.....	9
5.2 Reinforcing steel.....	11
6 TEST PROTOCOL.....	14
7 INSTRUMENTATION.....	21
7.1 Strain gauges.....	21
7.1.1 Longitudinal strain gauges.....	21
7.1.2 Transverse strain gauges.....	21
7.1.3 Safety restraint strain gauges.....	21
7.2 Linear voltage displacement transducers.....	22
7.3 Spring potentiometers.....	25
7.4 Accelerometers	27

7.5	GPS system.....	27
7.6	Video cameras	27
7.7	Data acquisition system.....	27
7.8	Control system.....	28
8	TEST RESULTS	29
8.1	Test EQ1	29
8.2	Test EQ2.....	33
8.3	Test EQ3.....	38
8.4	Test EQ4.....	42
8.5	Test EQ5.....	46
8.6	Test EQ6.....	49
8.7	Test EQ7.....	53
8.8	Test EQ8.....	57
8.9	Test EQ9.....	61
8.10	Test EQ10.....	65
9	SUMMARY AND CONCLUSIONS.....	70
9.1	Summary.....	70
9.2	Conclusions	75
	REFERENCES.....	78
	APPENDIX A: INSTRUMENTATION LAYOUT	81

LIST OF FIGURES

Figure 3.1	Column reinforcing details.....	4
Figure 4.1	Test specimen.....	5
Figure 4.2	Inclined safety columns.....	6
Figure 4.3	Pre-test setup.....	7
Figure 5.1	Column concrete stress-strain relationship.....	11
Figure 5.2	Column longitudinal reinforcement stress-strain relationship.....	12
Figure 5.3	Column transverse hoop reinforcement stress-strain benchmarking.....	12
Figure 6.1	Desired ground motions in terms of (a) pseudo-acceleration and (b) displacement response spectra at 1% damping ratio.....	17
Figure 6.2	EQ1 (a) pseudo-acceleration and (b) displacement response spectra at 1% damping ratio.....	17
Figure 6.3	EQ2 and EQ4 (a) pseudo-acceleration and (b) displacement response spectra at 1% damping ratio.....	18
Figure 6.4	EQ3 and EQ6 (a) pseudo-acceleration and (b) displacement response spectra at 1% damping ratio.....	18
Figure 6.5	EQ5 (a) pseudo-acceleration and (b) displacement response spectra at 1% damping ratio.....	19
Figure 6.6	EQ7 (a) pseudo-acceleration and (b) displacement response spectra at 1% damping ratio.....	19
Figure 6.7	EQ8, EQ9, and EQ10 (a) pseudo-acceleration and (b) displacement response spectra at 1% damping ratio.....	20
Figure 7.1	Curvature, shear, and fixed-end rotation LVDTs and the (a) South and (b) North faces.....	22
Figure 7.2	Column-to-top mass LVDTs.....	23
Figure 7.3	Bond slip bracket installation: (a) assembly, (b) placed on longitudinal bars, (c) encapsulated with debonding foam, and (d) final installation.....	24
Figure 7.4	Dilation LVDT installation (a) target welded to a transverse hoop, (b) LVDT assembly, and locations on the West face.....	25
Figure 7.5	Horizontal spring potentiometer locations.....	26
Figure 7.6	Inclined spring potentiometer locations.....	26
Figure 8.1	Column displacement during EQ1.....	29
Figure 8.2	Column base East face during EQ1 at (a) peak West displacement, (b) peak East displacement, and (c) post-test.....	30
Figure 8.3	Column response during EQ1 in terms of base moment and curvature.....	31

Figure 8.4	Column response during EQ1 in terms of base shear and drift ratio.	32
Figure 8.5	Longitudinal reinforcement tensile strain demand during EQ1.	32
Figure 8.6	Transverse hoop reinforcement tensile strain demand during EQ1.	33
Figure 8.7	Column displacement during EQ2.	34
Figure 8.8	Column base East face during EQ2 at (a) peak West displacement, (b) East positive displacement, and (c) post-test.	35
Figure 8.9	Column response during EQ2 in terms of base moment and curvature.	35
Figure 8.10	Column response during EQ2 in terms of base shear and drift ratio.	36
Figure 8.11	Longitudinal reinforcement tensile strain demand during EQ2.	37
Figure 8.12	Transverse hoop reinforcement tensile strain demand during EQ2.	37
Figure 8.13	Column displacement during EQ3.	38
Figure 8.14	Column base East face during EQ3 at (a) peak West displacement, (b) peak East displacement, and (c) post-test.	39
Figure 8.15	Column base West face after test EQ3.	40
Figure 8.16	Column response during EQ3 in terms of base moment and curvature.	40
Figure 8.17	Column response during EQ3 in terms of base shear and drift ratio.	41
Figure 8.18	Longitudinal reinforcement tensile strain demand during EQ3.	41
Figure 8.19	Transverse hoop reinforcement tensile strain demand during EQ3.	42
Figure 8.20	Column displacement during EQ4.	43
Figure 8.21	Column base East face during EQ4 at (a) peak West displacement, (b) peak East displacement, and (c) post-test.	44
Figure 8.22	Column response during EQ4 in terms of base moment and curvature.	44
Figure 8.23	Column response during EQ4 in terms of base shear and drift ratio.	45
Figure 8.24	Longitudinal reinforcement tensile strain demand during EQ4.	45
Figure 8.25	Transverse hoop reinforcement tensile strain demand during EQ4.	46
Figure 8.26	Column displacement during EQ5.	47
Figure 8.27	Column base East face during EQ5 at (a) peak West displacement, (b) peak East displacement, and (c) post-test.	47
Figure 8.28	Column response during EQ5 in terms of base moment and curvature.	48
Figure 8.29	Column response during EQ5 in terms of base shear and drift ratio.	48
Figure 8.30	Longitudinal reinforcement tensile strain demand during EQ5.	49
Figure 8.31	Transverse hoop reinforcement tensile strain demand during EQ5.	49
Figure 8.32	Column displacement during EQ6.	50
Figure 8.33	Column base East face during EQ6 at (a) peak West displacement, (b) peak East displacement, and (c) post-test.	51

Figure 8.34	Column response during EQ6 in terms of base moment and curvature.....	51
Figure 8.35	Column response during EQ6 in terms of base shear and drift ratio.	52
Figure 8.36	Longitudinal reinforcement tensile strain demand during EQ6.....	52
Figure 8.37	Transverse hoop reinforcement tensile strain demand during EQ6.....	53
Figure 8.38	Column displacement during EQ7.....	54
Figure 8.39	Column base East face during EQ7 at (a) peak West displacement, (b) peak East displacement, and (c) post-test.	54
Figure 8.40	Column response during EQ7 in terms of base moment and curvature.....	55
Figure 8.41	Column response during EQ7 in terms of base shear and drift ratio.	55
Figure 8.42	Longitudinal reinforcement tensile strain demand during EQ7.....	56
Figure 8.43	Transverse hoop reinforcement tensile strain demand during EQ7.....	56
Figure 8.44	Column displacement during EQ8.....	58
Figure 8.45	Column base East face during EQ8 at (a) peak West displacement, (b) peak East displacement, and (c) post-test.	58
Figure 8.46	Column response during EQ8 in terms of base moment and curvature.....	59
Figure 8.47	Column response during EQ8 in terms of base shear and drift ratio.	59
Figure 8.48	Longitudinal reinforcement tensile strain demand during EQ8.....	60
Figure 8.49	Transverse hoop reinforcement tensile strain demand during EQ8.....	60
Figure 8.50	Column displacement during EQ9.....	62
Figure 8.51	Column base East face during EQ9 at (a) peak West displacement, (b) peak East displacement, and (c) post-test.	62
Figure 8.52	Column response during EQ9 in terms of base moment and curvature.....	63
Figure 8.53	Column response during EQ9 in terms of base shear and drift ratio.	63
Figure 8.54	Longitudinal reinforcement tensile strain demand during EQ9.....	64
Figure 8.55	Transverse hoop reinforcement tensile strain demand during EQ9.....	64
Figure 8.56	Column displacement during EQ10.....	66
Figure 8.57	Column base East face during EQ10 at (a) peak West displacement, (b) peak East displacement, and (c) post-test.	66
Figure 8.58	Column response during EQ10 in terms of base moment and curvature.....	67
Figure 8.59	Column response during EQ10 in terms of base shear and drift ratio.	67
Figure 8.60	Longitudinal reinforcement strain demand during EQ10.	68
Figure 8.61	Transverse hoop reinforcement strain demand during EQ10.	68
Figure 9.1	Drift ratios achieved during tests.	71
Figure 9.2	Displacement components at peak displacements.	72

Figure 9.2	Column base East face post test (a) EQ1, (b) EQ2, (c) EQ3, (d) EQ4, (e) EQ5, (f) EQ6, (g) EQ7, (h) EQ8, (i) EQ9, and (j) EQ10.....	73
Figure 9.4	Extracted longitudinal reinforcement.....	74
Figure 9.5	South face of the column post-test.....	75

LIST OF TABLES

Table 5.1	Column as-built concrete mix proportions per cubic yard of concrete.	9
Table 5.2	Column concrete compressive strength.....	10
Table 5.3	Measured reinforcement strengths.	13
Table 6.1	Idealized, monotonic response of the analytical model.....	15
Table 6.1	Ground motion selections.....	15
Table 6.2	Ground motion scale factors.....	15
Table 6.3	Ground motion selection for extended testing.....	16
Table 6.4	Ground motion scale factors for extended testing.....	16
Table 7.1	Shake table capacities.....	28
Table 9.1	Peak response quantities.....	70

1 Introduction

Bridge failures during earthquakes in the 1970s through 1990s [Penzien 1971; Mellon 1987; Abolhassa 1989; Housner 1994; Kawashima 1995] generated substantial investigations into the causes of unacceptable performance. Experimental investigations sought and identified successful retrofit techniques, which were duly implemented through Caltrans' Seismic Retrofit Program. In parallel, seismic design guidelines evolved with these advances. One major philosophical change occurred as designs adopted a ductility approach to achieve performance objectives [Unjoh 2002; Marquez 2010].

To achieve performance levels, seismic guidelines require details to ensure plastic deformations are sustainable under cyclic loading. Experimental investigations have, and continue to provide much needed evidence as to what constitutes safe and sustainable levels. Shen, Yen, and O'Fallon [2005] assert, "the advancing of seismic design methodology and specifications is closely associated with findings and verifications produced by laboratory testing." These experiments are the basis for empirically based design equations and confidence in the adopted design philosophy.

To provide assurance that the desired and sustainable behavior is achieved through current seismic design guidelines, a 1.22-m (4-ft) diameter reinforced concrete bridge column was tested under dynamic loading conditions with simulated ground motions produced by a shake table. This was the first test of current seismic U.S. seismic guidelines at full-scale. The single cantilevered column had a nonlinear response dominated by flexural yielding at the base. Test specimen design was based on current Caltrans design specifications. To mobilize its capacity, a concrete block weighing 2.32 MN (521.9 kip) was cast on top of the 7.32-m (24-ft) column.

Test objectives were to produce lateral demands at targeted nonlinear deformations and to monitor the dynamic response for comparison with a small-scale shake table test conducted at the University of California, Berkeley. Validation of current design practices and analysis methods were of primary interest in this project. For single column bent supported on a fixed foundation, the design ductility is less than or equal to four for the direction transverse to the bridge deck [Caltrans 2006a]. Resistance to forces generated at this design level was investigated in the third test, EQ3. Experimental results at higher and lower level demands are also presented.

The test specimen was densely instrumented to obtain high quality response measurements under various ground motions. A total of ten earthquake simulations were conducted covering a range of limit states. Tests were conducted over a span of two days on the NEES shake table at the University of California, San Diego's Englekirk Structural Engineering Center on September 20th and 21st, 2010.

2 Literature Review

To date, only one prior test program has reported shake table tests of full-scale bridge columns. Kawashima et al. [2009] investigated the failure mechanism of three full-scale columns with a diameter of 1.8 m (5.9 ft). Of these, only one specimen was designed according to current Japanese standards. An unanticipated failure of this column involved the flow of crushed core concrete through the reinforcing cage. Similarities in the design philosophies and design requirements of the in Japan and the U.S. include this phenomenon as an area of concern. Sasaki and Kawashima [2009] reported on shear strength scale effects under dynamic loads utilizing the same test program. They reported shear strength as proportional to $D^{-1/5}$ or $D^{-1/3}$ depending on yielding of transverse reinforcement.

Investigations prompted by the 1971 San Fernando, were limited in scale due to capacity of laboratory equipment. Not until 2005 with the opening of the E-Defense table in Japan and the NEES@UCSD shake table at the University of California, San Diego were full scale bridge column experiments feasible. This limited full-scale experiments to pseudo-static [Stone 1989] or in-situ testing [Douglas 1985; Eberhard 1993; Gilani 1996]. The advantages of in-situ testing are the precise boundary conditions and system interaction that cannot be replicated in a laboratory. While investigation by Douglas and Buckle [1985] and Giani, Chavez, and Fenves [1996] were limited to free and forced vibration testing, Eberhard et al. [1993] applied lateral loads to examine performance, which resulted in flexural cracking of columns and abutment damage.

3 Design of the Experiment

The column was designed according to Caltrans Seismic Design Criteria [Caltrans 2006a] and Bridge Design Specifications [Caltrans 2004]. It was not based on a prototype structure, but representative of single column bents commonly found in California. Uni-axial shake table excitation subjected the test specimen to loading in the East-West direction only. Boundary conditions, fixed at the base and free at the top, corresponded to a bent subjected to ground excitation in the transverse direction of the bridge deck. The idealized condition neglects the complexities of system interaction such as multiple span interaction through deck coupling, superstructure restraint in the longitudinal direction of the deck, and foundation or abutment response.

The 1.22-m (4-ft) diameter column spanned 7.31 m (24 ft) above the footing. With a height-to-diameter aspect ratio of six, the test specimen was intended to respond in the nonlinear range with a predominant flexural behavior. A capacity based design aimed to preclude other failure modes. A design ductility of four was established for the test specimen based on the Seismic Design Criteria [Caltrans 2006a]. For this scenario, the probabilistic design spectrum corresponded to a 5% in 50 years probability of exceedance [Caltrans 2006a] and was obtained through ARS Online [Caltrans 2010].

Longitudinal reinforcement consisted of eighteen #11 (35.8-mm diameter) bars concentrically spaced around the column in a single layer. Butt-welded, double #5 (15.9-mm diameter) hoops, spaced at 152 mm (6 in.) on-center were used as transverse reinforcement. The term “double” refers to two hoops bundled together at each 152 mm spacing. Clear cover to the hoops was 51 mm (2 in.). Column reinforcement layout and the test specimen’s geometry are provided in Figure 3.1. Complete construction drawings are available at the project space on the NEEShub data repository website [NEES 2011]

A longitudinal reinforcement ratio, ρ_l , of 1.55%, typical of current practice, was provided for the column. The transverse reinforcement provided a volumetric confining ratio, ρ_s , of 0.953%. Reinforcement complied with minimum and maximum requirements [Caltrans 2004; Caltrans 2006a].

The as-built estimated axial load at the column base was 2.53 MN (569.7 kip). Accounting for the measured concrete strength at day one of testing, this axial load produced an axial load ratio, $N/A_g f'_c$, of 5.3%.

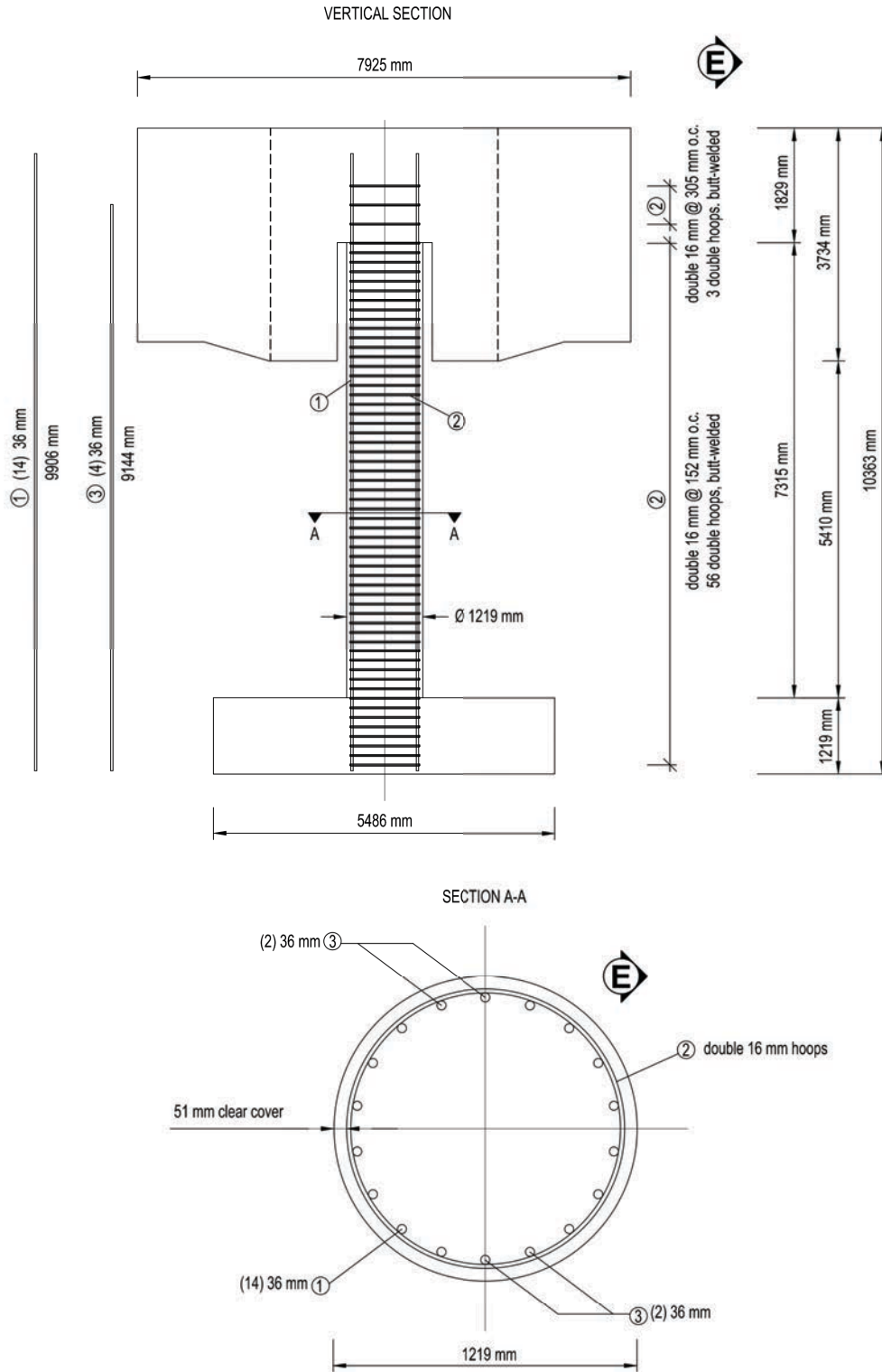


Figure 3.1 Column reinforcing details.

4 Test Setup

The test specimen included a cantilevered reinforced concrete column, footing, and superstructure mass; see Figure 4.1. The column represented a full scale bridge column designed to current Caltrans design guidelines. The footing was secured to the shake table with post-tensioning to prevent decompression under maximum expected overturning moment and provide shear transfer without sliding. A fixed base test setup isolated nonlinear response to the element of interest. The superstructure mass provided the targeted column axial load and the mass necessary to generate nonlinear response.



Figure 4.1 Test specimen.

Input excitation consisted of a single horizontal component produced by the uni-axial shake table whose dimensions are 7.6 m (25 ft) wide and 12.2 m (40 ft) long [NEES 2010]. Safety restraints, secured to the shake table, surrounded the test specimen to provide protection to site personnel and equipment. Two types of restraints were provided: inclined safety columns and arched restraint towers.

Column displacement was limited to a 10% drift ratio. This restriction was imposed by inclined safety columns placed on either side of the column in the direction of shaking, see Figure 4.2. These also provided gravity load restraint in the event of collapse. They were inclined 11.6° off vertical and were designed to contact the angled portion on the underside of the superstructure block at the limiting drift ratio. Safety columns consisted of dual W32x302 sections connected by stiffener plates. Headed reinforcing bars were welded to the flanges of the W-sections and anchored in a concrete footing. The W-sections were also embedded 38 mm (1.5 in.) in the footing. These footings were post-tensioned to the shake table, but were independent from the column's footing. Large timbers were secured to the top of the safety columns for energy dissipation at impact between the concrete block and safety column.

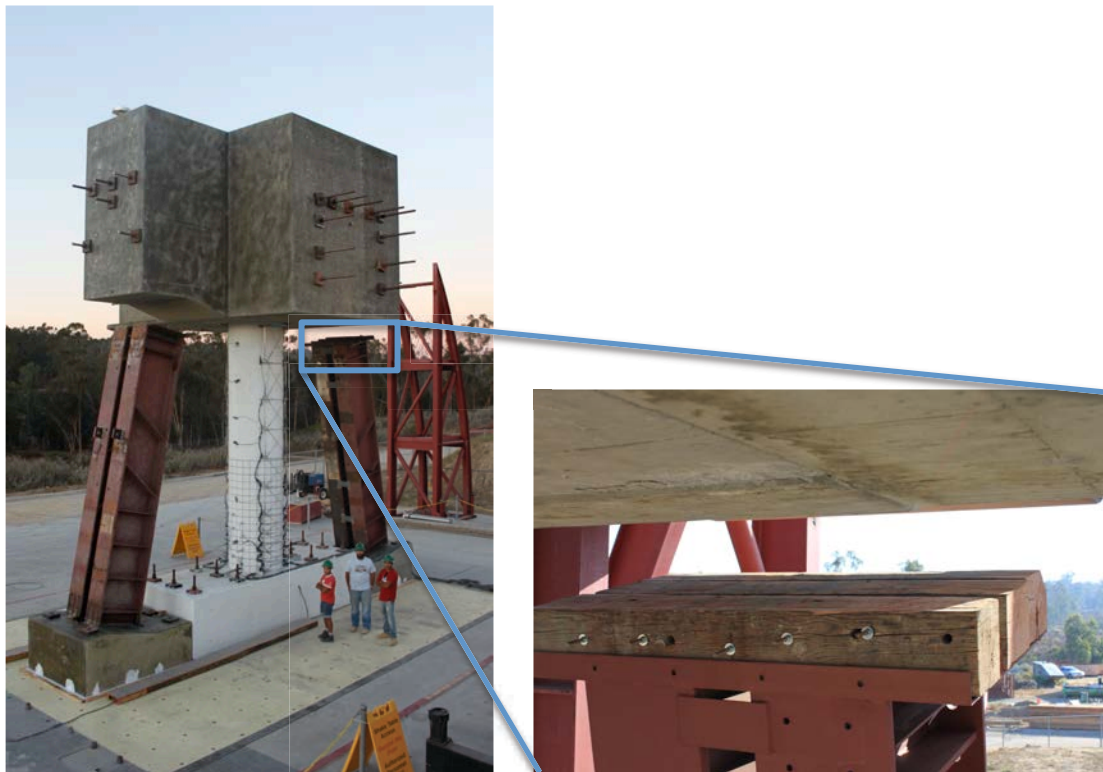


Figure 4.2 Inclined safety columns.

To preclude out-of-plane motion, the arched safety restraints located at the corners of the specimen were fitted with guides. Pairs of steel tubes were aligned in the direction of shaking and welded to the arched safety towers. A clear 6.4 mm (0.25 in.) gap between the guide and concrete block was greased to reduce friction should contact initiate during testing. The final test setup including the arched safety restraints is shown in Figure 4.3.



Figure 4.3 Pre-test setup.

4.1 COLUMN

The 1.22-m (4-ft) diameter column had a moment to shear ratio of 6.0. The free height to the center of mass of the superstructure mass was 7.31 m (24 ft). To ensure the column was unencumbered by the superstructure to the full 7.31 m, a gap was provided between the two. This gap is visible in Figure 4.3 where it appears the column is a peg in an oversized socket. However, a full moment resisting connection was provided at the top of the column where longitudinal reinforcement extended into the superstructure mass. Intentionally roughened construction joints were located at the top of the column and footing.

4.2 FOOTING

The footing was designed according to Caltrans Seismic Design Criteria [Caltrans 2006a] and Bridge Design Specifications [Caltrans 2004] guidelines. It consisted of a 5.49-m (18-ft) long, 1.83-m (6-ft) wide, 1.22-m (4-ft) deep reinforced concrete block. The moment resisting connection between the footing and column was designed similar to a superstructure “T” joint (Caltrans, 2006a). It was reinforced with twelve 36-mm diameter (#11) bars top and bottom and 13-mm diameter (#4) transverse stirrups and ties. Reinforcing details can be found in construction drawings available in the project archive [NEES 2011]. The footing was post-tensioned to the shake table with considerations to prevent decompression under maximum

expected overturning moment and prevent sliding at maximum shear transfer relative to the shake table.

4.3 SUPERSTRUCTURE MASS

The superstructure consisted of five cast-in-place concrete blocks. These blocks were arranged in a cruciform to accommodate the placement of the safety restraints on the table. The blocks were post-tensioned together and had a combined estimated weight of 2.32 MN (521.9 kip). This weight utilized the measured concrete unit weight with the specified geometry and accounted for the block reinforcement, through holes for post-tensioning, and post-tensioning bars. The rotational mass moment of inertia about the center of mass was calculated as $2.50 \times 10^{10} \frac{kN \cdot m^2}{g}$ ($3.62 \times 10^6 \frac{kip \cdot in^2}{g}$). This calculation relied also on the specified geometry and estimated weight.

Through post-tensioning ensured the total mass was mobilized as a single block. It was designed to ensure decompression would not occur under combined gravity and seismic loading. Minimum reinforcement was provided for each block. The reinforcement ratio was assigned per ACI 316 [ACI 2005] requirements, and was distributed as skin reinforcement on each face of the blocks. Specified block dimension and reinforcing details can be found in construction drawings available in the project archive [NEES 2011].

The central block was cast on top of the column and provided anchorage for the column's longitudinal reinforcement for a full moment resisting connection. The combined block geometry was designed so its center of mass coincided with the top of the column. To ensure an unencumbered column height of 7.32 m (24 ft), a breakout was provided between the column and the central block for the bottom 1.91 m (6.25 ft) of the block. A 1.52-m (5-ft) diameter corrugated pipe embedded in the block resulted in a 152.4-mm (6-in.) gap between the block and the column. The corrugated pipe was utilized as stay-in-place formwork.

5 Material Properties

5.1 CONCRETE

The specified concrete strength of the column was 27.6 MPa (4.0 ksi) for a targeted axial load ratio of 6.1% based on an expected concrete strength of $1.3f'_c$. Maximum aggregate size for the mix was specified as 25.4 mm (1.0 in.) and the mix conformed to Caltrans aggregate grading (Caltrans, 2006b). The mix design included type II Portland cement with a water to cement ratio of 0.44 including 25 percent contribution from fly ash, and had an anticipated 101.6 mm (4.0 in.) slump. Prior to placing the concrete, 0.019 m^3 (5 gallons) of water was added to each delivery truck with 6.1 m^3 (8 yd^3) of concrete containing 1.03 m^3 (273 gallons) of water. The resulting water to cement ratio was 0.43. Each batch was further supplemented with 1479 ml (50 oz) of superplasticizer to improve workability and achieved a measured slump of 159 mm (6.25 in.) and 165 mm (6.5 in.). The mix proportions, averaged between the two batches, are provided in Table 5.1.

Table 5.1 Column as-built concrete mix proportions per cubic yard of concrete.

Material	Proportion
Cement	230 kg (509 lb) *
Fly ash – Class F	77 (169)
Fine aggregate	634 (1400)
Aggregate: 1-1/2" x 3/4"	0 (0)
Aggregate: 1" x #4	620 (1368)
Aggregate: 3/8" x #8	134 (298)
Water (34.8 gallons)	131 (290)
Entrapped air	1%
Water reducing admixture	600 ml (20.3 oz)
Superplasticizer	185 ml (6.3 oz)
Total	1792 kg (3952 lb)

At the time of casting, 152.4-mm (6-in.) diameter by 304.8-mm (12-in.) high concrete test cylinders were taken. These gave an average concrete unit weight of 23.58 kN/m³ (150.1 pcf). Cylinders were tested under monotonic compression in sets of three samples at twenty-nine, forty-two, and forty-three days. Commencement of shake table testing corresponded to an age of forty-two days in the column concrete. The forty-three day age corresponded to the second day of shake table testing. Of the three samples in a set, two samples were taken from the first batch of concrete delivered to the site and one sample was from the second batch of concrete. This gave emphasis to the concrete strength in the plastic hinge region. Table 5.2 summarizes the results of these compression tests. A complete stress-strain relationship to peak load was obtained for one sample of each set of cylinders; see Figure 5.1. The strain was obtained as the average measurement from three concrete strain gauges oriented in the longitudinal direction. The sample was taken from the first batch of concrete delivered to the site.

Table 5.2 Column concrete compressive strength.

Age (Days)	f'_c MPa (ksi)
21	37.0 (5.4) *
29	40.3 (5.8) *
42	40.9 (5.9) +
43	42.0 (6.1) ‡

* Average of three samples

+ Average of five samples

‡ Average of six samples

The modulus of elasticity of the concrete, E_c defined here as the slope of the secant line from the origin to the point at $0.5f'_c$, was obtained from the stress-strain curves in Figure 5.1 as 22877 MPa (3317 ksi). This was found as the average value of three concrete breaks. This modulus of elasticity is only 79% of the anticipated modulus calculated from equation 3.11 [Caltrans 2006a] based expected concrete compressive strength and unit weight.

The unconfined concrete compressive strain at maximum compressive stress, ϵ_{co} , was obtained from Figure 5.1 and found to be 0.0026. This was based on an average strain from three samples at 42 or 43 days, where the maximum compressive stress was based on the average from five or six samples, respectively, rather than the maximum compressive stress of the single sample shown in Figure 5.1. This unconfined concrete compressive strain at maximum compressive stress was 30% greater than the 0.002 value specified for design [Caltrans 2006a].

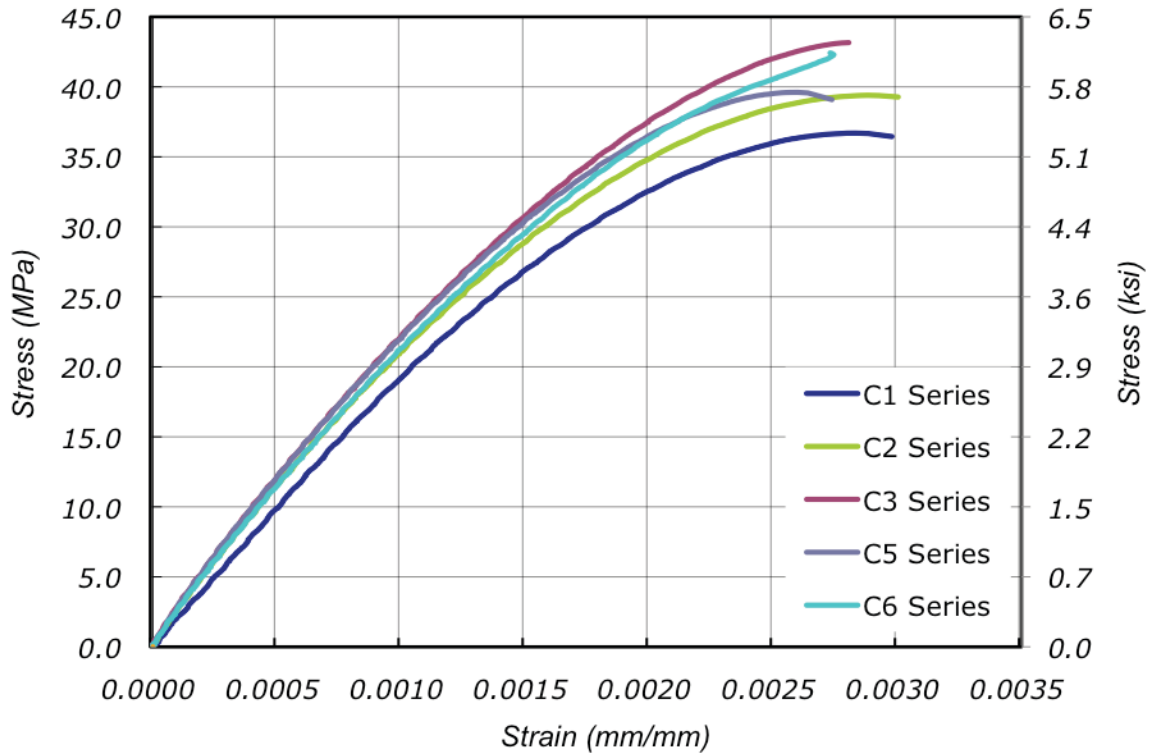


Figure 5.1 Column concrete stress-strain relationship.

5.2 REINFORCING STEEL

Column longitudinal and transverse reinforcement were specified as Grade 60 (414 MPa) steel conforming to ASTM A706 [2009]. The #11 (35.8-mm diameter) longitudinal reinforcement had a yield strength of 518.5 MPa (75.2 ksi) and an ultimate strength of 706.7 MPa (102.4 ksi). These strengths, reiterated in Table 5.3 along with other mechanical properties of the reinforcement, were obtained from monotonic tension tests. The yield strength is based on the average of two samples and the ultimate strength is based on the average of three samples. Test coupons were instrumented with a pair of strain gauges, from which the strain measurement was obtained. A complete stress-strain curve for one sample is provided Figure 5.2.

Five samples taken from the #5 (15.9-mm diameter) transverse hoops tested under monotonic tension did not exhibit a yield plateau. These samples were cut from three bent hoops outside of the weld-affected region. The butt welds of these hoops were proof tested and all failed outside of the weld. Yield strength based on the mill cert of the straight #5 bars was expected to be 454 MPa (65.8 ksi) and the ultimate tensile strength was expected to be 600 MPa (87.0 ksi). The ultimate tensile strength based on five samples was 592.2 MPa (85.9 ksi). Strain was calculated as the average strain recorded by a pair of strain gauges. One gauge was located on the concave side of the bar and the other on the convex side. The stress-strain relationship of two samples is provided in Figure 5.3. Specimen 1, 2, and 3 had strain gauges that saturated prematurely and are therefore excluded from Figure 5.3.

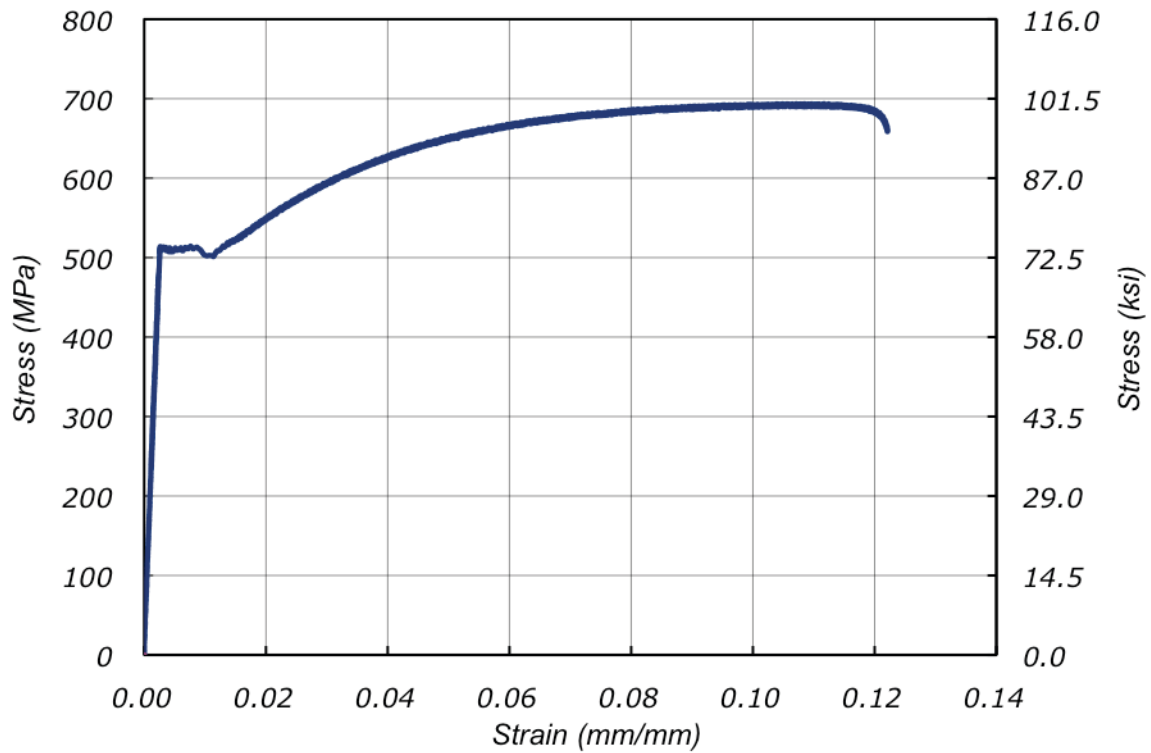


Figure 5.2 Column longitudinal reinforcement stress-strain relationship.

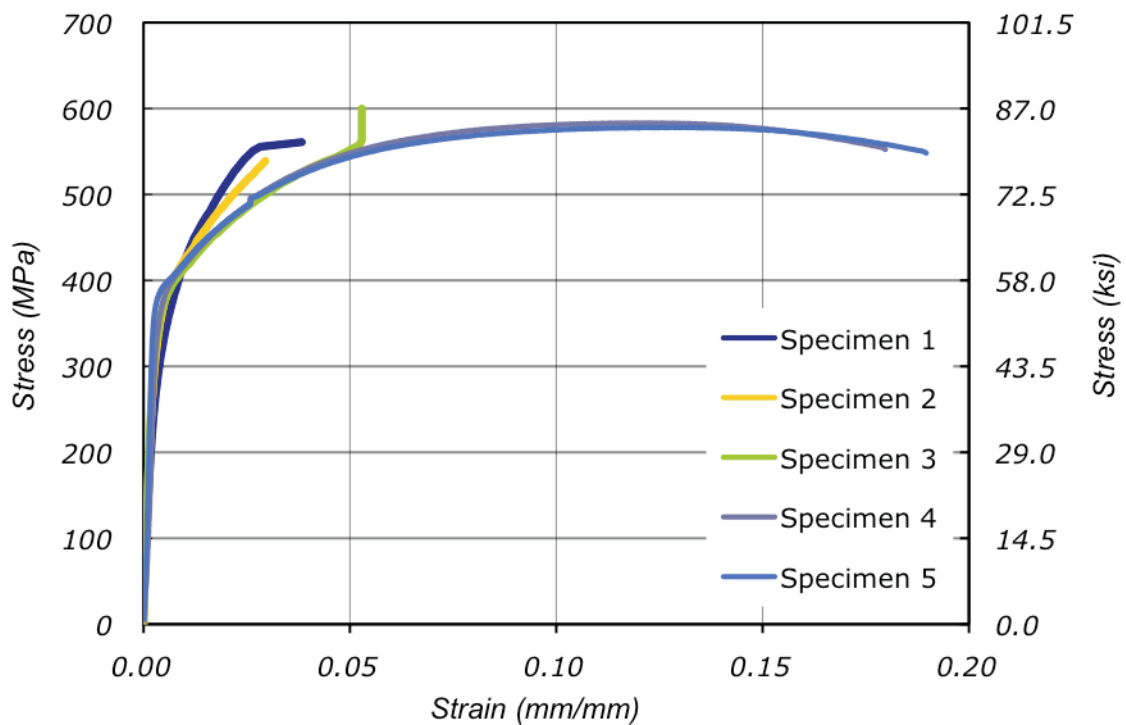


Figure 5.3 Column transverse hoop reinforcement stress-strain benchmarking.

Table 5.3 Measured reinforcement strengths.

Reinf.	ϵ_y (%)	f_y MPa (ksi)	E_s MPa (ksi)	ϵ_{sh} (%)	E_{sh} MPa (ksi)	ϵ_u (%)	f_u MPa (ksi)
#11 long.	0.26	518.5 (75.2)	196057 (28426)	1.1	5515.5 (800.0)	12.2	706.7 (102.4)
#5 transv.	-	337.9 (54.8)*		-	-	12.5	592.2 (85.9)

Footings and superstructure reinforcement was specified as Grade 60 (414 MPa) steel conforming to ASTM A615 [2009]. Normal weight concrete was utilized in both of these components. Samples from each of these provided an average concrete unit weight of 23.47 kN/m³ (149.8 pcf) and 23.68 kN/m³ (150.7 pcf) for the footing and superstructure, respectively. The concrete in the footing had a specified strength of 27.6 MPa (4.0 ksi), and the mix design was the same as utilized for the column. The concrete strength on the day one of testing was 41.9 MPa (6.1 ksi). The superstructure mass included high-early strength concrete to accommodate the project schedule. The specified strength of this mix design was 35 MPa (5.1 ksi) with an expected strength of 31.3 MPa (4.7 ksi) at seven days.

6 Test Protocol

Six earthquake simulation tests were planned in the loading protocol. The test objectives were to achieve desired column displacements. The displacements were selected in terms of target displacement ductilities as 1, 2, 4, and 8. However, to investigate the effects of lower intensity aftershocks, the test sequence was not conducted with continually increasing demands. The protocol included a repetition of the target ductility of 2 and 4 after subsequently testing at a higher ductility demand. The resulting protocol called for tests with input motions capable of producing target ductilities in the following sequence: 1, 2, 4, 2, 8, and 4. Tests at a repeated target ductility utilized the same input motion as the initial trial. This provided the opportunity to investigate the effect of damping and damage accumulation.

The selection of input table motions relied on the Pacific Earthquake Engineering Research (PEER) Center's strong motion database [PEER 2007]. Considering a site located in San Francisco, California, earthquake recordings from a strike slip fault mechanism were given preference. Preference was also given to records that could produce the desired response without scaling. Ground motion selections were based initially on their 2% damped, elastic response spectrum. The equal displacement concept, displacement response spectrum, and analytically based fundamental period were used to identify possible candidates for the targeted ductility ratios. Displacement ductility was based on an idealized yield displacement determined analytically as 88 mm (3.47 in.) [Carrea 2010].

Based on nonlinear dynamic time history analyses [Carr 2002; Carrea 2010], possible input motions were further reassessed. The lumped plasticity model, with which the yield displacement was calculated, was calibrated against a full-scale, pseudo-static test by Stone and Cheok [1989], which had similar design properties. The idealized moment-curvature response was refined to account for measured material properties such as a lower than anticipated concrete modulus. The resulting idealized monotonic behavior can be characterized by the parameters in Table 6.1.

After analyzing possible candidates, four historical earthquake recordings were selected as shake table input motions. Three input motions were selected from the 1989 Loma Prieta earthquake. The fourth record was sourced from the Takatori station during the 1995 Kobe earthquake. These records are identified in Table 6.2. Analytical predictions indicated the Takatori record was stronger than necessary to achieve the target ductility and exceeded the safety limit imposed due to ratcheting when run in sequence with the other motions. Therefore, the amplitude reduced and polarity inverted as indicated in Table 6.3.

Table 6.1 Idealized, monotonic response of the analytical model.

Limit state	Curvature (rad/m)	Moment (kN-m)	Displacement (mm)	Shear force (kN)
First cracking	2.93×10^{-4} (7.43×10^{-6} rad/in)	839 (619 kip-ft)	4 (0.17 in.)	97.0 (21.8 kip)
Nominal or idealized yield	4.73×10^{-3} (1.20×10^{-4} rad/in)	5793 (4273 kip-ft)	88 (3.47 in.)	781.8 (175.8 kip)
Ultimate	7.56×10^{-2} (1.92×10^{-3} rad/in)	6282 (4633 kip-ft)	506 (19.95 in.)	705.0 (158.5 kip)

Table 6.2 Ground motion selections.

Test	Earthquake	Date	Moment magnitude	Station	Component
EQ1	Loma Prieta	10/18/1989	6.9	Agnew State Hospital	090
EQ2	Loma Prieta	10/18/1989	6.9	Corralitos	090
EQ3	Loma Prieta	10/18/1989	6.9	LGPC	000
EQ4	Loma Prieta	10/18/1989	6.9	Corralitos	090
EQ5	Kobe	01/16/1995	6.9	Takatori	000
EQ6	Loma Prieta	10/18/1989	6.9	LGPC	000

Table 6.3 Ground motion scale factors.

Test	Target displacement ductility	Scale factor	Table PGA (g)
EQ1	1.0	1.0	-0.199
EQ2	2.0	1.0	0.409
EQ3	4.0	1.0	0.526
EQ4	2.0	1.0	0.454
EQ5	8.0	-0.8	-0.533
EQ6	4.0	1.0	-0.512

Due to significant structural integrity after the planned test sequence, the scope was expanded and an additional four tests were conducted. These tests utilized the Takatori ground motion from the Kobe earthquake, see Table 6.4, at different amplitudes. The scale factors for the ground motions in the extended test sequence are provided in Table 6.5.

Table 6.4 Ground motion selection for extended testing.

Test	Earthquake	Date	Moment magnitude	Station	Component
EQ7	Kobe	01/16/1995	6.9	Takatori	000
EQ8	Kobe	01/16/1995	6.9	Takatori	000
EQ9	Kobe	01/16/1995	6.9	Takatori	000
EQ10	Kobe	01/16/1995	6.9	Takatori	000

Table 6.5 Ground motion scale factors for extended testing.

Test	Target displacement ductility	Scale factor	Table PGA (g)
EQ7	Not applicable	1.0	0.646
EQ8	Not applicable	-1.2	-0.829
EQ9	Not applicable	1.2	0.819
EQ10	Not applicable	1.2	0.851

For comparison with these input motions, the 975 year return period probabilistic seismic hazard for the San Francisco site is provided with their response spectra in Figure 6.1. Obtained through ARS Online [Caltrans 2010b], the 5% damped design response spectra was transformed to 1% damping with a 1/0.8 amplification across the entire period range [FEMA-273 1997]. The site considered, latitude 37.77 and longitude -122.42, had stiff soil with an average small strain shear wave velocity, V_{s30} , of 350 m/s (1,148 ft/s) in the upper 30 m (98 ft) of the soil column.

The response spectra for the ten tests are provided in Figure 6.2 through Figure 6.7. The elastic pseudo-acceleration and displacement response spectra are provided for each test along with the response spectra of the desired ground motion at 1% damping. The response spectra for EQ1 are provided in Figure 6.2. EQ2 and EQ4 are repetitions of the same ground motion and are plotted together in Figure 6.3. Similarly, Figure 6.4 contains the response spectra of both EQ3 and EQ6. The response spectra of EQ5 and EQ7 are provided in Figure 6.5 and Figure 6.6, respectively. Tests EQ8, EQ9, and EQ10 utilized the same ground motion so their response spectra are all contained in Figure 6.7.

The response spectra of the desired ground motions were obtained after filtering historical records found in the PEER Ground Motion Database [PEER 2007]. The records were band pass filtered using an FIR filter of order 5000 with cutoff frequencies of 0.25 and 25-Hz. The table acceleration feedback was also band pass filtered using the same FIR filter before obtaining the response spectra.

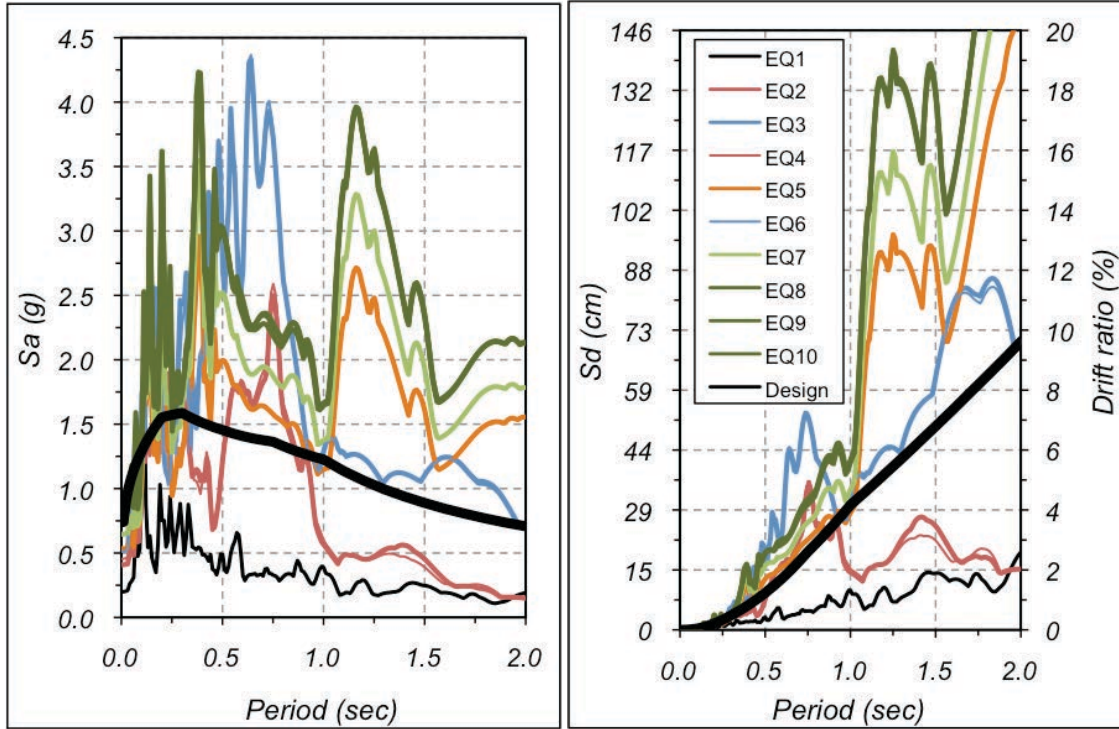


Figure 6.1 Desired ground motions in terms of (a) pseudo-acceleration and (b) displacement response spectra at 1% damping ratio.

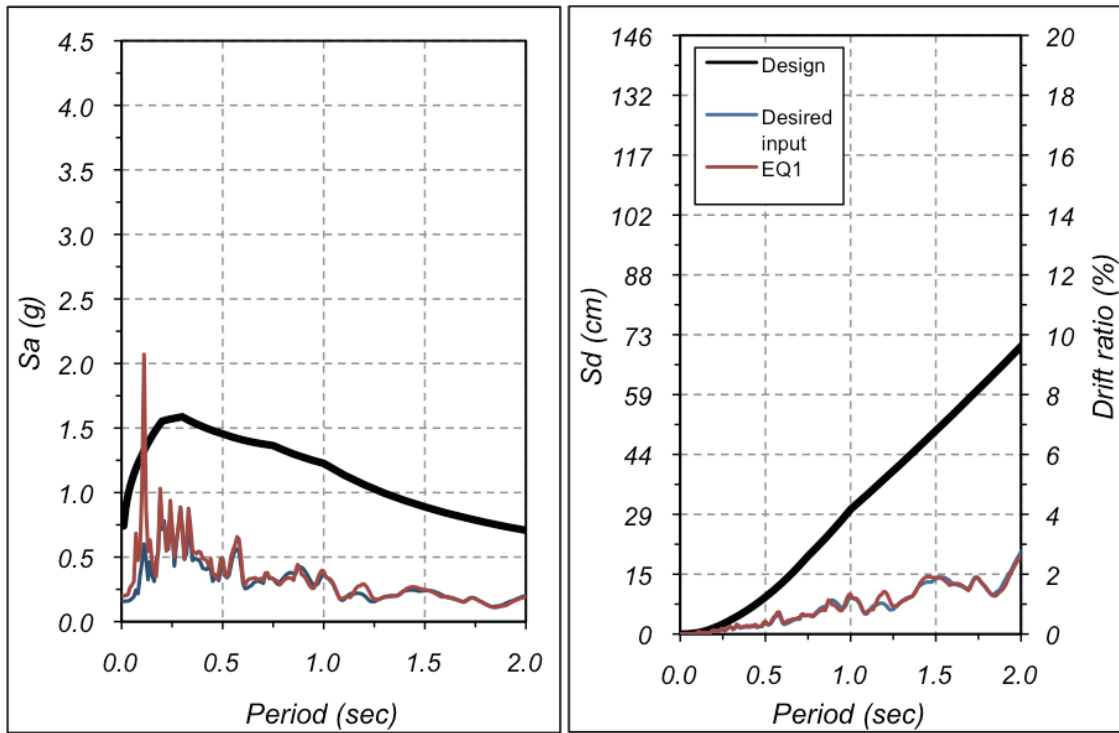


Figure 6.2 EQ1 (a) pseudo-acceleration and (b) displacement response spectra at 1% damping ratio.

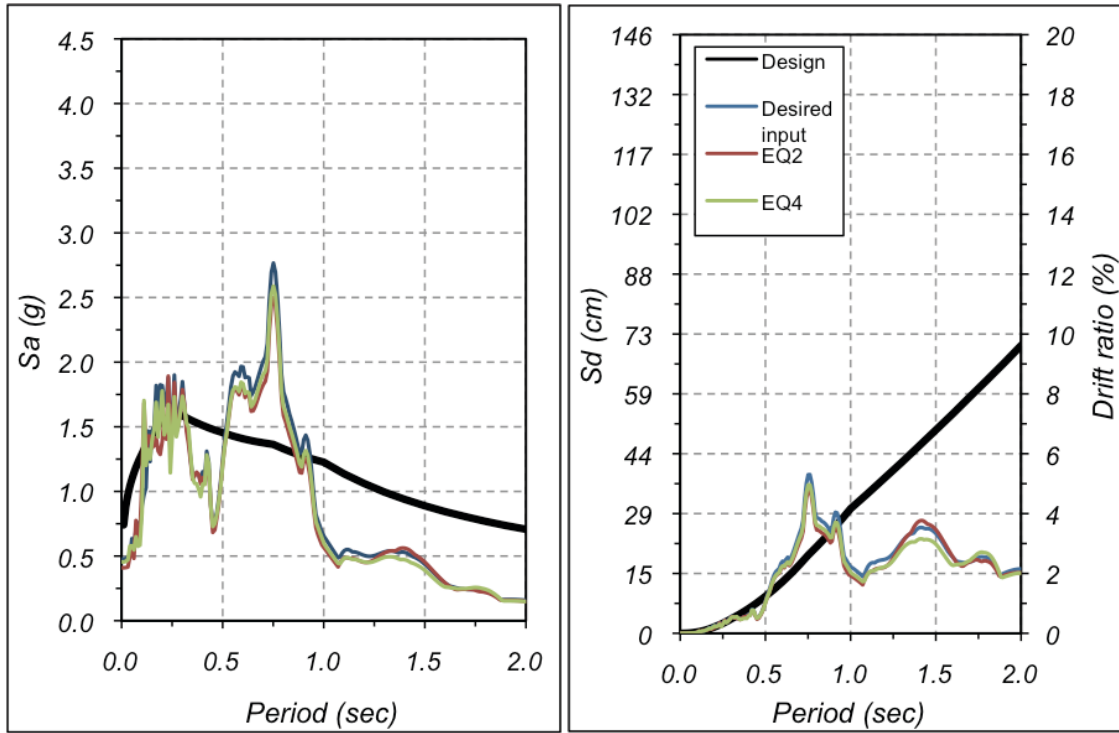


Figure 6.3 EQ2 and EQ4 (a) pseudo-acceleration and (b) displacement response spectra at 1% damping ratio.

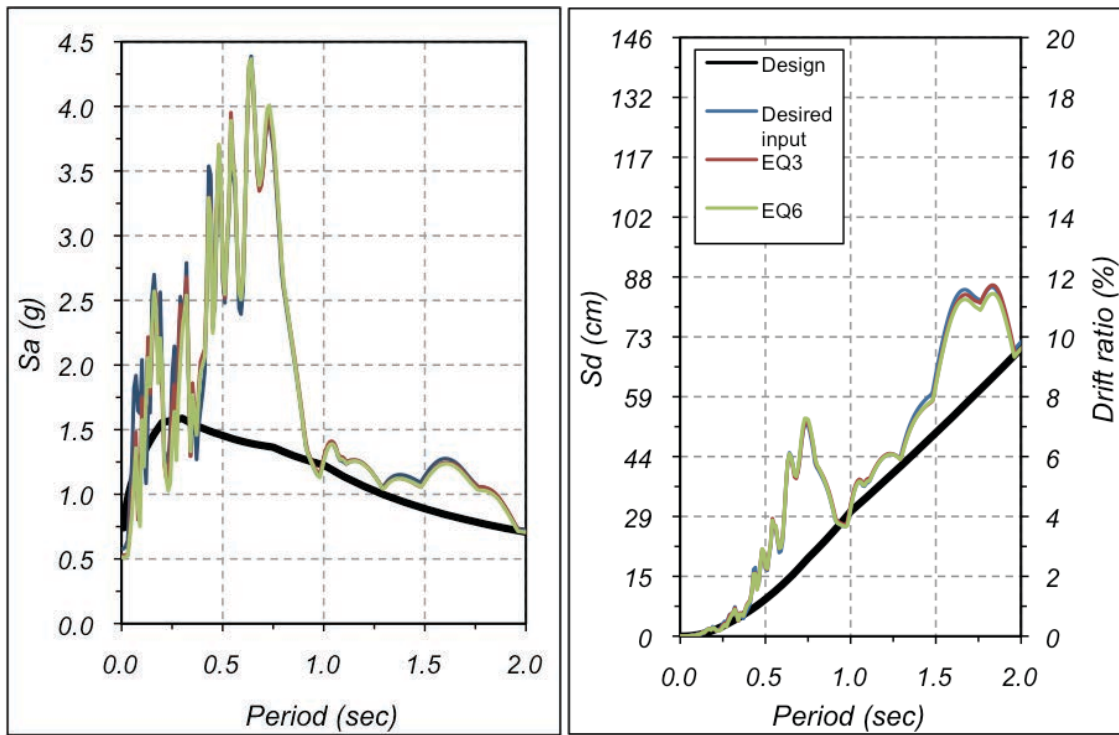


Figure 6.4 EQ3 and EQ6 (a) pseudo-acceleration and (b) displacement response spectra at 1% damping ratio.

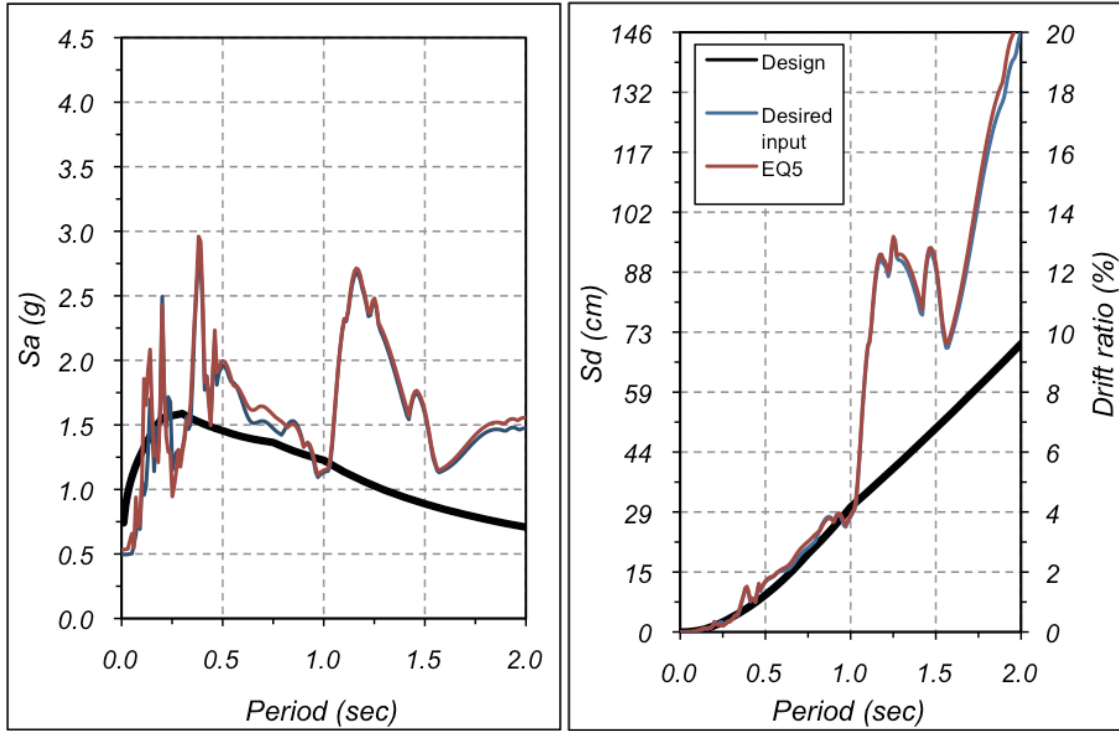


Figure 6.5 EQ5 (a) pseudo-acceleration and (b) displacement response spectra at 1% damping ratio.

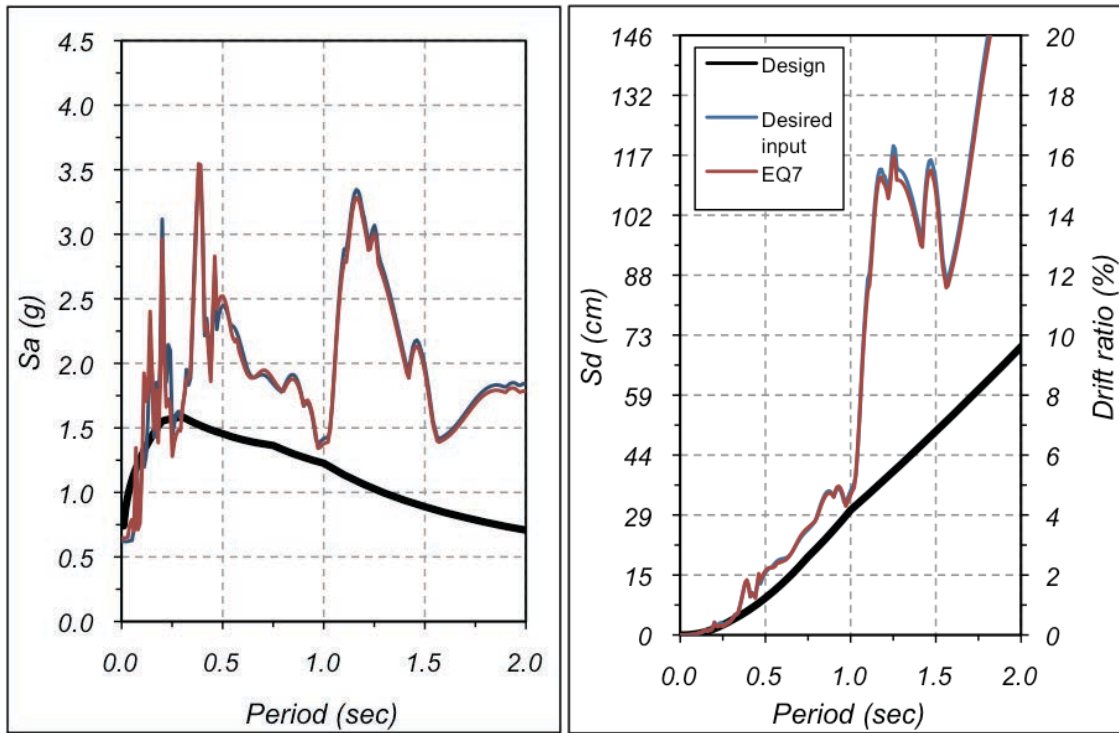


Figure 6.6 EQ7 (a) pseudo-acceleration and (b) displacement response spectra at 1% damping ratio.

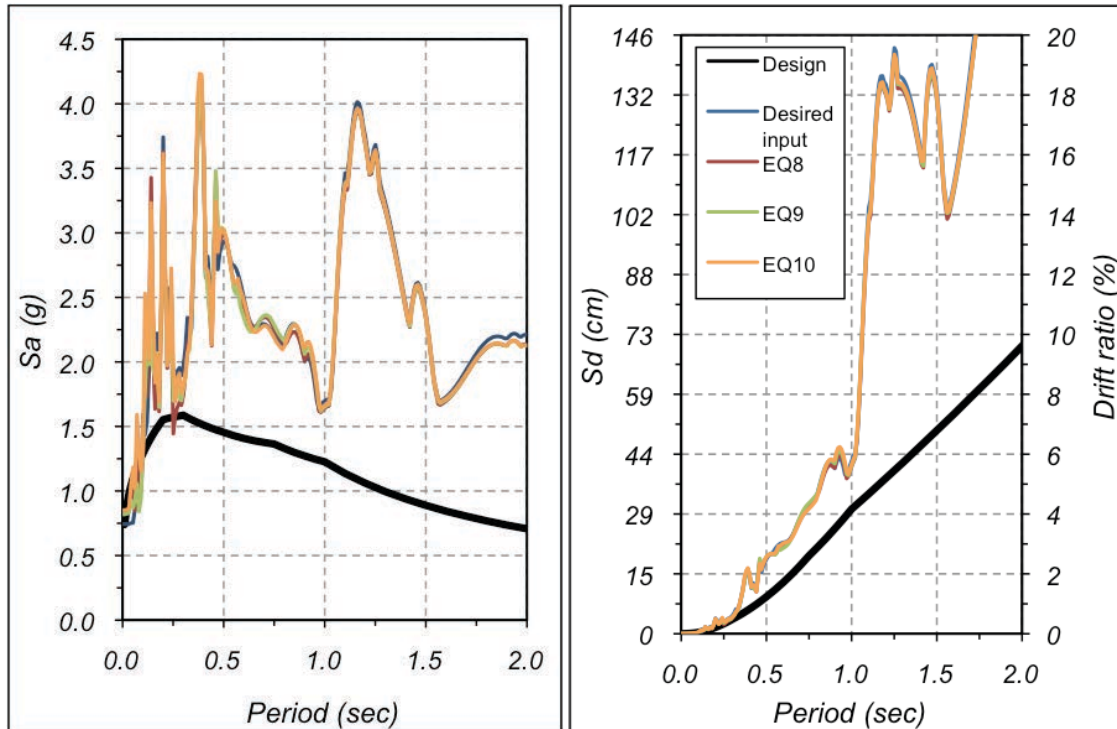


Figure 6.7 EQ8, EQ9, and EQ10 (a) pseudo-acceleration and (b) displacement response spectra at 1% damping ratio.

Before the first earthquake simulation, two white noise table motions were conducted. A white noise table motion with 0.03-g root mean square amplitude was used to check the instrumentation for quality control assurance. The same input motion was repeated before testing commenced and then repeated between subsequent earthquake tests. This was implemented to observe the period shift and mode shape changes caused by damage accumulation.

7 Instrumentation

The test specimen was densely instrumented with 278 channels of data acquisition. These included strain gauges, linear and string potentiometers, accelerometers, and Global Positioning System (GPS) receivers to measure internal, local, and global deformations during testing. Detailed instrumentation plans are provided in Appendix A and available at the project space on the NEEShub data repository website [NEES 2011].

7.1 STRAIN GAUGES

7.1.1 Longitudinal strain gauges

Electrical resistance strain gauges were symmetrically installed on two longitudinal reinforcing bars at both East and West faces of the column to monitor axial strains. These gauges were placed in pairs on both sides of each bar in the direction of shaking to monitor any bending in the bar. In total, 64 gauges with a 5 mm (0.2 in.) gauge length were installed on the four longitudinal bars. Prior to installation of the gauges, the steel reinforcement was filed to expose a smooth surface free of mill scale and deformations.

7.1.2 Transverse strain gauges

Strain gauges were installed on the exterior face of the transverse hoops at the East and West sides of the column. Twenty-two foil resistance strain gauges with a 5 mm (0.2 in.) gauge length were installed; 11 gauges were located on either. The purpose of these gauges was to monitor the hoops' axial dilation caused by radial dilation of the concrete core and longitudinal bars buckling. Prior to installation of the gauges, the steel reinforcement was filed to expose a smooth surface free of mill scale and deformations

7.1.3 Safety restraint strain gauges

Eight strain gauges were installed on the flanges of the four inclined columns used as safety restraints. Two gauges per column were installed as pairs on opposite faces; one on the East and one on the West face. These gauges were intended to estimate the impact force should the column reach a 10% drift ratio.

7.2 LINEAR VOLTAGE DISPLACEMENT TRANSDUCERS

Linear displacement sensors with either a 50-mm (2-in.) or 100-mm (4-in.) stroke were installed externally to monitor column deformations; they are referred to as curvature Linear Variable Differential Transformers (LVDTs) or shear deformation LVDTs. These potentiometers were mounted on 9.5-mm (3/8-in) threaded rods cast horizontally in the column in the North-South direction perpendicular to the direction of shaking. This removed the LVDTs from regions of potential spalling to decrease the likelihood of sensor damage. The rods were placed parallel and as close as possible to the expected neutral axis position to move them from the region of potential spalling and prevent dislocation during concrete crushing. They were encased in rubber hose to debond them from the concrete core. Surgical tubing surrounded threaded couplers at each end of the threaded rod to accommodate extensions once the steel form was removed. To reduce rod vibrations where needed, approximately 5-mm (2-in.) long segments at the ends of rods were epoxied to the concrete.

A 203-mm (8-in.) vertical spacing of the rods was used starting 50.8 mm (2 in.) above the column base and extending one column diameter, whereas 610-mm (24-in.) and 787-mm (31-in.) spacings were used outside of that area. Both curvature and shear LVDTs were installed on the South face of the column, whereas only curvature LVDTs were mounted on the North face, see Figure 7.1. Four vertical spring LVDTs were installed to determine the fix-end rotation of the column. They were mounted on the four curvature rods located 51mm (2 in.) above the column-footing interface and they targeted the top of the footing as shown in Figure 7.1.

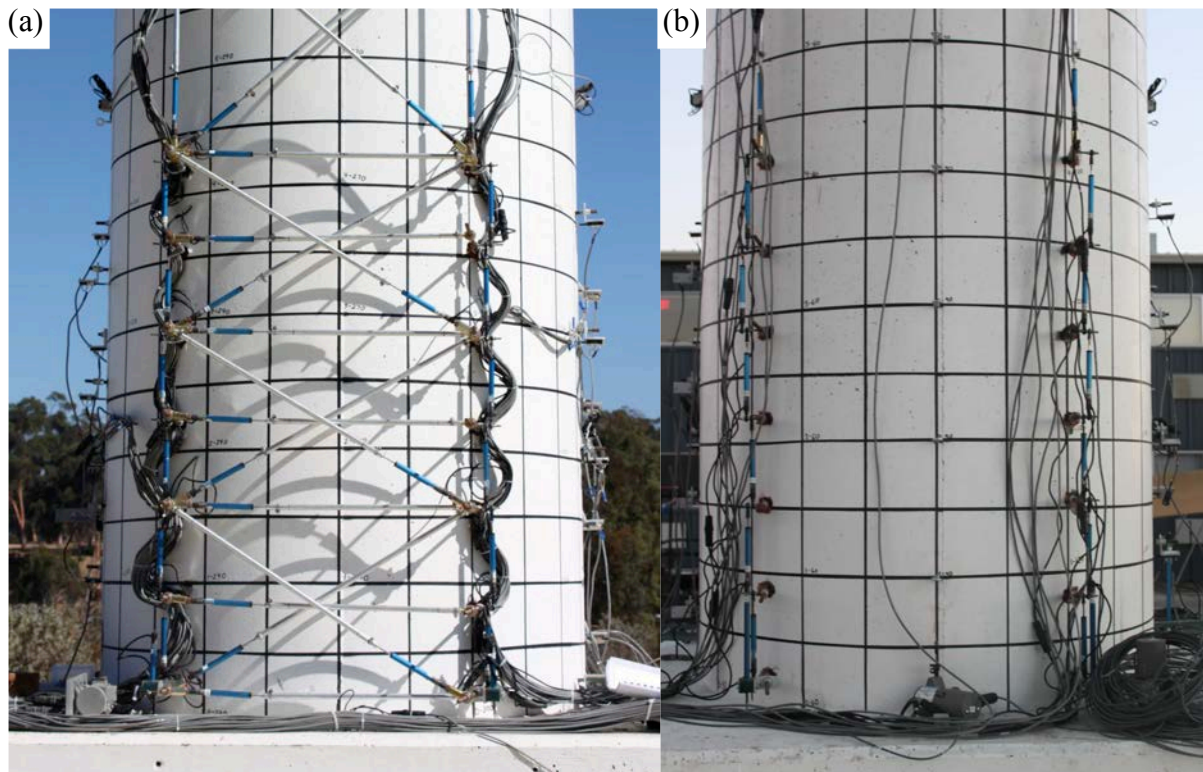


Figure 7.1 Curvature, shear, and fixed-end rotation LVDTs and the (a) South and (b) North faces.

Two horizontal spring loaded LVDTs were installed to monitor the relative rotation between the column and the superstructure mass. These sensors were mounted on the lower face of the central block and they targeted the East and West faces of the column, see Figure 7.2.

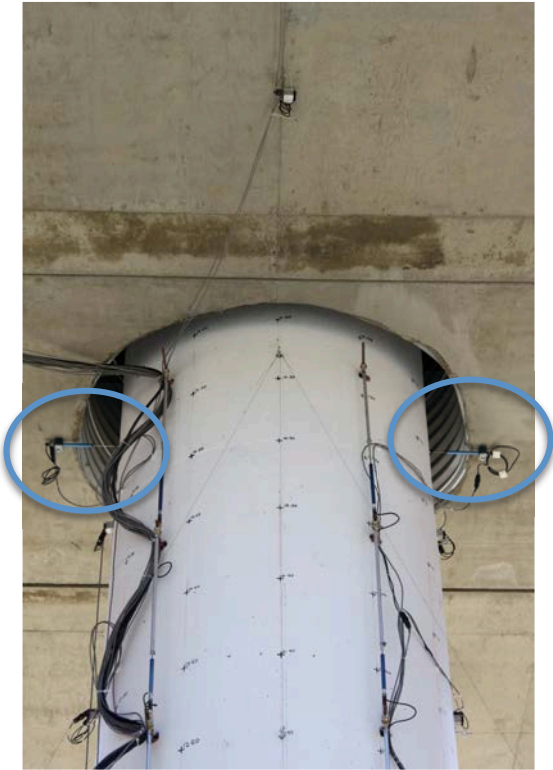


Figure 7.2 Column-to-top mass LVDTs.

Vertical LVDTs were installed to measure bond slip between the longitudinal bars and the concrete of the footing. One bar on both East and West faces of the column was monitored. Steel brackets, see Figure 7.3, were clamped on these bars using three sharpen screws and they were placed just below the column-footing interface. Two concave steel targets were welded to each brace to prevent slip of the spring LVDTs. The distances from the center of the bar to the center of each target were 119 mm (4.7 in.) and 208 mm (8.2 in.). Epoxy filled the gap between the collar and the longitudinal bar and the screws were ground flush to the exterior of the collar. The assembly was then encapsulated in expansive foam to debond it from and allow movement within the surrounding footing concrete, see Figure 7.3(c). The LVDTs were placed on a rigid support bolted to the footing away from the column. Access to the bracket was made possible by removing the expansive foam after casting the footing. Two LVDTs were used to capture the rotation and vertical movement of the bracket.

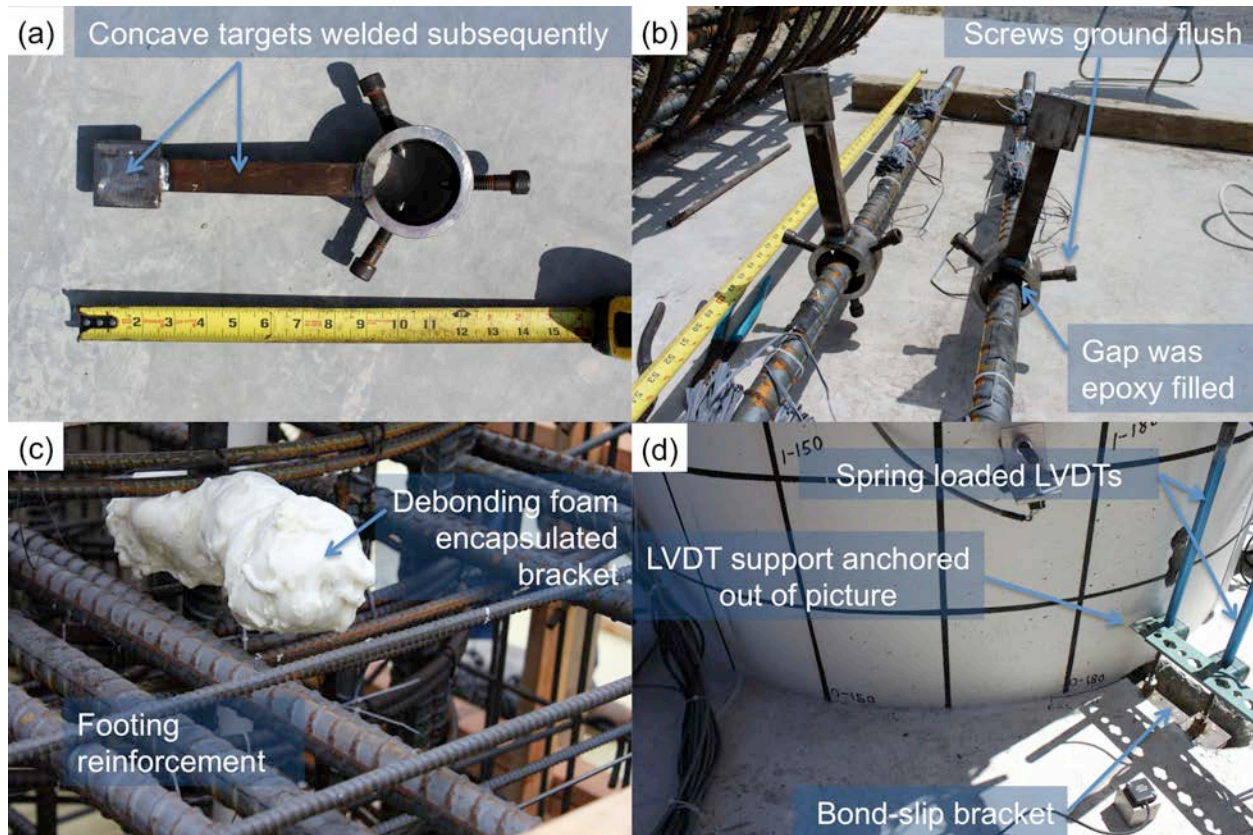


Figure 7.3 Bond slip bracket installation: (a) assembly, (b) placed on longitudinal bars, (c) encapsulated with debonding foam, and (d) final installation.

Spring loaded linear displacement sensors with a 25.4 mm (1-in.) stroke were installed to measure the radial dilation of the concrete core in the plastic hinge region; they are referred to as dilation LVDTs, see Figure 7.4. These potentiometers were mounted on steel rods that were cast into the column. The rods passed horizontally through the column along the diameter of its cross section. They were encased in steel pipes to inhibit bond with the surrounding concrete. However, a 127-mm (5-in.) long segment at the rod's center remained exposed to fix the rods in a stable area of the column cross section. These sensors were aligned to concave steel targets that were welded to the exterior face of the hoops, see Figure 7.4(a).

A 25.4 mm (1 in.) stroke LVDT was installed to monitor shear slip between the base of the column and the footing along their interface. This potentiometer was placed on the column-footing interface at the South side. In total, 107 LVDTs were installed on the column.



Figure 7.4 Dilation LVDT installation (a) target welded to a transverse hoop, (b) LVDT assembly, and locations on the West face.

7.3 SPRING POTENTIOMETERS

The relative horizontal displacement between the shake table and the column was measured at different heights using five cable-extension position transducers; they are referred to as horizontal string potentiometer. These instruments were mounted to the stiffener plates of the West safety restraint. Because the upper portion of the column was embedded in the superstructure, four string potentiometers were installed between the restraining towers and the sides blocks to measure the relative horizontal displacement of the column top. The horizontal string potentiometer layout is shown in Figure 7.5 with only one of the four string pots between the arched safety restraint and the mass block visible. In tests up to and including the white noise test after EQ3, the string potentiometers measuring top block displacement at the elevation of the top of the column were located on the four corners of the block. For the remaining tests, the potentiometers on the East side of the block were relocated to the West side and placed in series with the potentiometers on this side. This was done to ensure adequate stroke in the sensors at the limiting drift.



Figure 7.5 Horizontal spring potentiometer locations.

Three sensors were installed to monitor the relative displacement of the column at 5.41 m (17.75-ft) above the top of the footing. They were placed on the North side of the column: one was vertical, whereas the others two were inclined as shown in Figure 7.6. This configuration allows the computation of the column elongation.



Figure 7.6 Inclined spring potentiometer locations.

7.4 ACCELEROMETERS

Twenty-three accelerometers were installed to monitor the dynamic response of the specimen. These sensors were used to measure vertical and horizontal accelerations. The DC coupled, silicone MEMS accelerometers were uniaxial with ± 5 g dynamic range. They were installed on the East and West faces of the column in different locations along its height. Because of the column tip was embedded in the superstructure, two vertical and two horizontal accelerometers were placed on the North and South faces of the superstructure to measure the center of mass acceleration. The horizontal acceleration at the base of the column was measured using two accelerometers placed on the footing at North and South sides. The data of these sensors allowed the computation of the inertia forces generated on the specimen from the base excitation.

Vertical accelerometers were installed on the platen and on the footing to monitor the possible rotation of the shake table and column foundation in the shaking direction. Vertical and horizontal accelerometers were mounted on the superstructure mass to monitor its longitudinal, transverse and rotational response.

The possible impact between the superstructure and the wood blocks located atop of the safety columns was measured by four accelerometers and four strain gauges previously. Eight accelerometers were installed on the restraining towers to measure their response, which is included in the column's top displacement since they were used as an assumed rigid reference.

7.5 GPS SYSTEM

A network of three NAVCOM ANT-2004T antennae provided global displacement monitoring. Two GPS antennae were mounted on top of the superstructure mass and one was used as a reference on the ground. These measured global displacement of the test specimen in three dimensions. The GPS acquisition system was separate from the table's data acquisition system. The dedicated standalone computer allowed continuous monitoring via three NAVCOM NTC-2030M receivers operating at 50-Hz.

7.6 VIDEO CAMERAS

Six video cameras were mounted on the shake table observing the plastic hinge region: four were secured to the footing pointing at the East and West faces of the column and two were installed on rigid supports bolted to the platen pointing to the North and South faces of the column. These cameras were connected to a PC based digital video recording system synchronized with the data acquisition system. Several independent video cameras were installed outside the shake table to record the tests from different angles.

7.7 DATA ACQUISITION SYSTEM

A data acquisition system, operating at 240-Hz, was used to interpret signals from the instrumentation channels and to convert them into a digital format. It consisted of eight PXI chassis or nodes, each chassis was loaded with an embedded controller based on Windows XP running Lab View applications and eight SCXI-1520 signal conditioning modules. With this

configuration, each chassis had a total of sixty-four channels. All eight chasses were triggered to record simultaneously before the command signal was sent by the control system. Therefore, there is a time lag between the data acquisition system recordings and the control system feedback data.

7.8 CONTROL SYSTEM

Base excitation was applied using the NEES@UCSD shake table located at the Englekirk Structure Engineering Center. The 7.6 x 12.2 m (25 x 40 ft) shake table allowed testing of the column under a wide range of ground motions, starting with low-intensity shaking and bringing the column progressively towards near-collapse conditions. Its performance parameters such as peak velocity and acceleration, stroke and force capacity of actuators, maximum gravity payload and overturning moment, and frequency bandwidth, available from NEES@UCSD web site [NEES 2010], are summarized in Table 7.1. Table command and feedback data operated at a sampling rate of 256-Hz.

Table 7.1 Shake table capacities.

Test		Metric	US Customary
Platen dimensions		7.6 m x 12.2 m	25 ft x 40 ft
Peak acceleration	Bare table	4.2g	
	400 ton payload	1.2g	
Peak velocity		1.8 m/sec	70.9 in./sec
Stroke		±0.75 m	±29.5 in.
Payload capacity		20 MN	2,248 tons
Overturning moment capacity	Bare table	35 MN-m	25,816 kip-ft
	400 ton payload	50 MN-m	36,880 kip-ft
Frequency bandwidth		0-33 Hz	

8 Test Results

8.1 TEST EQ1

The objective of this test was to induce a displacement ductility of 1.0. The peak displacement achieved, defined as the magnitude of the maximum displacement in the East or West direction, was 62 mm (2.44 in.) corresponding to a 0.85% drift ratio and there was no plastic deformation. Figure 8.1 shows the displacement time history with initial, peak, and residual quantities indicated. The residual displacement was 1 mm (0.03 in.) or a 0.01% residual drift ratio. Figure 8.2 (a) and (b) show the East face of the column base at maximum displacement in the West and East directions, respectively.

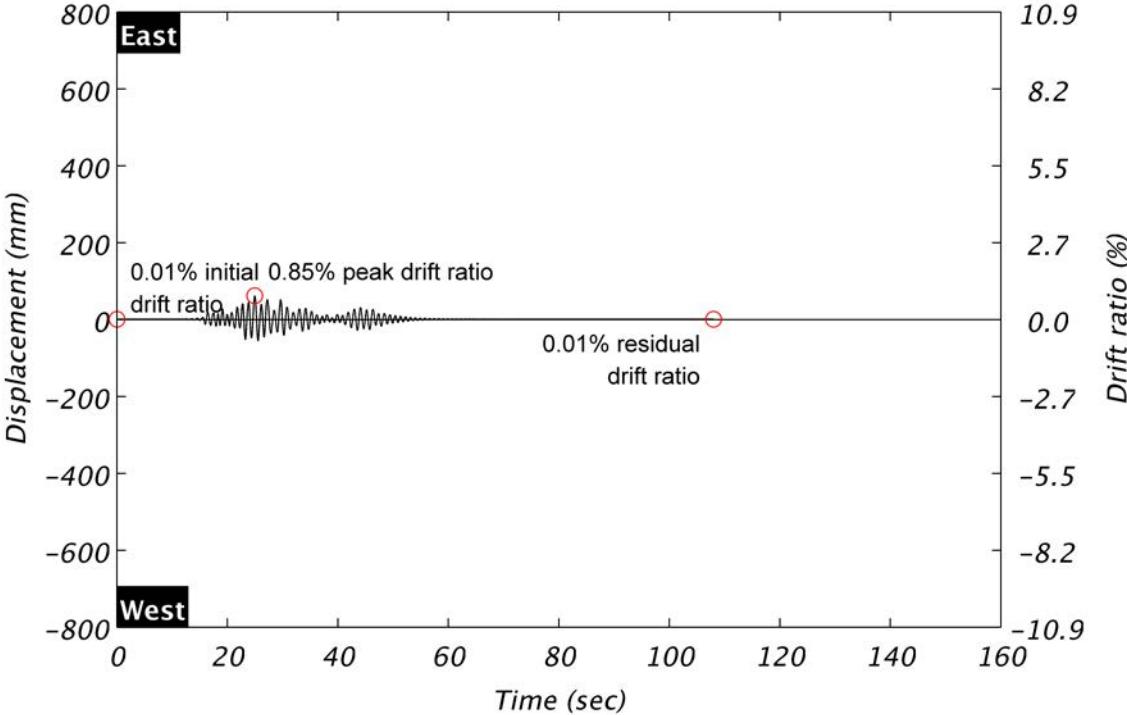


Figure 8.1 Column displacement during EQ1.

There was no observable damage in the column post-test. Hairline cracks, defined here as less than 0.1 mm (0.004-in), were found at the column to footing interface. The cracks were

discontinuous on the East and West sides of the column. No other cracks were observed in the test specimen. A post-test view of the East face of the column base is shown in Figure 8.2 (c).

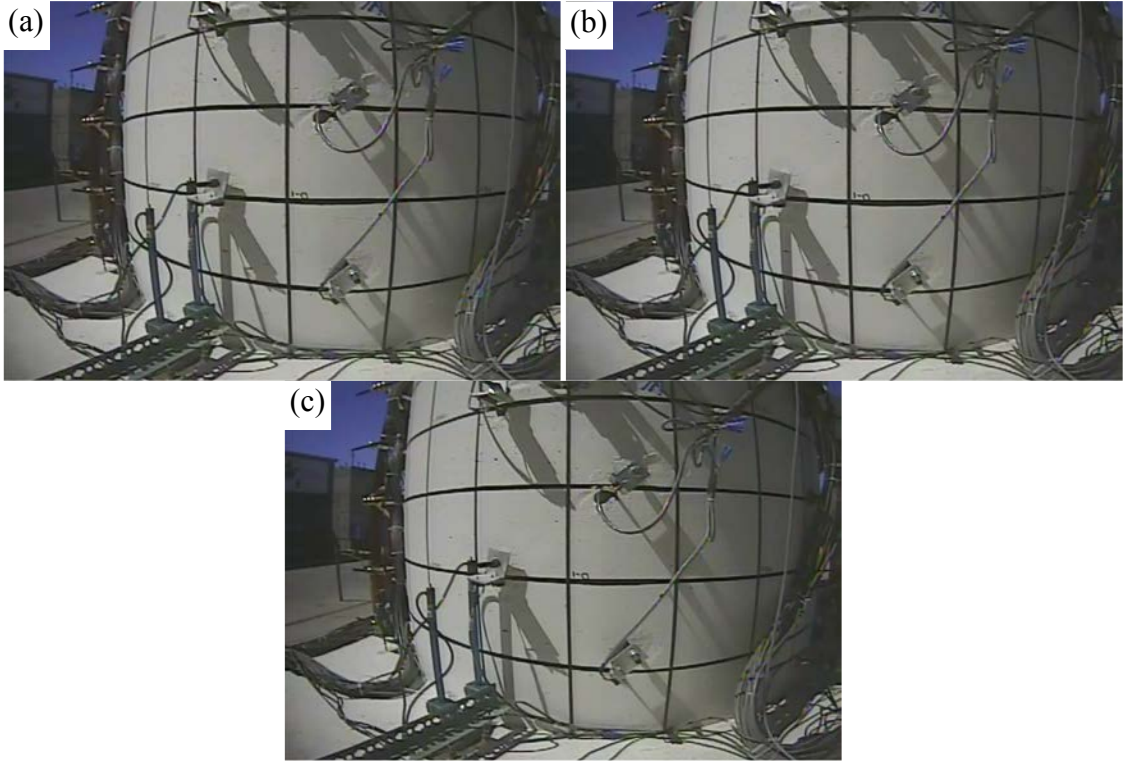


Figure 8.2 Column base East face during EQ1 at (a) peak West displacement, (b) peak East displacement, and (c) post-test.

An essentially linear elastic moment curvature response was obtained from the derived moment at the column base and the average curvature calculated near the column base, see Figure 8.3. The curvature was calculated over a 406 mm (16 in.) (1/3 column diameter) gauge length from 51 mm (2 in.) to 457 mm (18 in.) above the footing. The peak column base moment was 3,948 kN-m (2,912 kip-ft).

The idealized backbone curves shown in Figure 8.3 and Figure 8.4 are the monotonic response from the analytical tool developed in the ground motion selection process. The analytical prediction was significantly more stiff in terms of moment-curvature. For this reason, an experimental idealized curvature is defined as:

$$\varphi_{ye} = \frac{M_y}{EI_e} = 8.36 \times 10^{-3} \frac{rad}{m} \left(2.12 \times 10^{-4} \frac{rad}{in} \right)$$

where M_y is the nominal moment capacity and EI_e is the average of the secant slope to maximum and minimum moment-curvature response. This is the basis for defining curvature ductility throughout the test program.

Column base shear was derived from inertia forces in the superstructure block and column. The peak shear force was 500 kN (112.4 kip). The lateral shear force and displacement response shown in Figure 8.4 exhibits a linear elastic behavior. Better agreement was achieved

between analytical and experimental stiffness in terms of force-displacement response. The experimental idealized yield displacement, D_{ye} , is defined as:

$$\Delta_{ye} = \frac{V_y}{K_e} = 90 \text{ mm (3.54 in.)}$$

where V_y is the nominal shear capacity, and K_e is the average of the secant slope to maximum and minimum shear-displacement response. This is the basis for defining displacement ductility throughout the test program.

Localized yielding may have occurred in the longitudinal reinforcement. Peak recorded strains, averaged from pairs of strain gauges, reached 0.0022 mm/mm, see Figure 8.5. This corresponds to $0.85\epsilon_y$, where ϵ_y is the longitudinal yield strain of 0.0026 mm/mm obtained from material testing. Although localized yielding may have occurred outside of the monitored locations, a plastic hinge did not form. In addition to the average response, the corresponding individual gauge readings are shown with error bars in figures illustrating longitudinal strains. These are indistinguishable in Figure 8.5.

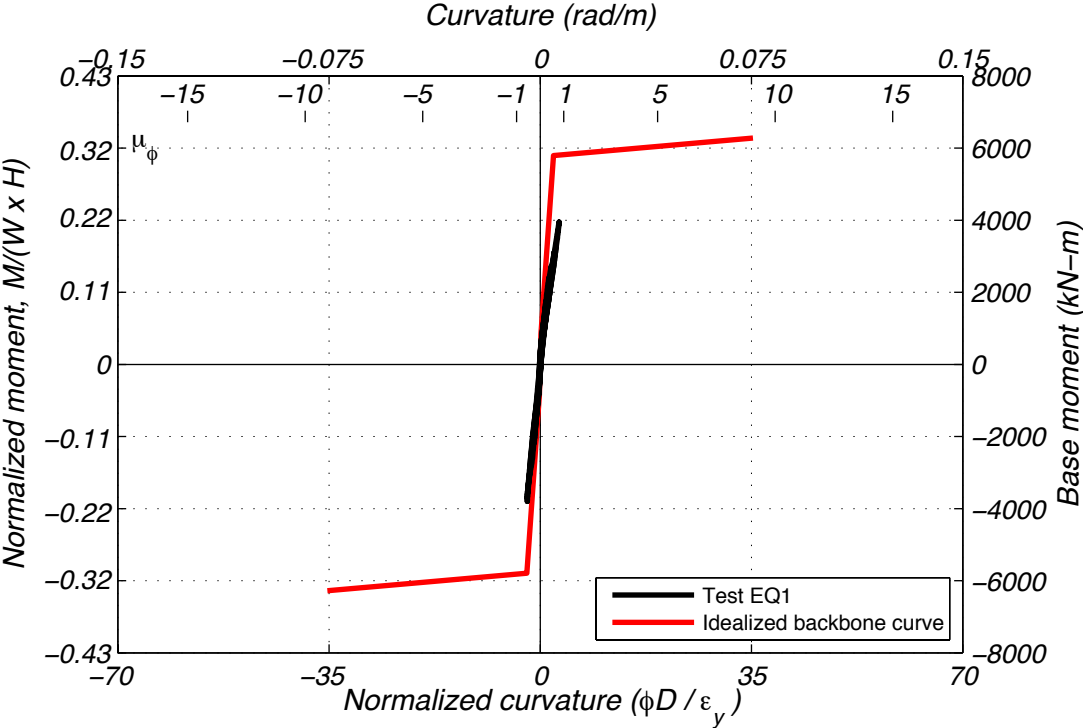


Figure 8.3 Column response during EQ1 in terms of base moment and curvature.

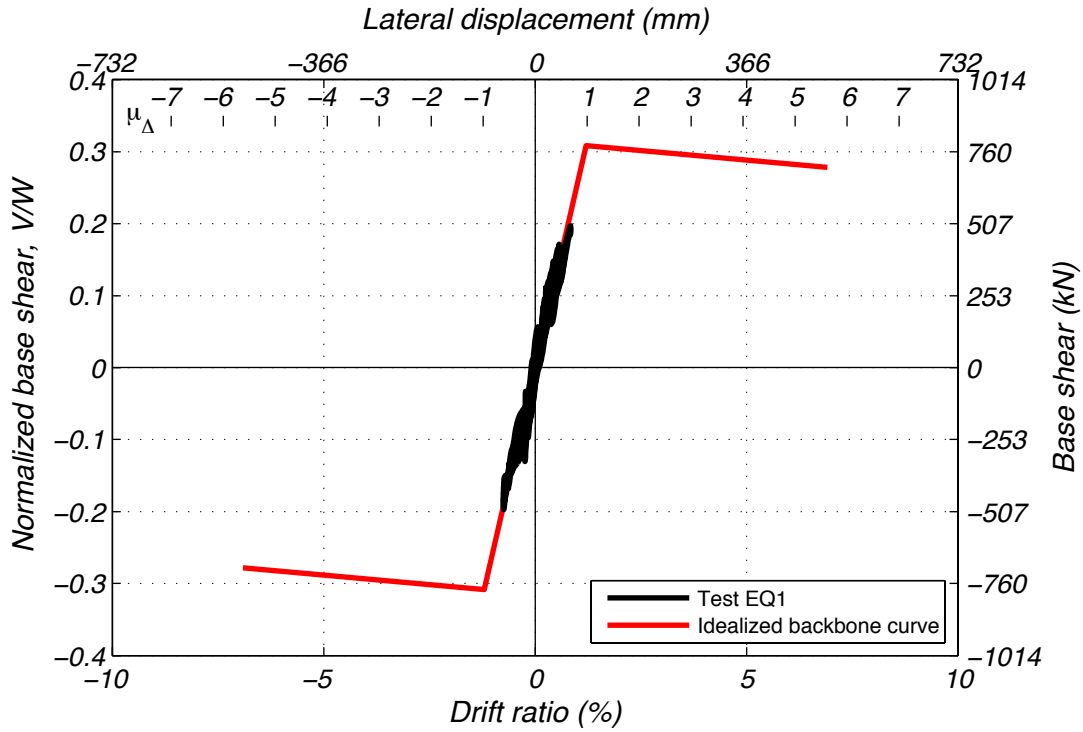


Figure 8.4 Column response during EQ1 in terms of base shear and drift ratio.

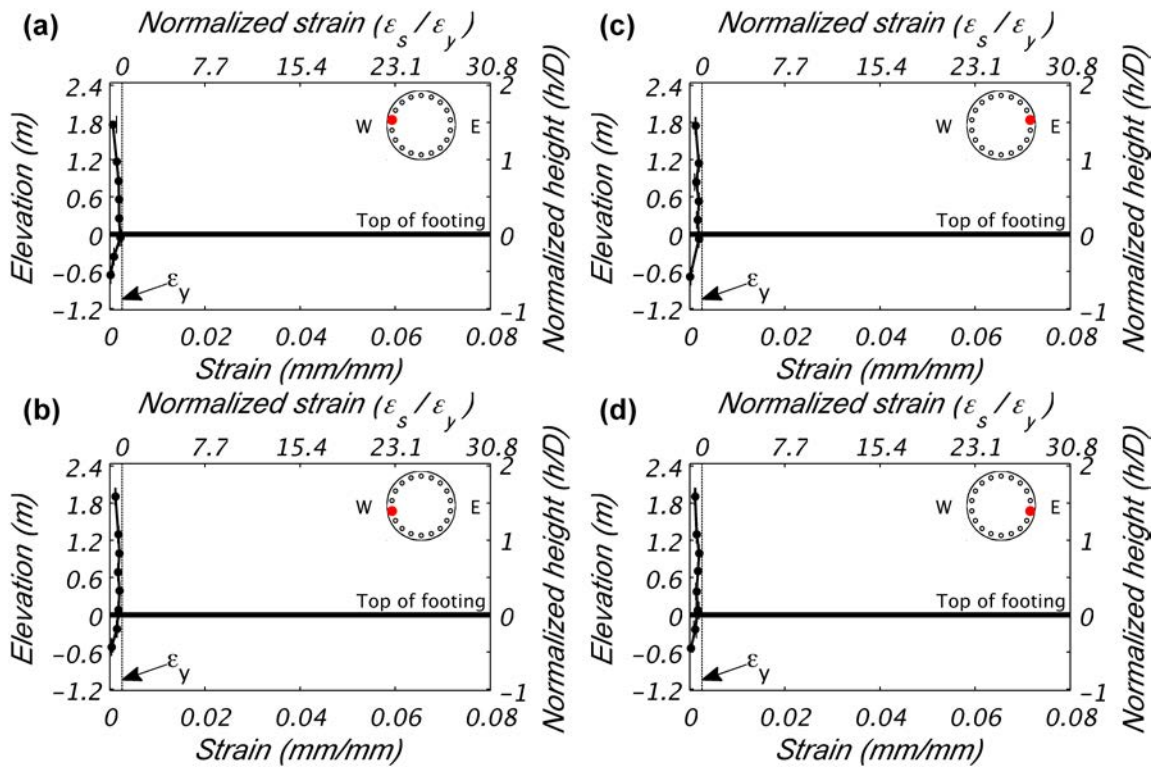


Figure 8.5 Longitudinal reinforcement tensile strain demand during EQ1.

Transverse hoop strains on the East and West faces of the column remained elastic. A single strain gauge was located on the outside of one of the bundled hoops on the East and West sides of the column. Figure 8.6 shows the maximum tensile values obtained in the instrumented hoops were larger on the West face with values approaching yield between 0.25 and 0.5 times the column diameter. Negligible strain increases were recorded on the East face.

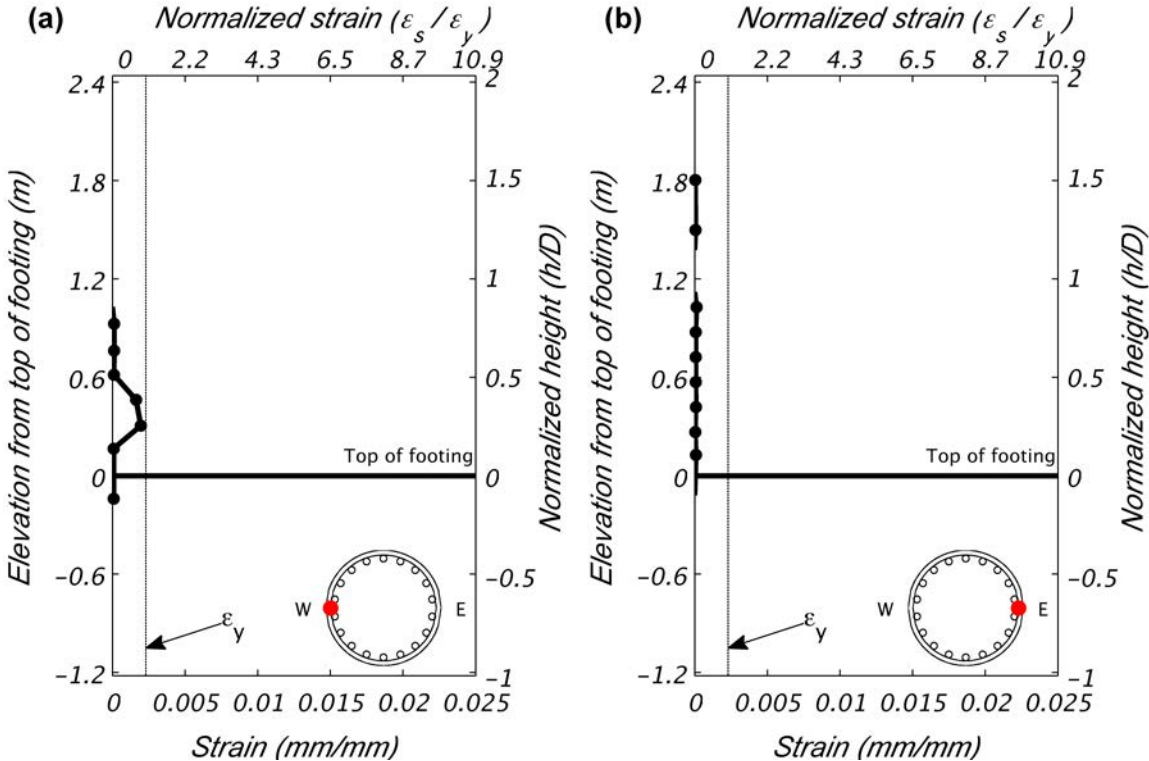


Figure 8.6 Transverse hoop reinforcement tensile strain demand during EQ1.

8.2 TEST EQ2

A displacement ductility of two was the target ductility for EQ2. The earthquake simulation produced a displacement ductility of 1.48 at the peak displacement of 133 mm (5.23 in.). This corresponds to a drift ratio of 1.82%. The residual displacement was a negligible 4 mm (0.16 in.) or 0.05% residual drift ratio. These values are indicated in the displacement time history of the top of the column in Figure 8.7. Figure 8.8 (a) and (b) show the East face of the column base at peak displacement in the West and East directions, respectively. A tensile crack is visible in Figure 8.8 (a) at approximately 10 in. above the footing. A post-test view of the East face of the column base is shown in Figure 8.8 (c). The video snapshot was taken before crack marking, so cracks are not visible in this figure.

Residual crack widths remained at hairline width after this test. Crack propagation occurred at the column to footing interface and additional cracks formed. Discontinuous hairline cracks spaced between 152 mm (6 in.) and 305 mm (12 in.) were found in the column from its

base to about 1.68 m (5.5 ft). Additional cracks were found between 3.91 m (12.5 ft) and 4.97 m (16.3 ft).

A nonlinear response was obtained in the moment-curvature relationship, see Figure 8.9. The peak column base moment was 5,896 kN-m (4,349 kip-ft), and peak shear force was 699 kN (157.3 kip). The lateral shear force and displacement response is shown in Figure 8.10.

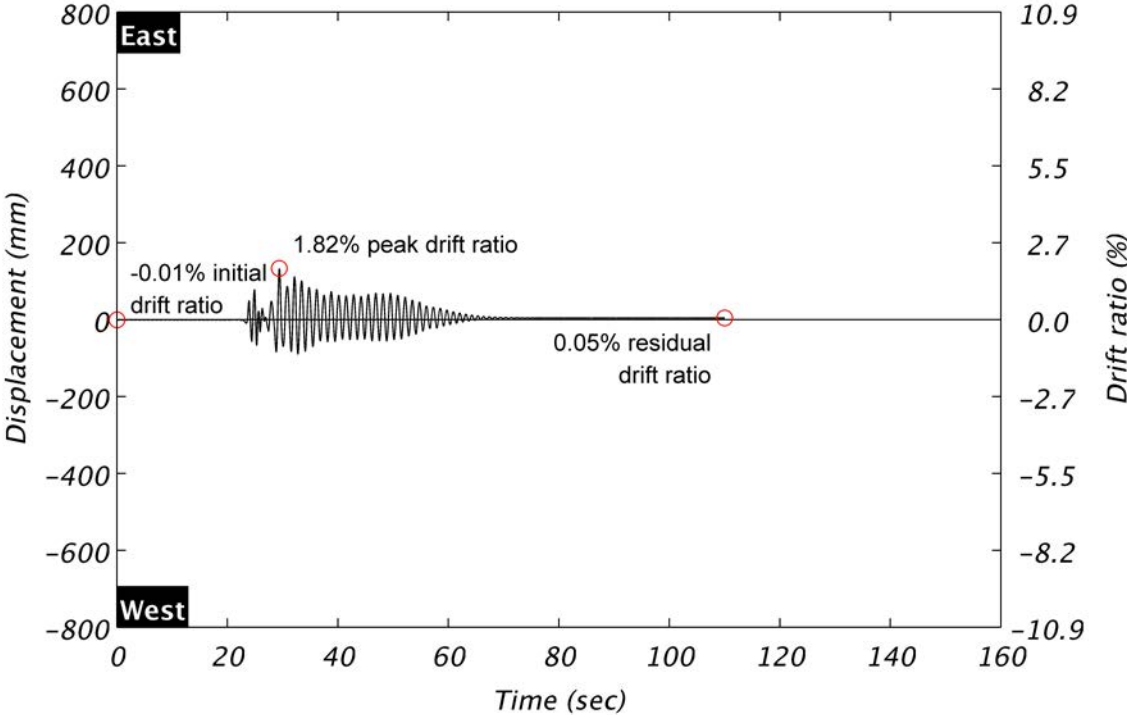


Figure 8.7 Column displacement during EQ2.

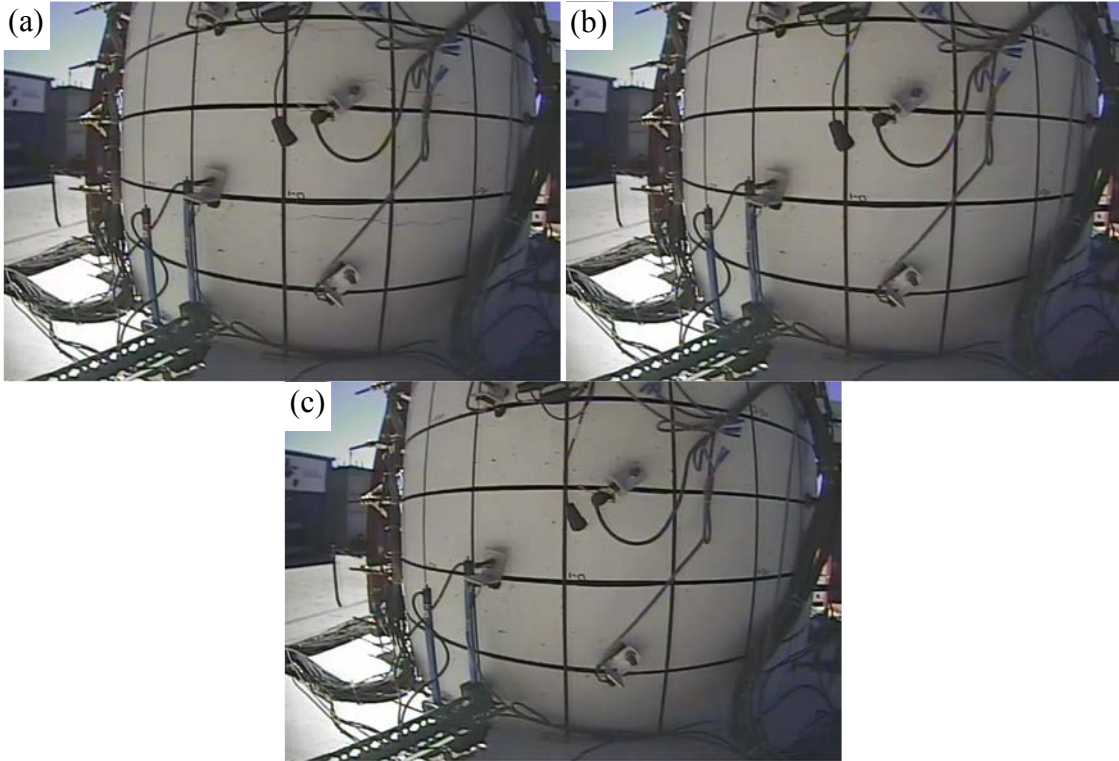


Figure 8.8 Column base East face during EQ2 at (a) peak West displacement, (b) East positive displacement, and (c) post-test.

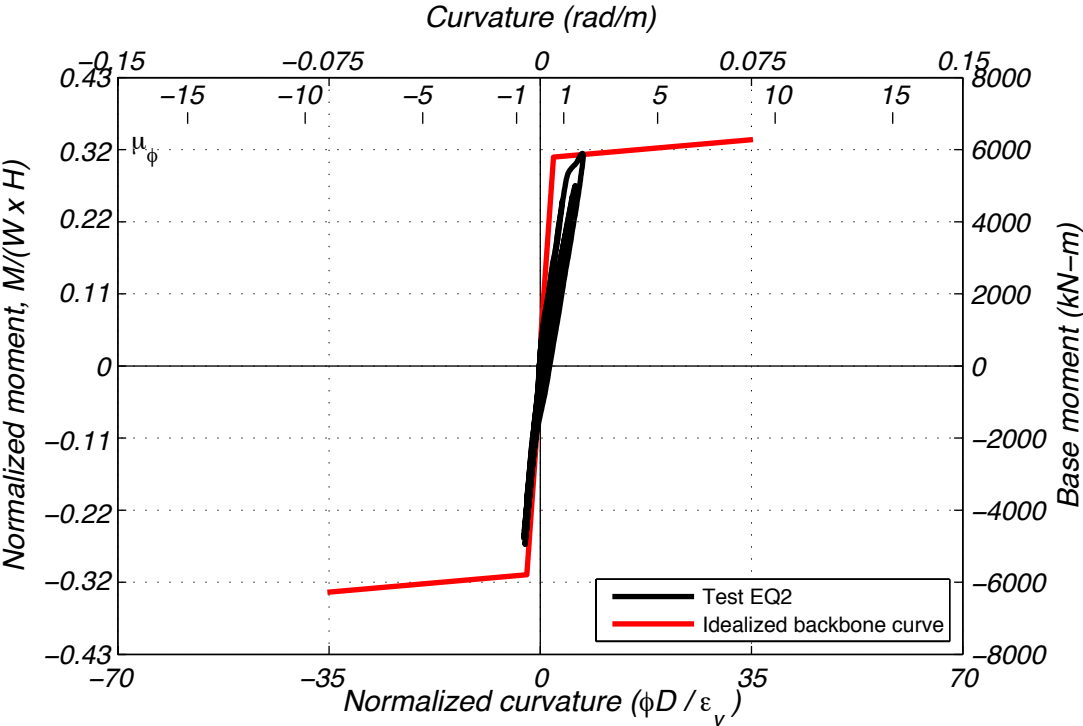


Figure 8.9 Column response during EQ2 in terms of base moment and curvature.

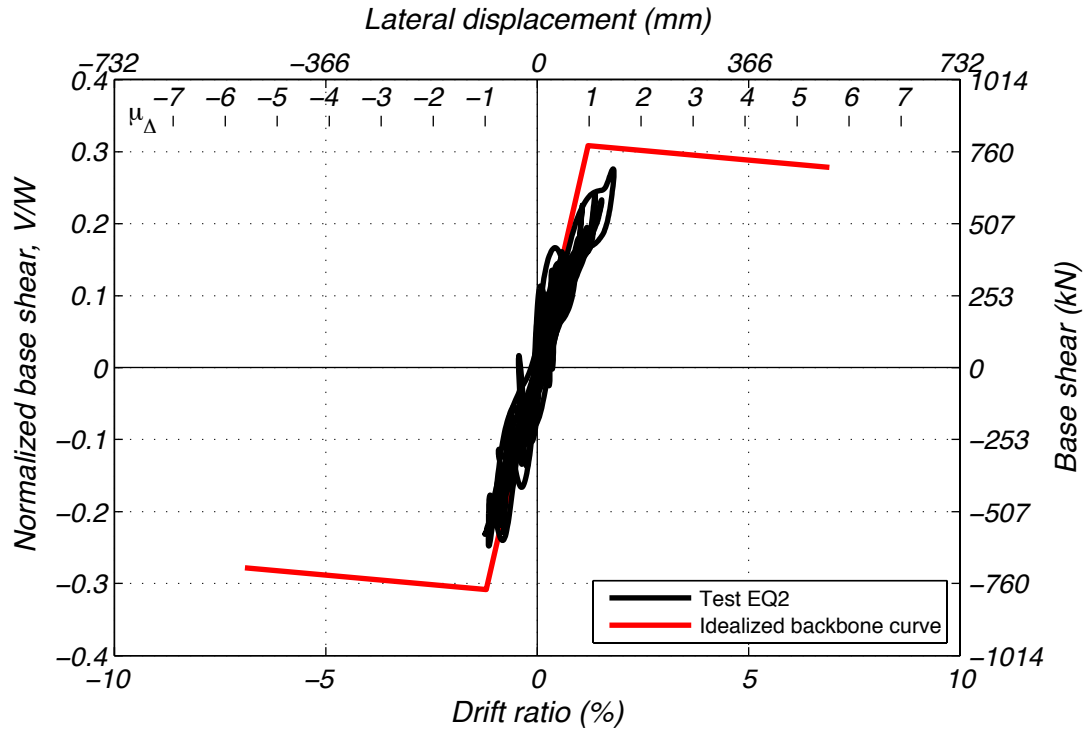


Figure 8.10 Column response during EQ2 in terms of base shear and drift ratio.

Localized yielding was measured by strain gauges near the column-to-footing interface, see Figure 8.11. Maximum tensile strain was 0.0132 mm/mm or $5.1\varepsilon_y$. All four instrumented bars achieved peak tensile strains on the order of yielding within one column diameter from the top of the footing. Although localized yielding occurred, a plastic hinge did not form. Transverse hoops strains also exceeded their yield strain at elevations between 0.25 and 0.5 times the column diameter on the West face, see Figure 8.12. Strains demands on the opposite face were minor.

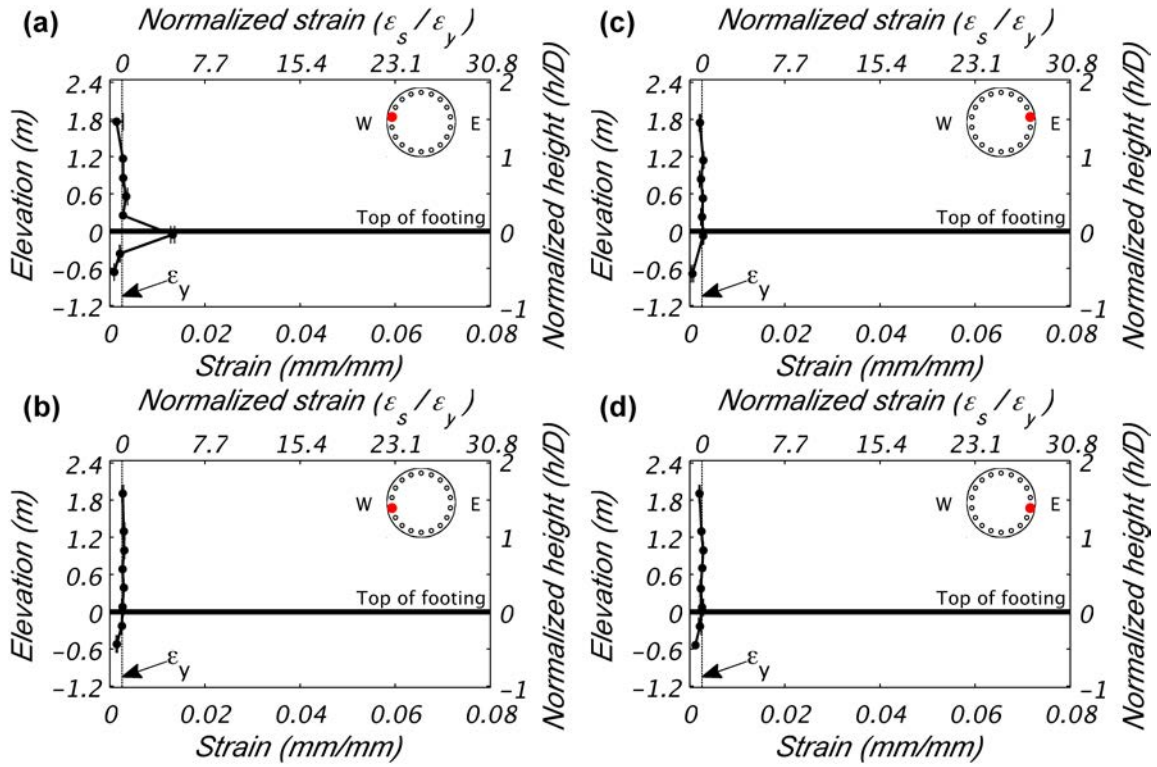


Figure 8.11 Longitudinal reinforcement tensile strain demand during EQ2.

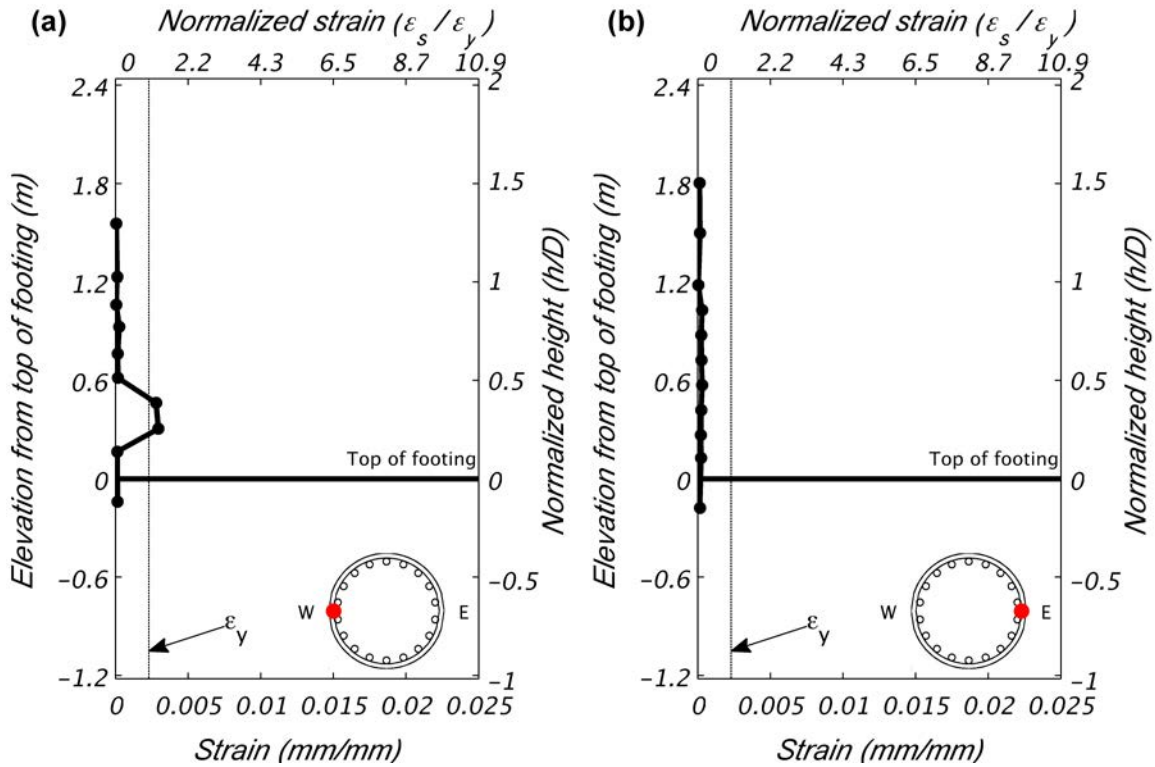


Figure 8.12 Transverse hoop reinforcement tensile strain demand during EQ2.

8.3 TEST EQ3

Test EQ3 represents a simulation of a design level earthquake. The target displacement ductility of four was achieved with only cosmetic damage. A peak displacement of 361 mm (14.20 in.) was measured at the top of the column. This corresponds to a displacement ductility of 4.01 or a drift ratio of 4.93%. A residual drift ratio of -0.87% or -63mm (-2.49 in.) resulted from the nonlinear response. These values are indicated in the displacement time history of Figure 8.13. This was the first instance of a residual drift. Figure 8.14 (a) and (b) show the East face of the column base at peak displacement in the West and East directions, respectively.

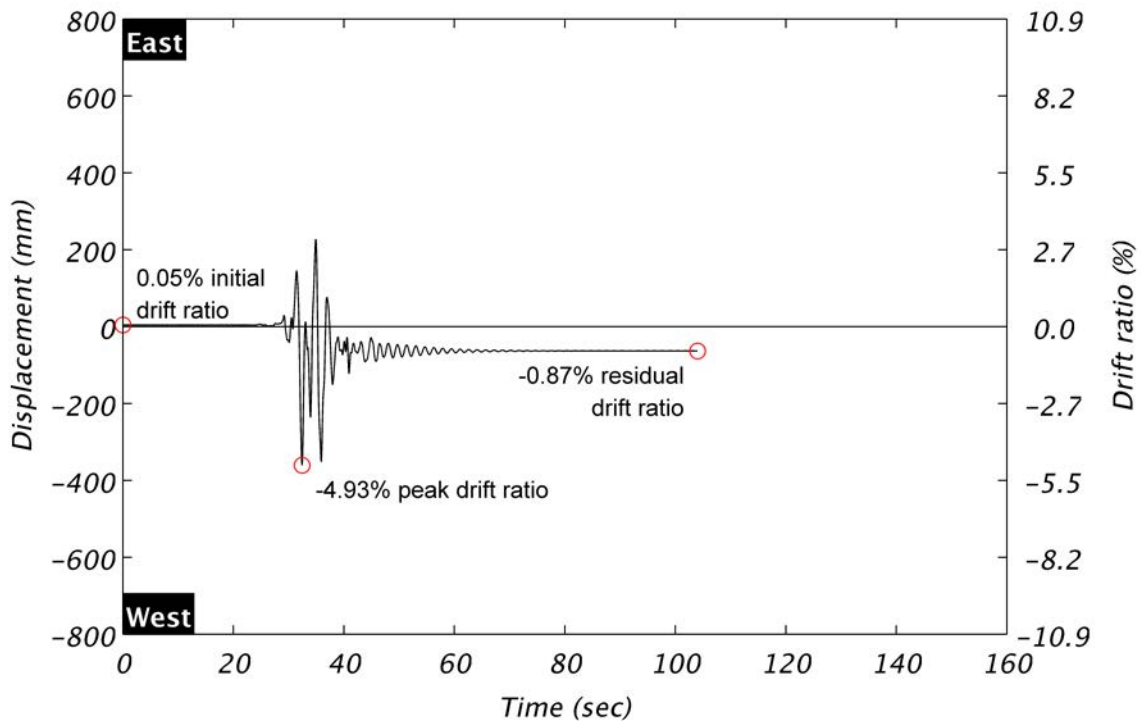


Figure 8.13 Column displacement during EQ3.

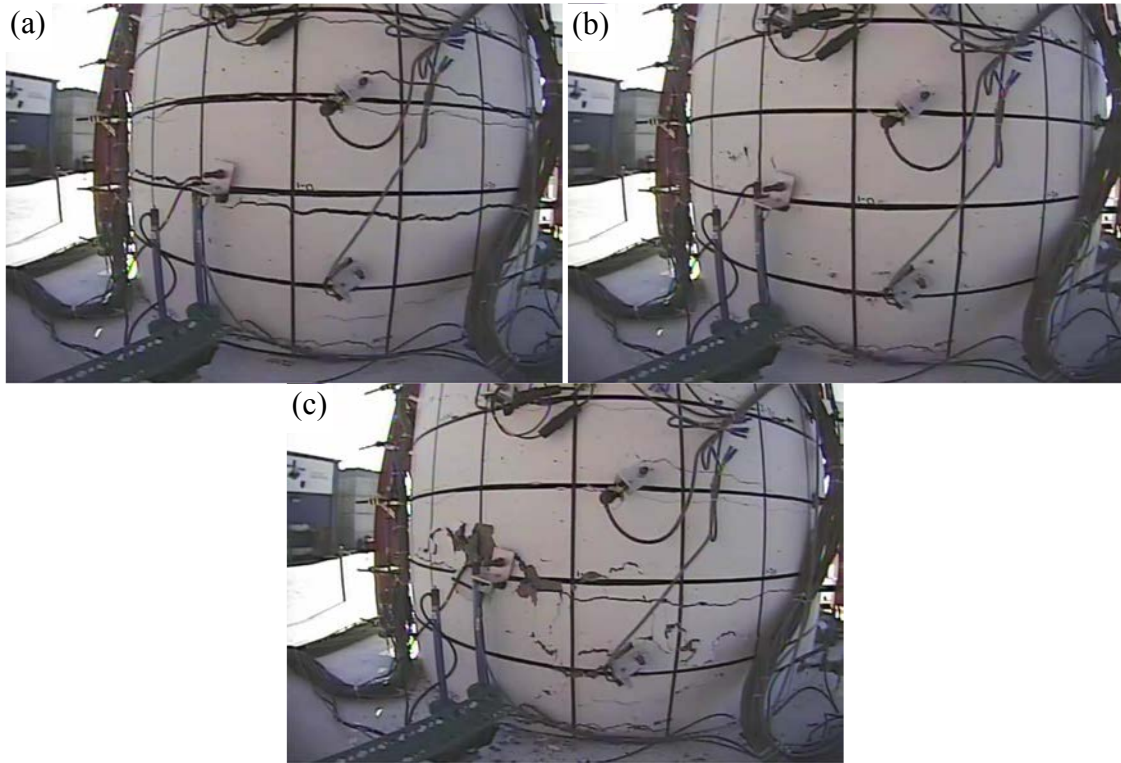


Figure 8.14 Column base East face during EQ3 at (a) peak West displacement, (b) peak East displacement, and (c) post-test.

Spalling of the concrete cover was initiated at this level of testing. Spalling occurred on the West face of the column, shown in Figure 8.15. The maximum residual crack width near the base of the column was 1.4 mm (0.055 in.). Significant cracking developed at the base of the column; see the post-test views of the East and West column faces in Figure 8.14(c) and Figure 8.15, respectively. The snapshot in this figure was taken before cracks had been marked, but the crack pattern and concrete flaking are visible.



Figure 8.15 Column base West face after test EQ3.

Significant nonlinearity was obtained in the moment-curvature response, see Figure 8.16. The peak column base moment was 6,594 kN-m (4,864 kip-ft). The peak shear force was 888 kN (199.6 kip). This was the largest shear force obtained in any of the tests. The lateral shear force and displacement response is shown in Figure 8.17. Contributions from a higher mode are evident in this figure.

Significant yielding was captured by strain gauges on all four instrumented longitudinal bars, see Figure 8.18. This occurred within one column diameter from the footing interface. The maximum tensile strain was 0.0298 mm/mm or $11.5\epsilon_y$. In this test, gauge pairs began to exhibit variation as evident in the error bars at some locations. Strain penetration into the footing is apparent, but demands were below yield at a depth below the footing of $\frac{1}{2}D$ or $17d_b$.

Peak transverse strain demands on the West face were consistent with demands from the prior test. Only two hoops on the West face of the column exceeded yield, see Figure 8.19. Hoop demands elsewhere increased, but were below yield. Despite modest transverse strain demand increases, the plastic hinge was fully formed as evident in the nonlinear moment and shear responses, longitudinal strain demands, and observed damage.

A residual displacement after test EQ3 denotes that target displacement ductilities are not relevant to subsequent tests. Target displacement ductilities used in the ground motion selection process were based on cracked section properties and zero initial displacement. No attempts were made to straighten or repair the column between tests.

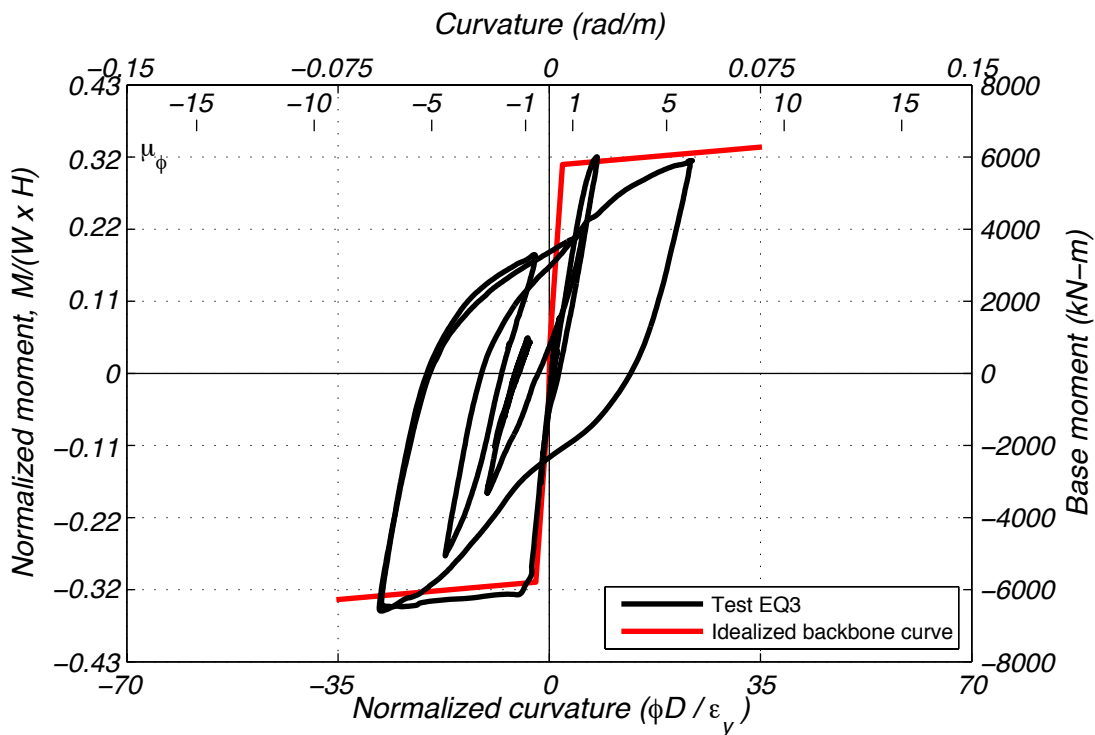


Figure 8.16 Column response during EQ3 in terms of base moment and curvature.

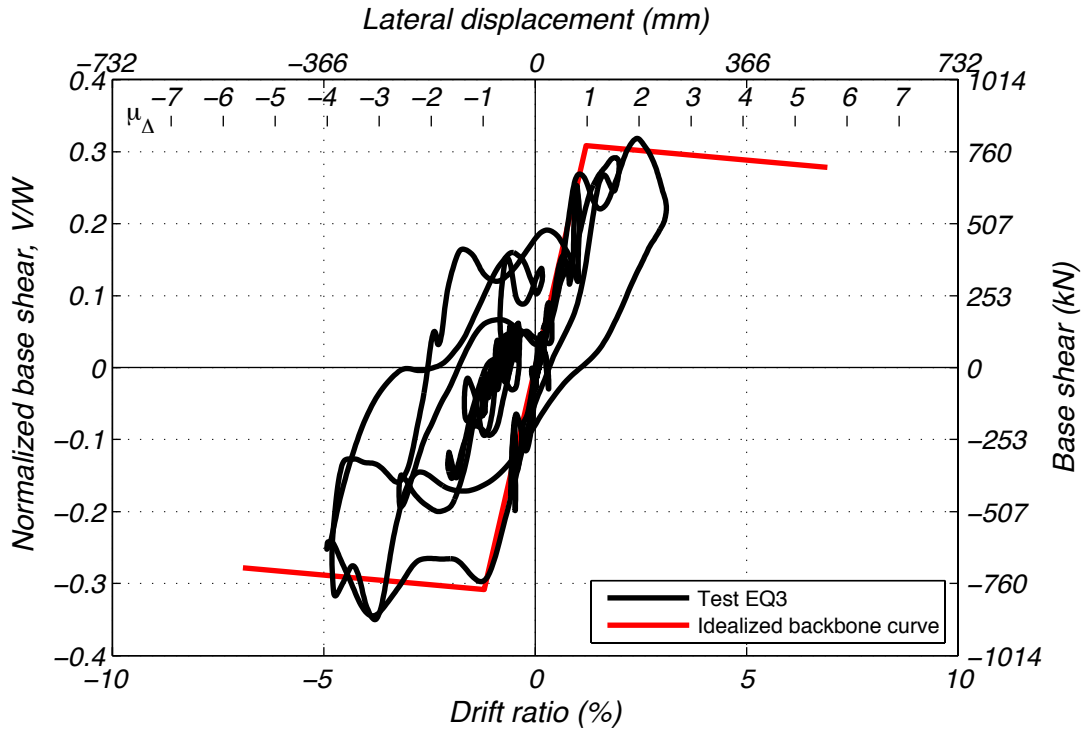


Figure 8.17 Column response during EQ3 in terms of base shear and drift ratio.

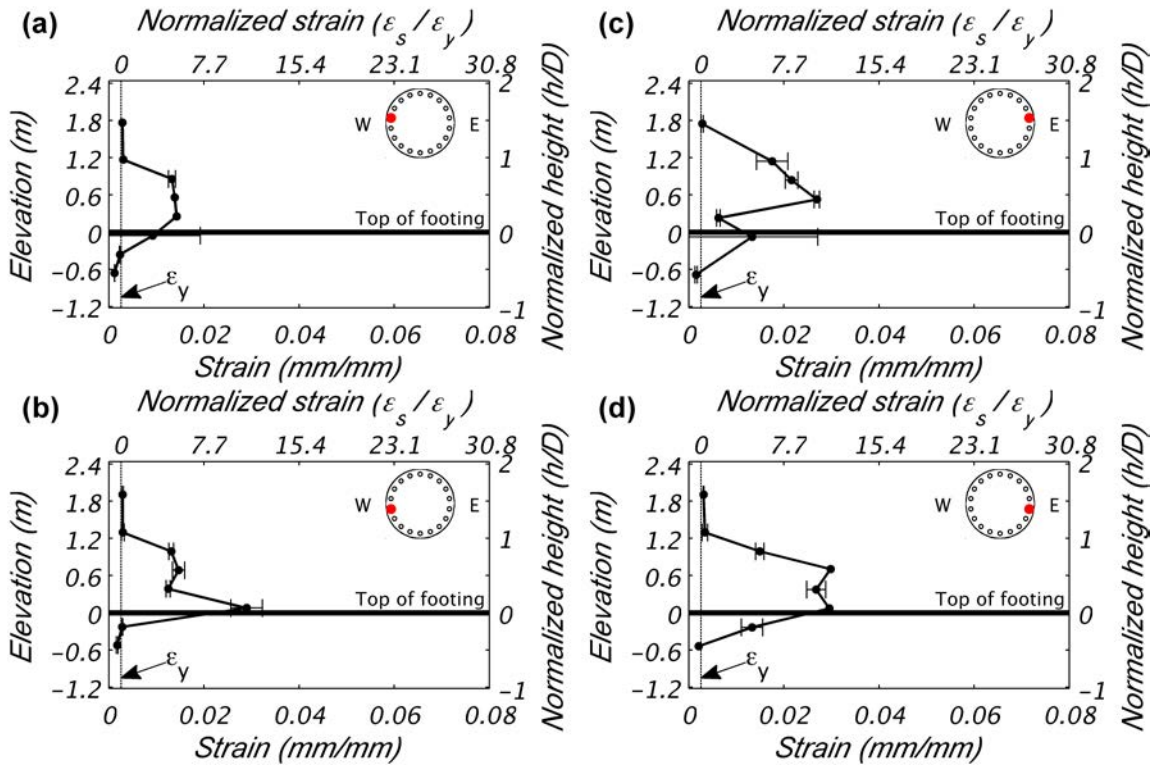


Figure 8.18 Longitudinal reinforcement tensile strain demand during EQ3.

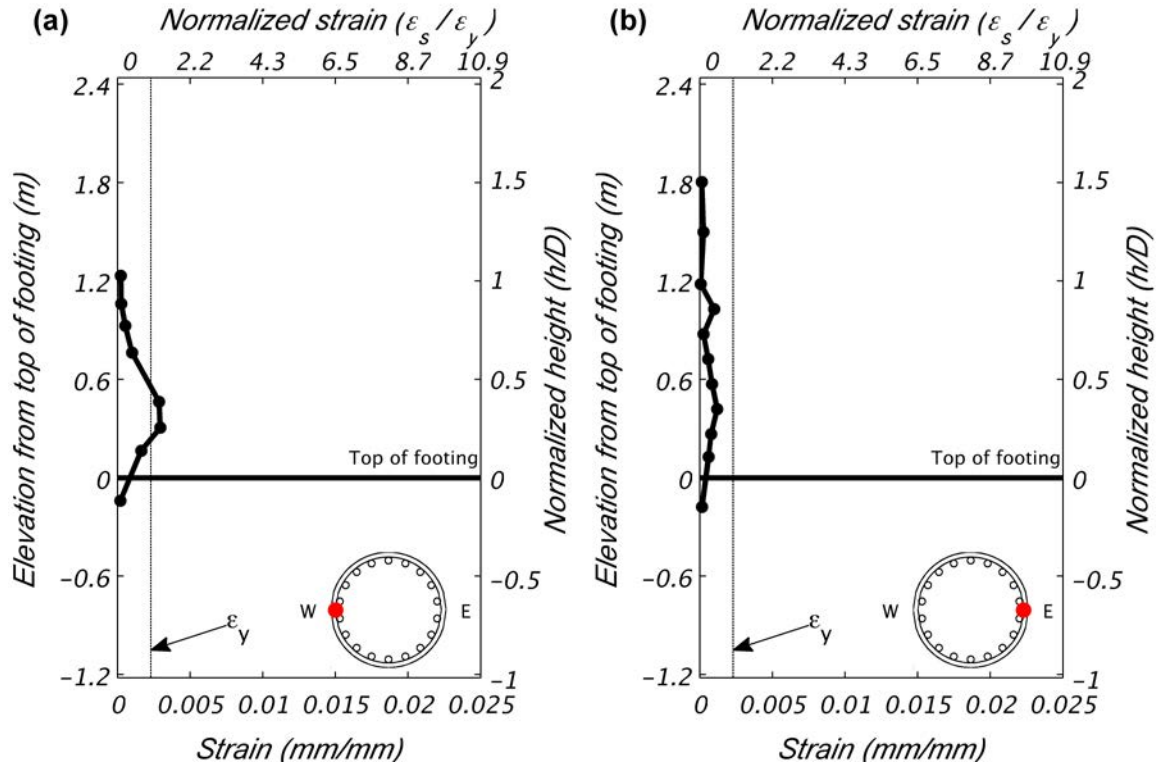


Figure 8.19 Transverse hoop reinforcement tensile strain demand during EQ3.

8.4 TEST EQ4

Test EQ4 simulated an aftershock to the design level event of EQ3. A residual displacement from the prior test remained as an initial offset. The aftershock simulation achieved a peak displacement of 170 mm (6.71 in.) or 2.33% drift ratio. A residual displacement, consistent with the residual from the prior test, of -59 mm (-2.33 in.) remained post-test. The displacement time history of the top of the column is shown in Figure 8.20. The input motion was the same as EQ2.

Figure 8.21 (a) and (b) show the East face of the column base at peak displacement in the West and East directions, respectively. Residual cracks were not marked post-test due to testing time constraints. Regions with spalling caused by test EQ3 enlarged, but damage was less significant than that induced by EQ3. A post-test view of the East face of the column base is shown in Figure 8.21 (c).

A nearly linear response was obtained in terms of moment-curvature, see Figure 8.22. This curve is offset along the curvature axis due to the residual deformation of EQ3. The peak column base moment was 3,745 kN-m (2,762 kip-ft). The peak shear force was 401 kN (90.2 kip). The lateral shear force and displacement response is shown in Figure 8.23. This figure also shows an offset along its horizontal axis and contains contributions from a higher mode.

Strain gauges on longitudinal reinforcement measured a maximum tensile strain of 0.0144 mm/mm or $5.5\epsilon_y$, see Figure 8.24. These strains were largely influenced by the residual from the prior test. Demands in this test were on the order of 0.005 mm/mm above the prior

residual. Figure 8.25 shows transverse strain demands were below yield with larger demands on the West face where spalling initiated in the prior test.

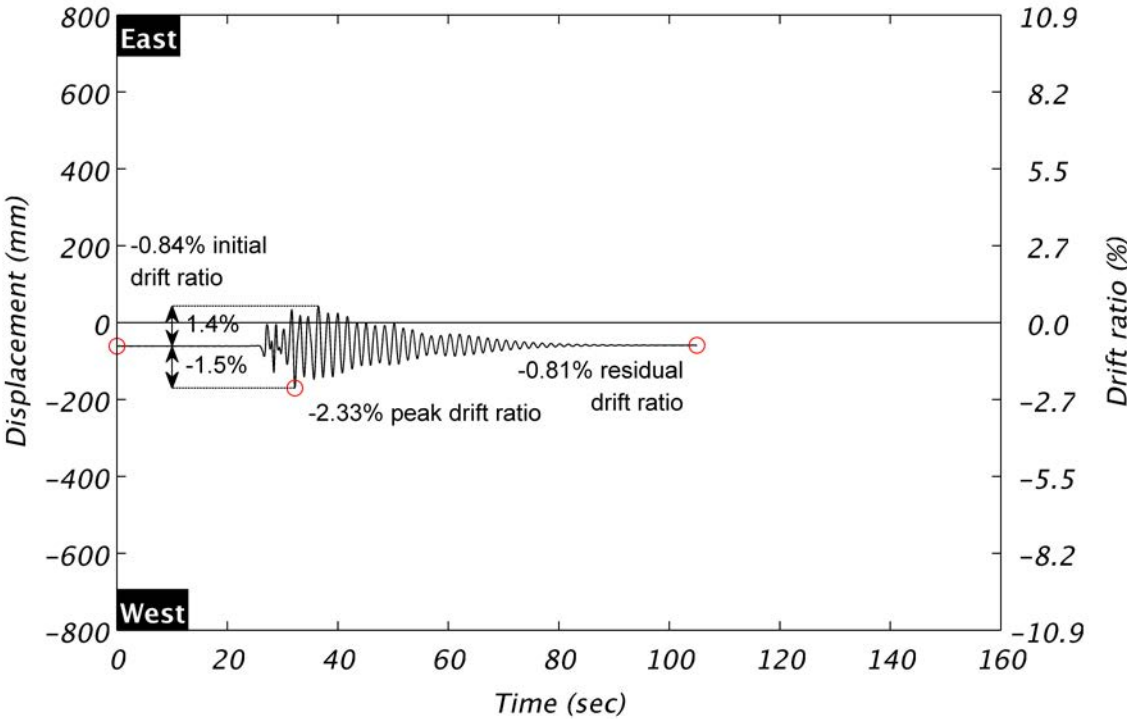


Figure 8.20 Column displacement during EQ4.

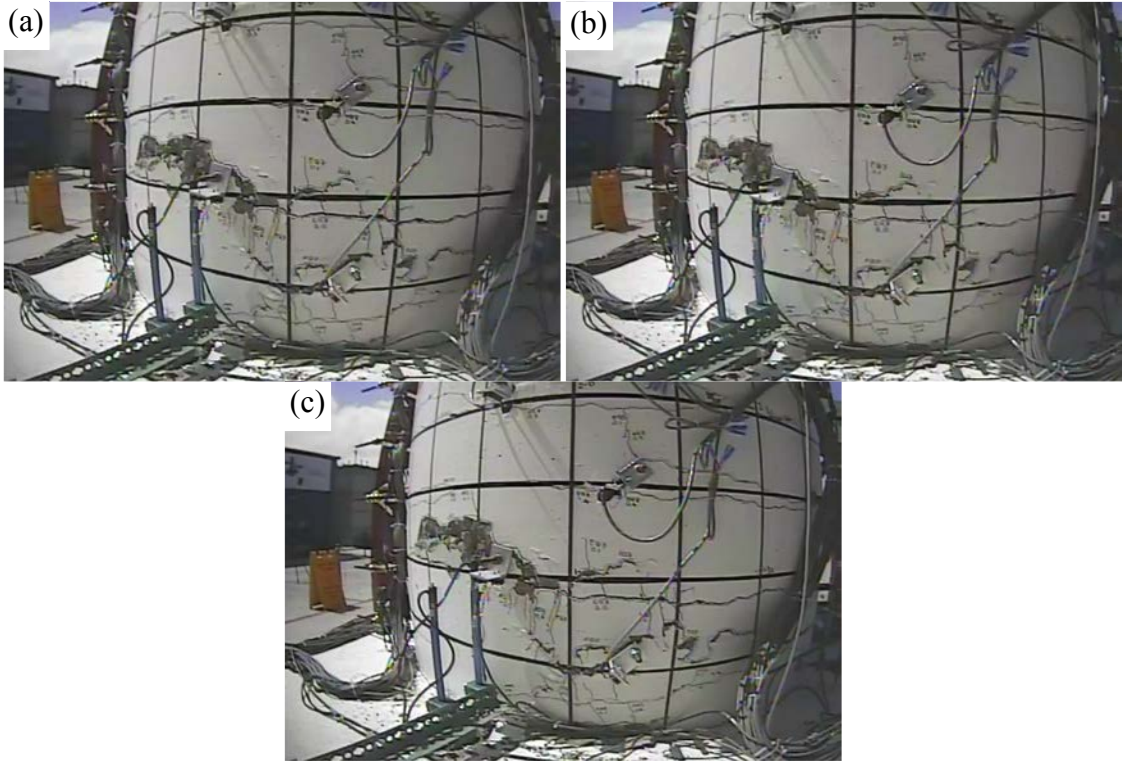


Figure 8.21 Column base East face during EQ4 at (a) peak West displacement, (b) peak East displacement, and (c) post-test.

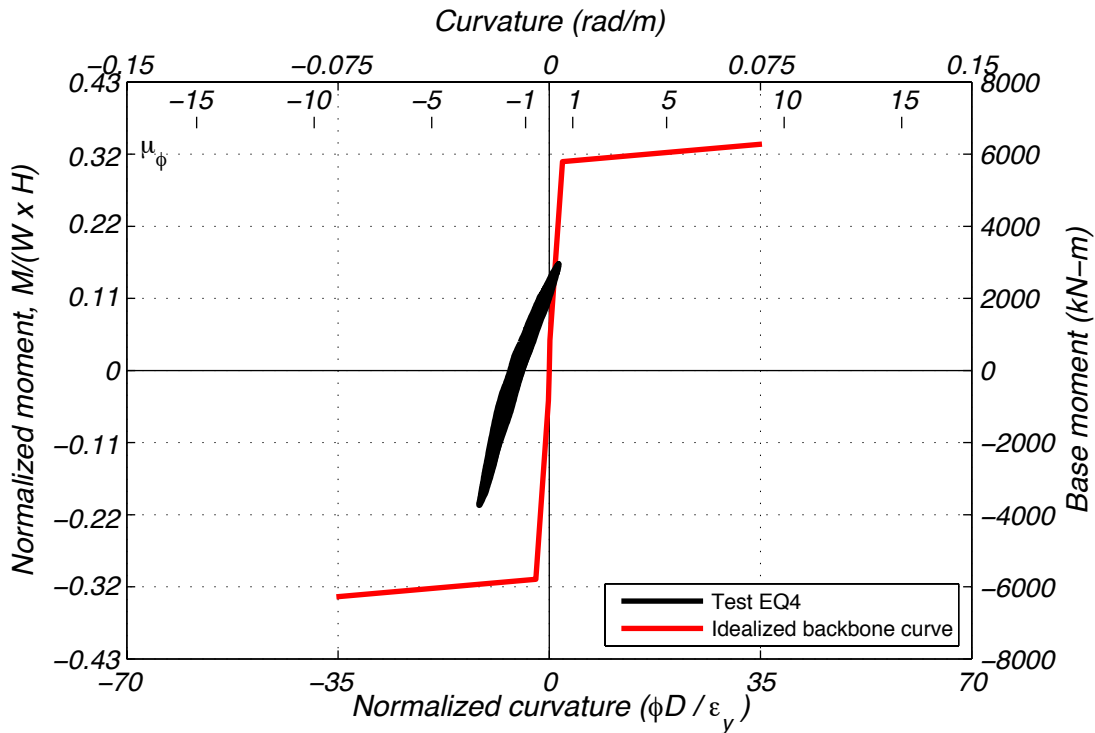


Figure 8.22 Column response during EQ4 in terms of base moment and curvature.

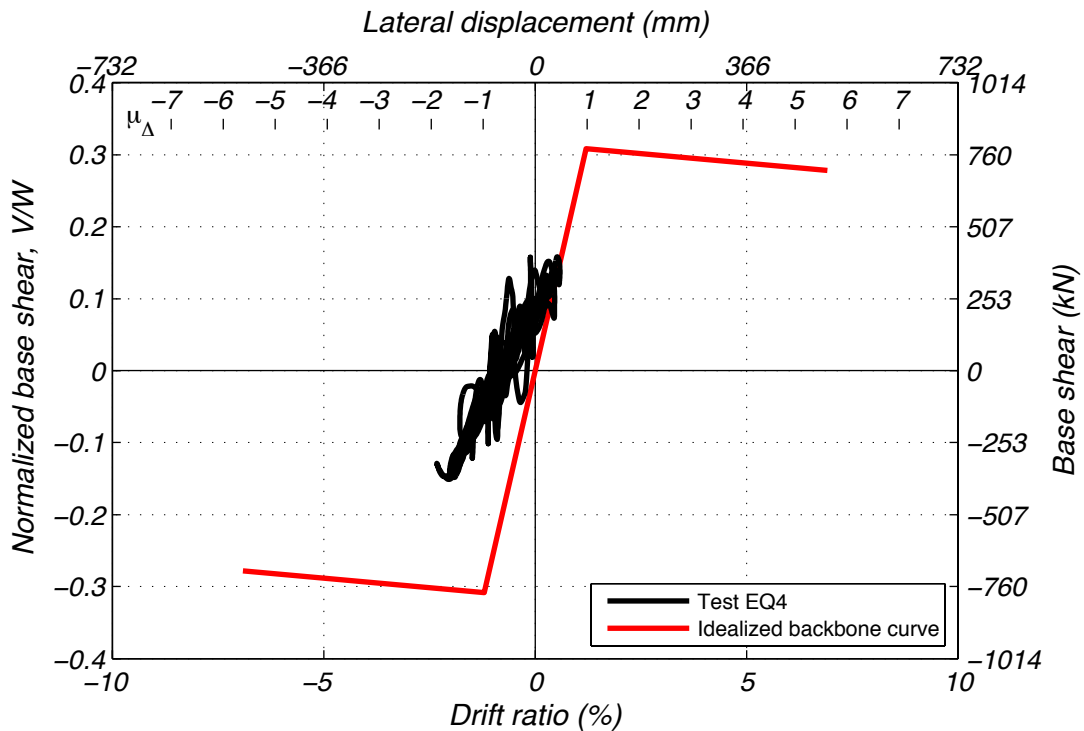


Figure 8.23 Column response during EQ4 in terms of base shear and drift ratio.

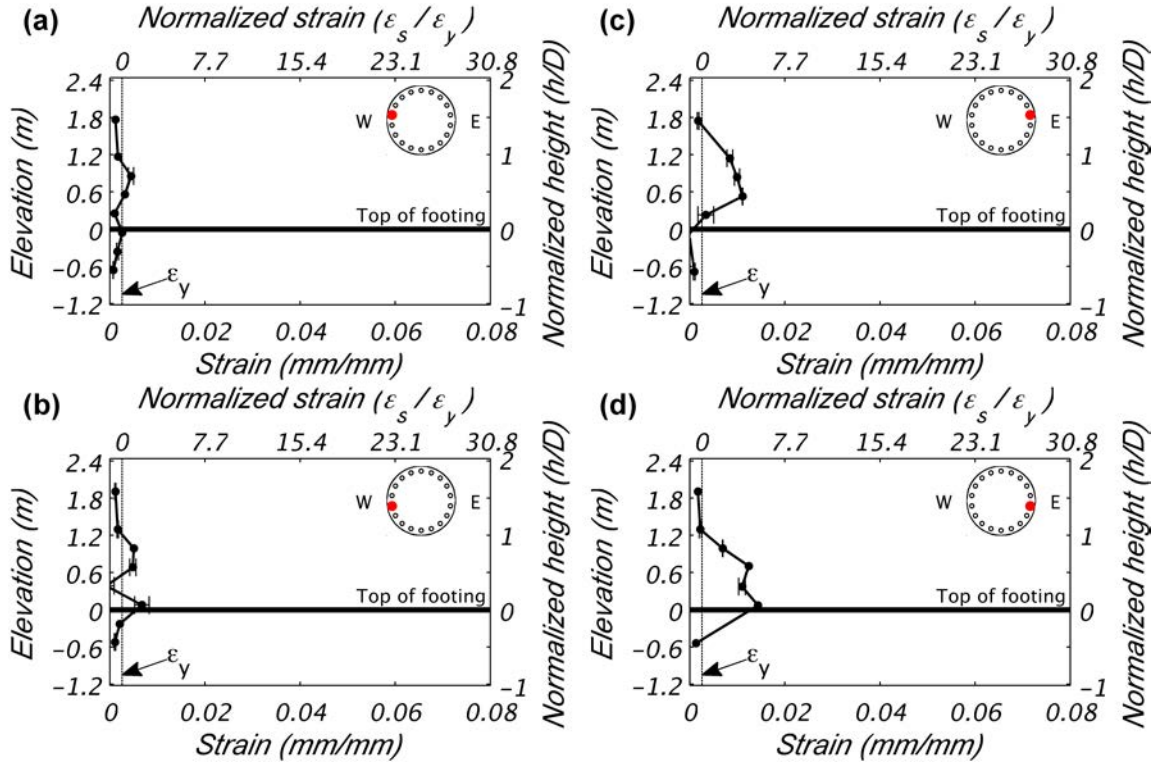


Figure 8.24 Longitudinal reinforcement tensile strain demand during EQ4.

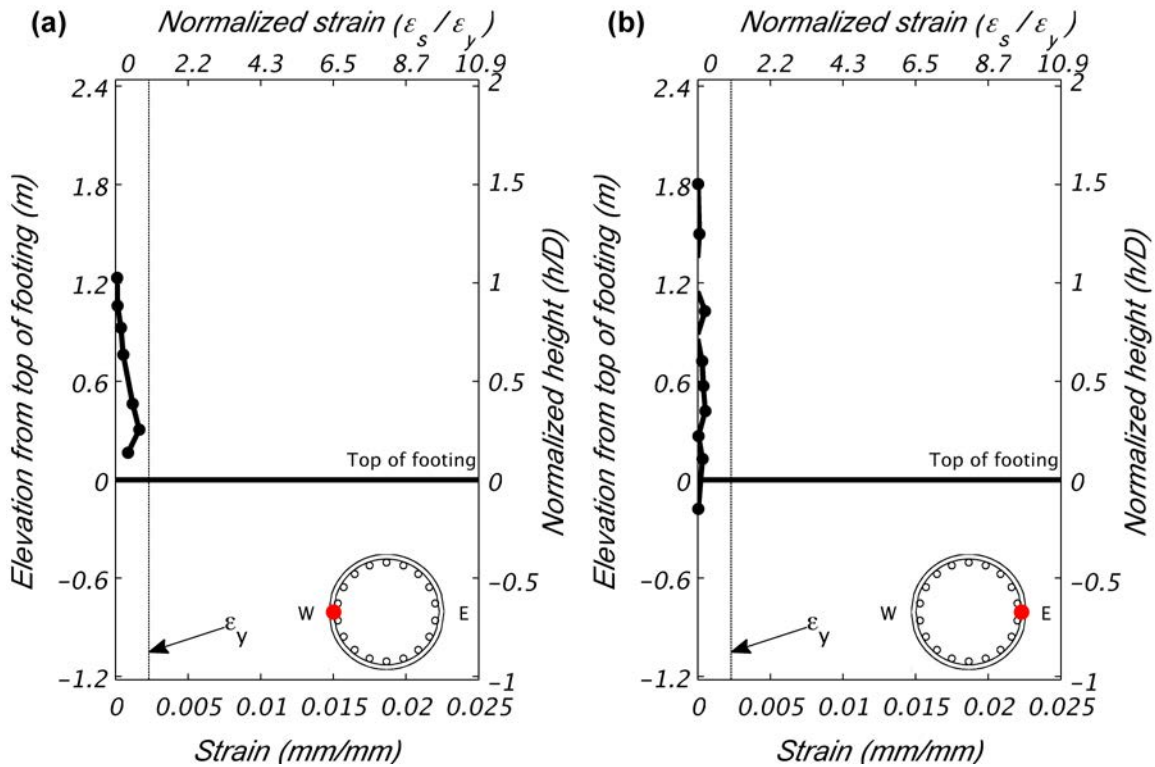


Figure 8.25 Transverse hoop reinforcement tensile strain demand during EQ4.

8.5 TEST EQ5

A peak displacement of 569 mm (22.40 in.) or 7.78% drift ratio was achieved. Displacement ductility at this peak displacement was 6.32. The residual displacement was 104 mm (4.11 in.) corresponding to 1.43% residual drift ratio, see Figure 8.26. The peak and residual drift ratios were to the East, which was opposite the initial drift ratio. Figure 8.27 (a) and (b) show the East face of the column base at peak displacement in the West and East directions, respectively.

Continued concrete spalling occurred and extended to 1.07 m (3.5 ft) above the column base. A post-test view of the East face of the column base is shown in Figure 8.27 (c). Concrete spalling is evident in this figure to a height of 0.76 m (2.5 ft), or 0.625 column diameters.

The peak column base moment was 7,241 kN-m (5,341 kip-ft), which was the second largest demand of any test. The moment-curvature response is shown in Figure 8.28. Large, stable hysteretic loops are evident. The peak shear force was 811 kN (182.5 kip). The lateral shear force-displacement response is shown in Figure 8.29.

The peak longitudinal strain measured was 0.0466 mm/mm, see Figure 8.30. Error bars at gauge elevation indicate that two strain gauges provided reliable measurements with their measurements indicated by the error bars. The absence of error bars means that only one gauge was reliable, and the absence of a solid black circle means neither gauge was viable during the test. Figure 8.31 illustrates the large demands placed on transverse reinforcement in this test. The 0.025 mm/mm demand on the West face was the largest of any test. However, nonlinear demands were all within 0.76 m (30 in.) or 0.63D from the column base.

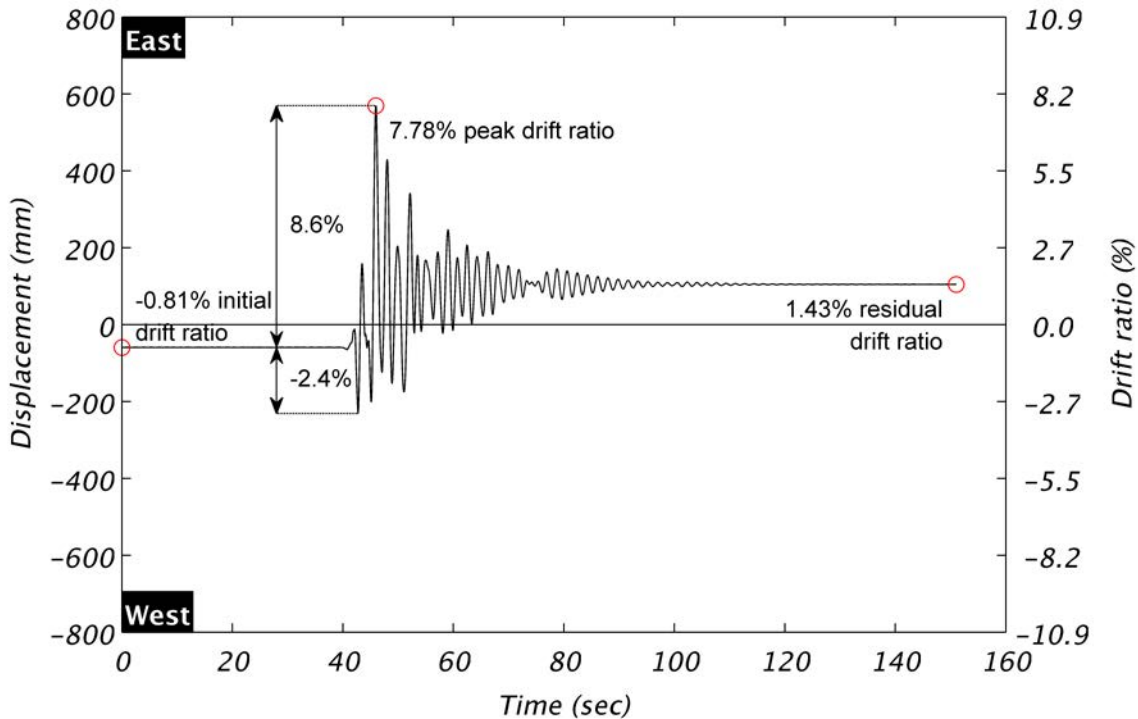


Figure 8.26 Column displacement during EQ5.

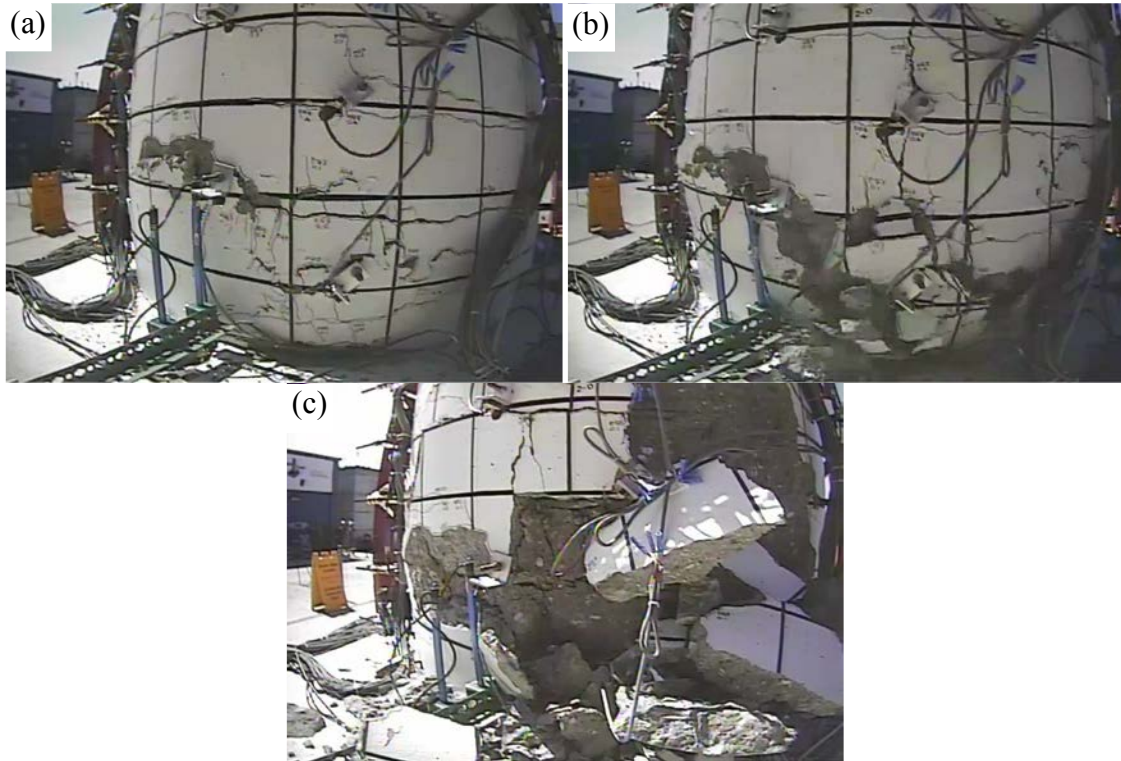


Figure 8.27 Column base East face during EQ5 at (a) peak West displacement, (b) peak East displacement, and (c) post-test.

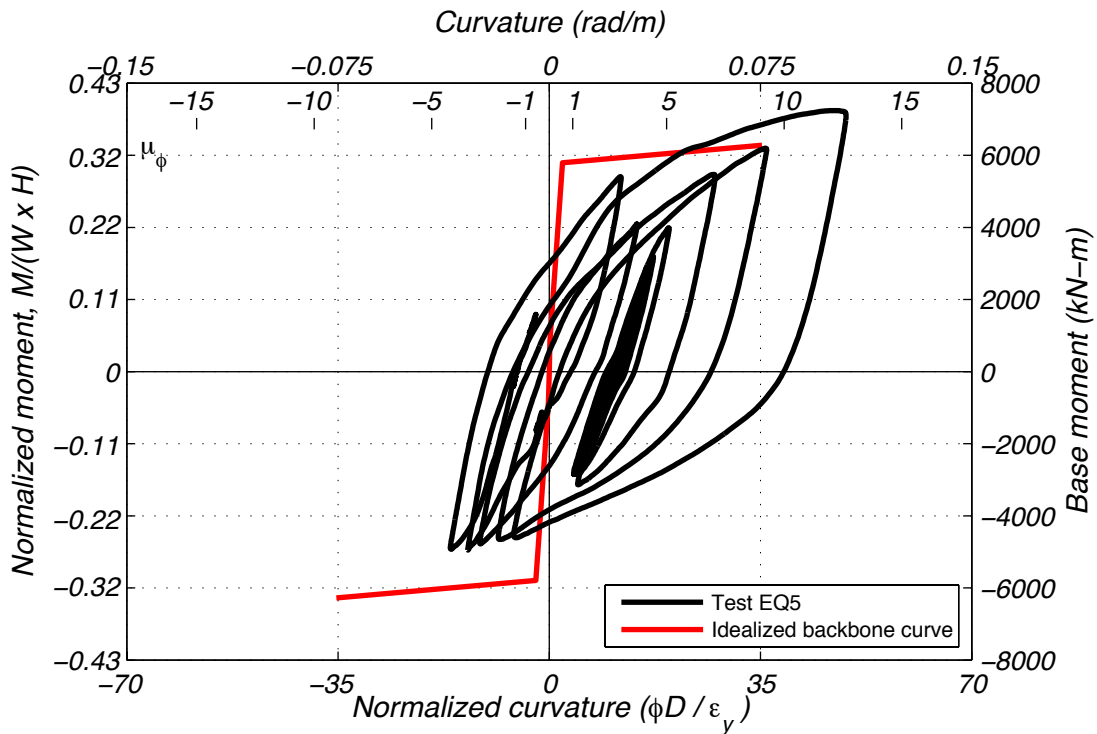


Figure 8.28 Column response during EQ5 in terms of base moment and curvature.

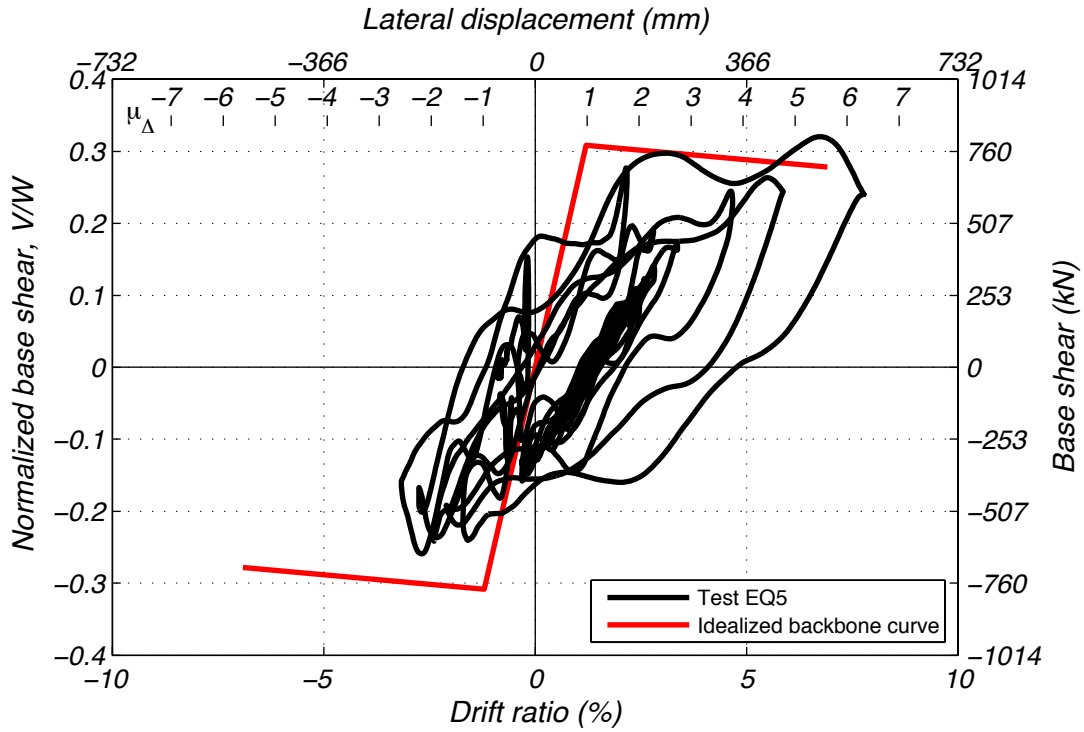


Figure 8.29 Column response during EQ5 in terms of base shear and drift ratio.

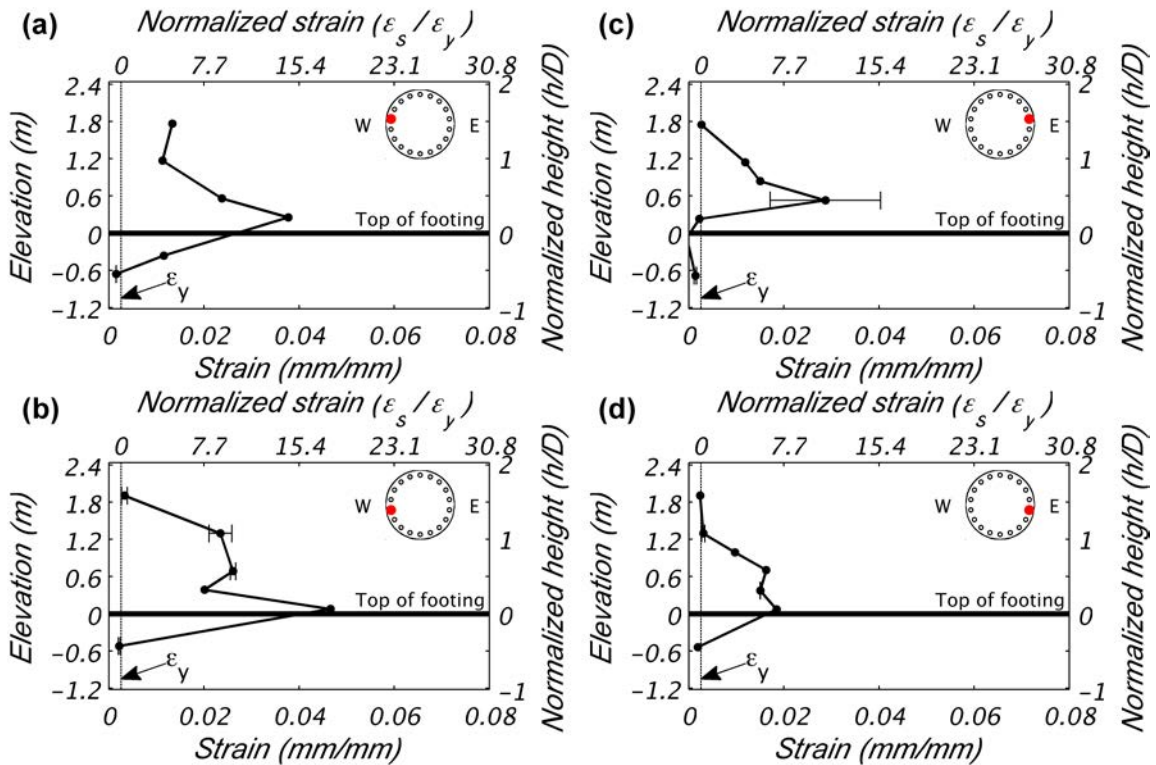


Figure 8.30 Longitudinal reinforcement tensile strain demand during EQ5.

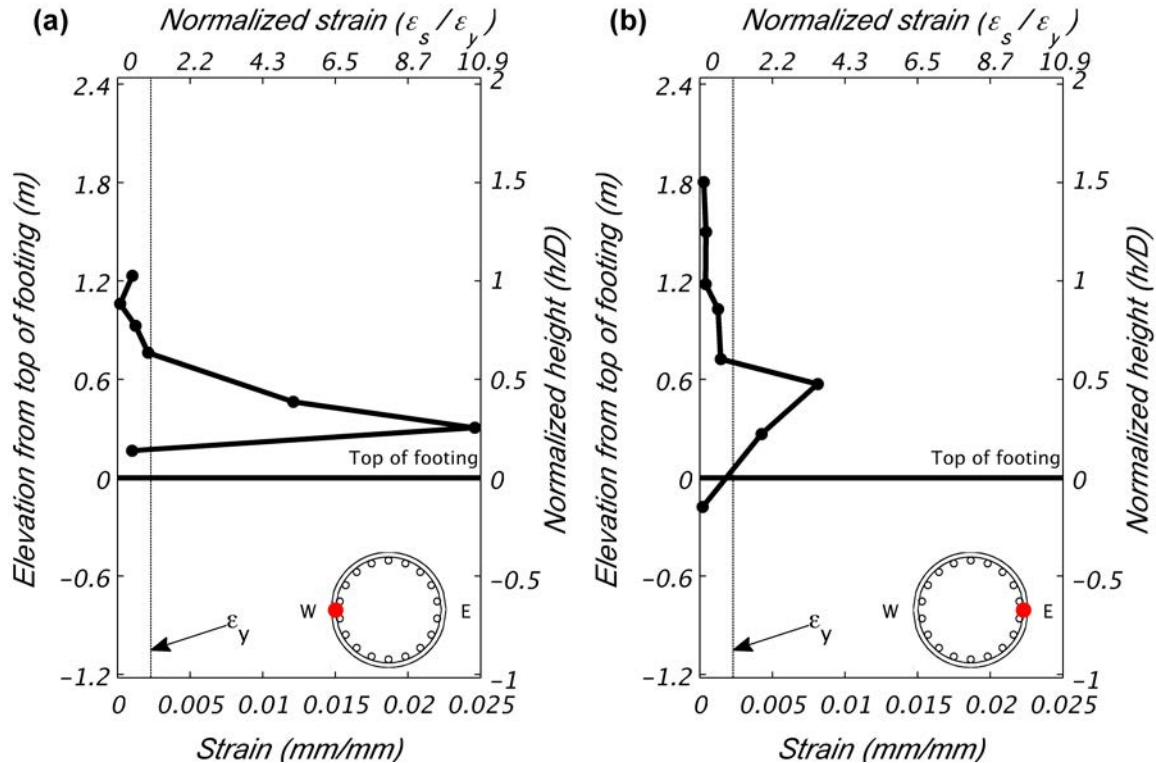


Figure 8.31 Transverse hoop reinforcement tensile strain demand during EQ5.

8.6 TEST EQ6

A repeat of test EQ3, the Los Gatos Presentation Center record from the Loma Prieta earthquake, resulted in a displacement ductility of 5.44. The peak displacement was 490 mm (19.28 in.) or a 6.69% drift ratio. Post-test, a residual displacement of 50 mm (1.97 in.) remained. This corresponds to 0.68% residual drift ratio. The displacement time history of the top of the column is shown in Figure 8.32. Figure 8.33 (a) and (b) show the East face of the column base at peak displacement in the West and East directions, respectively.

A post-test view of the East face of the column base is shown in Figure 8.33 (c). Concrete spalling and longitudinal reinforcement are visible, but spalling did not extend beyond the damage caused by test EQ5. The primary difference between Figure 8.33 (c) and Figure 8.27 (c) is the removal of spalled and loose concrete before test EQ6. The concrete core remained intact.

The peak column base moment was 6,500 kN-m (4,794 kip-ft). Stable hysteretic loops are present in the moment-curvature response of Figure 8.34. The peak shear force was 771 kN (173.4 kip). The lateral shear force and displacement response is shown in Figure 8.35.

Strain profiles are presented in Figure 8.36 and Figure 8.37 for longitudinal and transverse bars, respectively. Longitudinal and transverse strains were on the same order of magnitude as the prior test. Longitudinal strains beyond the elastic limit were measured at 1.8 m

(71 in.) or 1.5 column diameters above the footing. Longitudinal gauges at a depth of 0.6 m (24 in.) in the footing remained elastic.

EQ6 was the last test intended in the loading protocol. However, damage to this point was limited to concrete spalling. This provided the opportunity to extend the scope of testing.

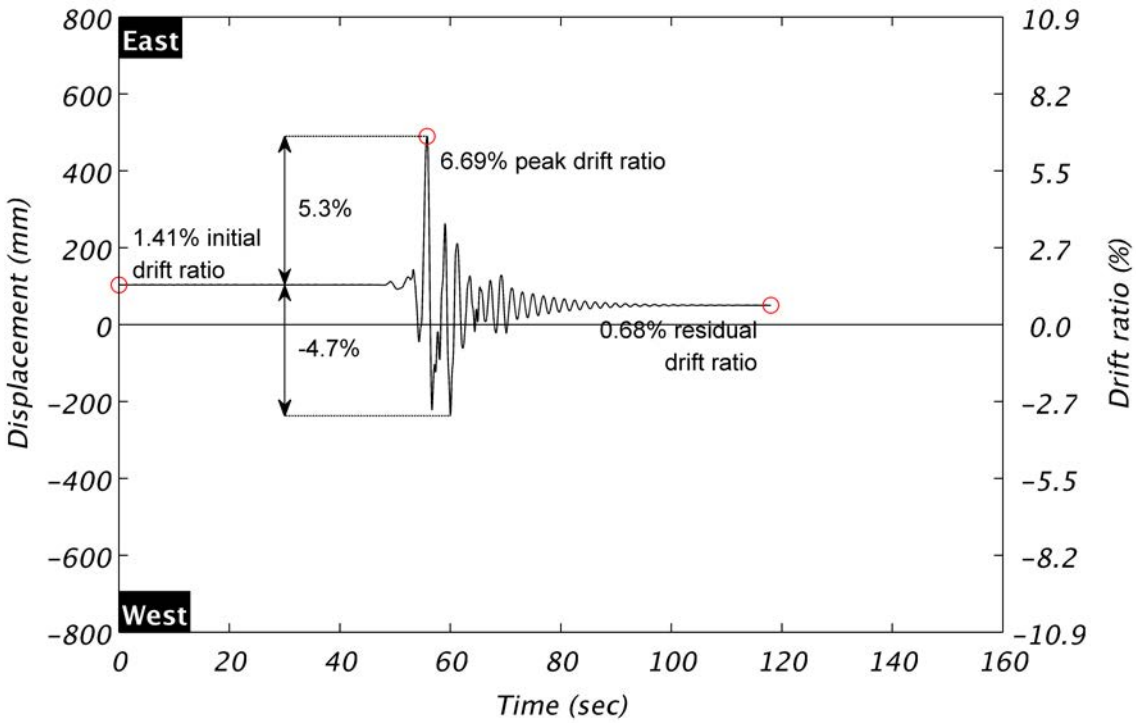


Figure 8.32 Column displacement during EQ6.

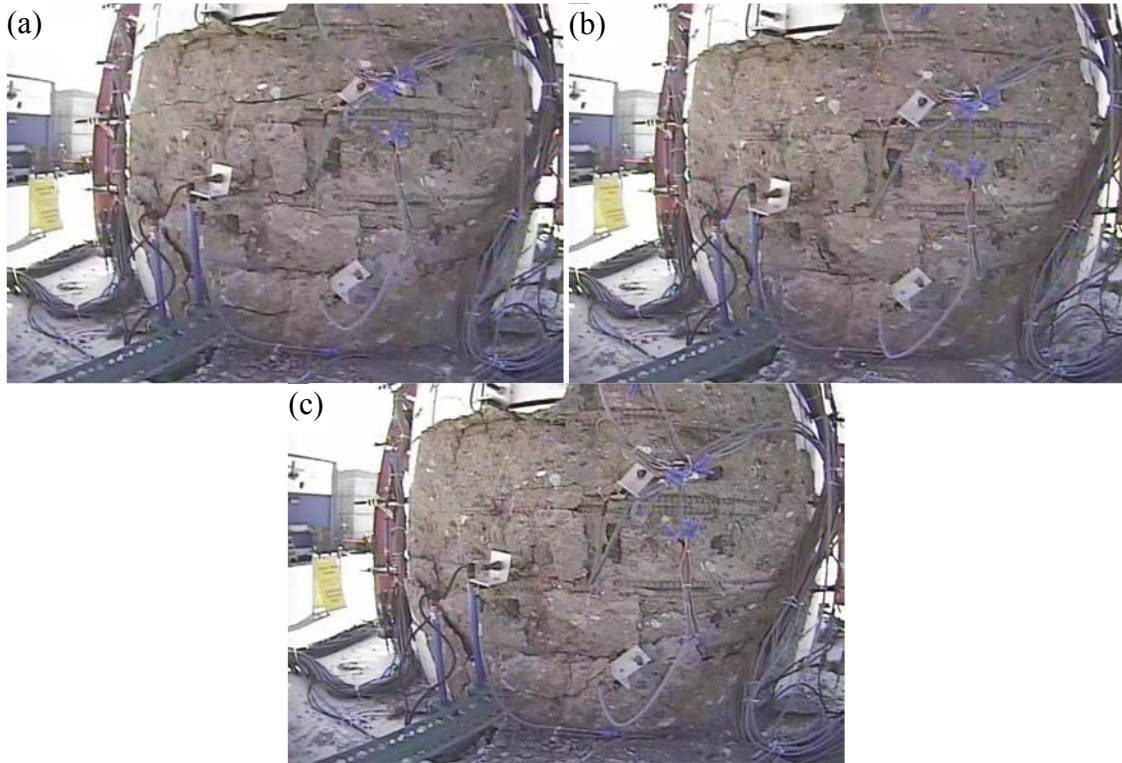


Figure 8.33 Column base East face during EQ6 at (a) peak West displacement, (b) peak East displacement, and (c) post-test.

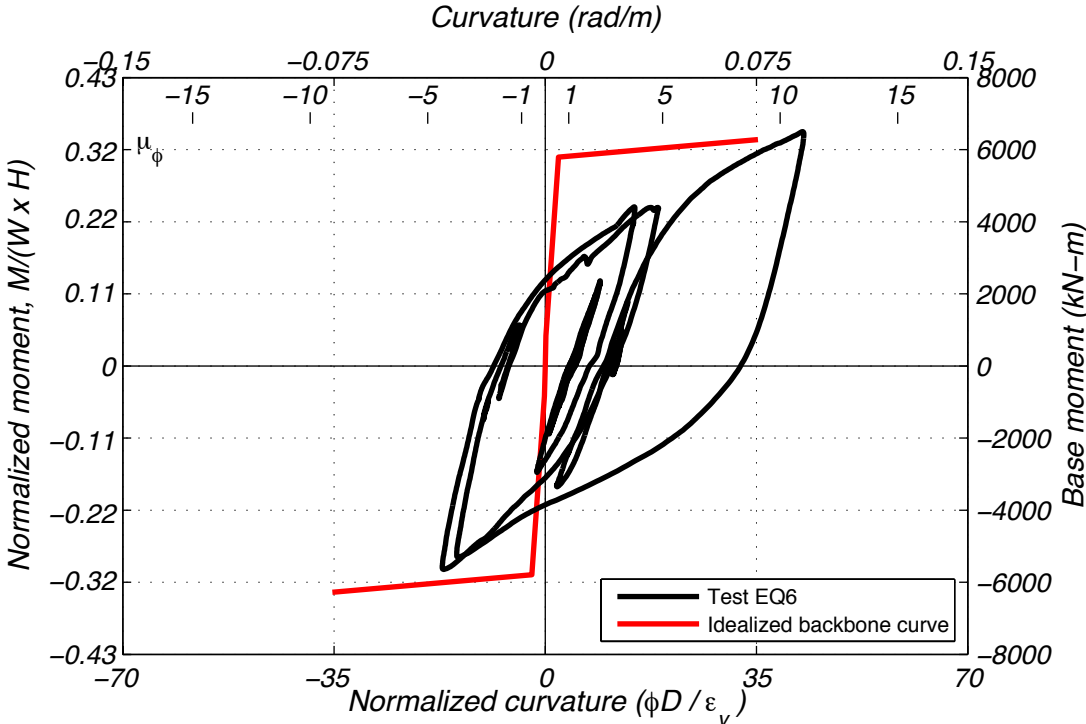


Figure 8.34 Column response during EQ6 in terms of base moment and curvature.

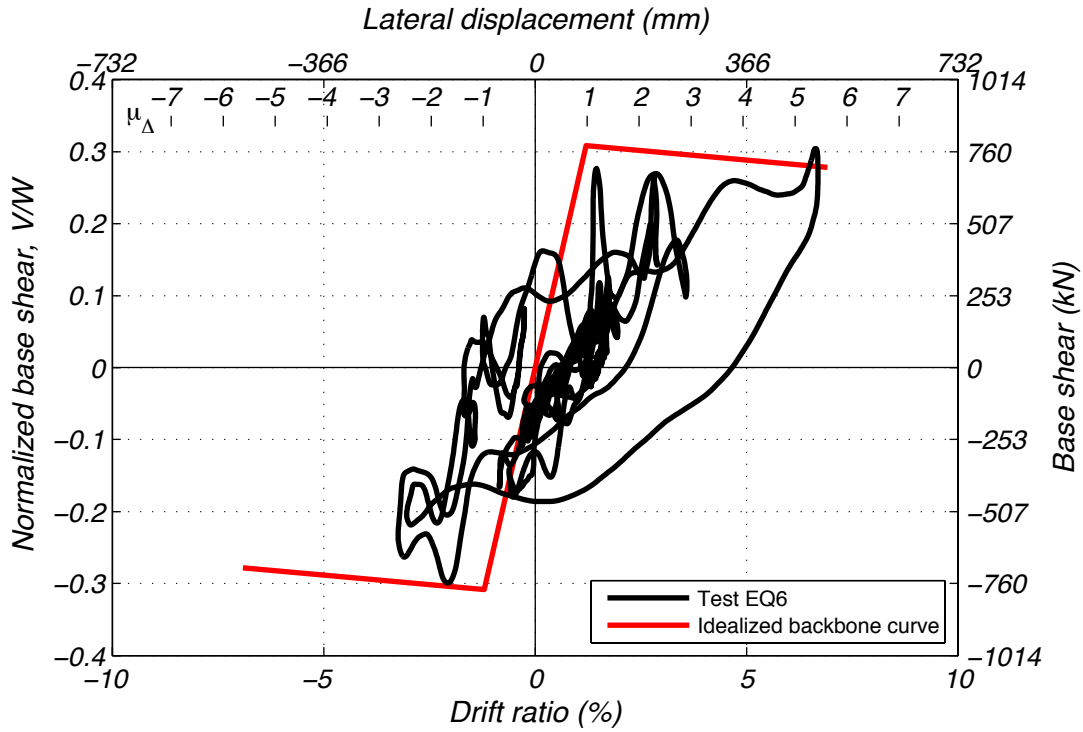


Figure 8.35 Column response during EQ6 in terms of base shear and drift ratio.

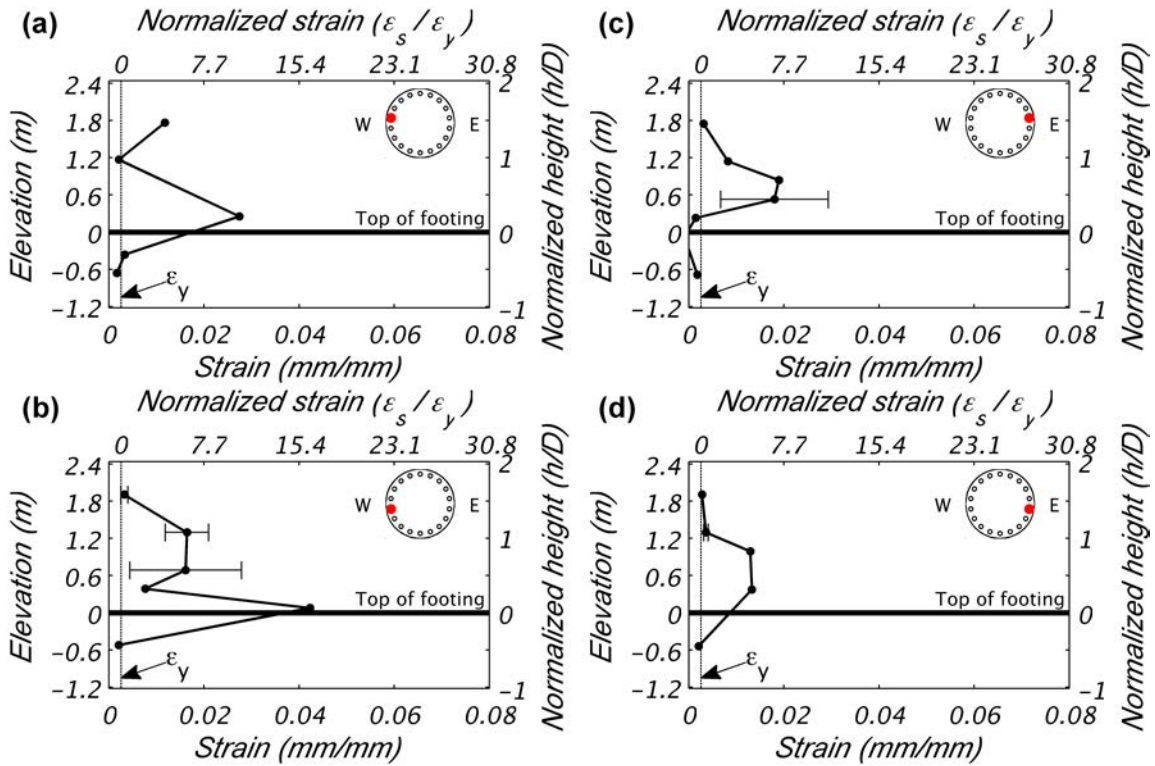


Figure 8.36 Longitudinal reinforcement tensile strain demand during EQ6.

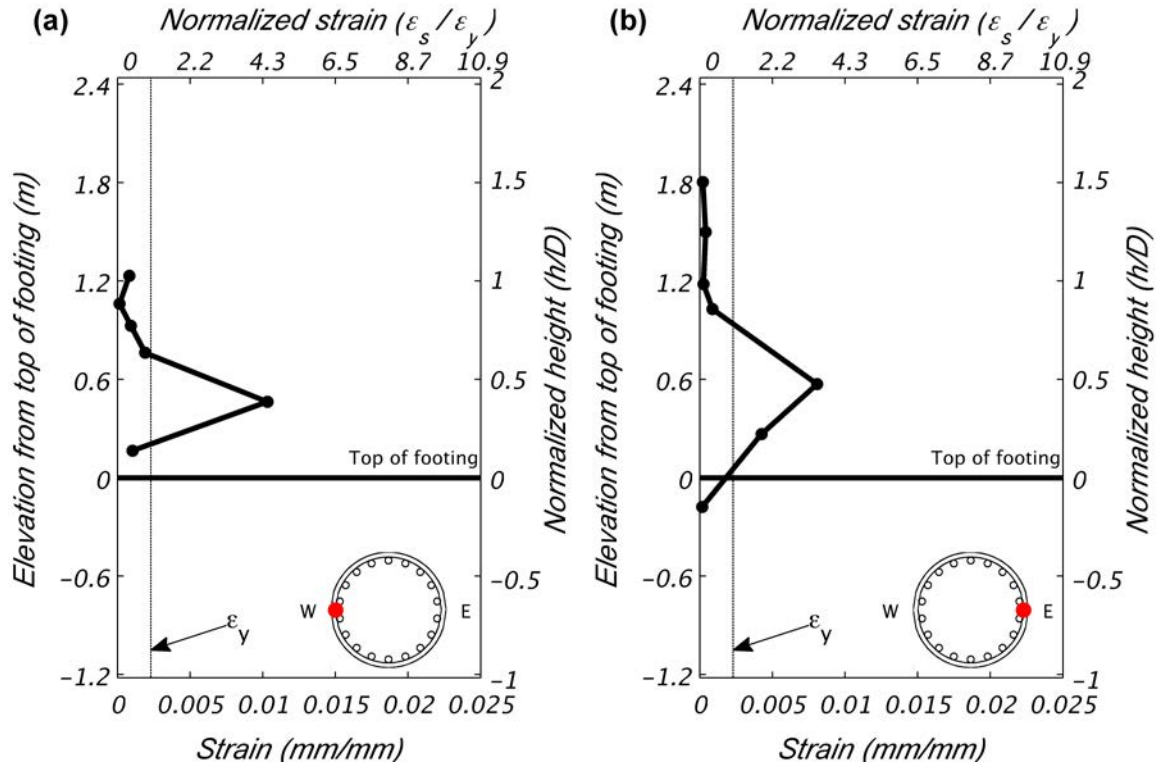


Figure 8.37 Transverse hoop reinforcement tensile strain demand during EQ6.

8.7 TEST EQ7

For extended testing, the Takatori record from the Kobe earthquake was utilized at different amplitudes to bring the column to a near collapse condition. In test EQ7, the Takatori motion was utilized at 100% of the original record. It resulted in a peak displacement of 553 mm (21.78 in.) or a 7.56% drift ratio. This corresponds to a displacement ductility of 6.15. A residual drift ratio of -1.98%, or -145 mm (-5.70 in.) column displacement, remained post-test, see Figure 8.38. Figure 8.39 (a) and (b) show the East face of the column base at peak displacement in the West and East directions, respectively.

A post-test view of the East face of the column base is shown in Figure 8.39 (c). Further spalling was induced and more of the longitudinal bars were exposed as the spalling penetrated deeper into the face of the column. The loss of bond with the longitudinal bars in this figure and video footage indicate the onset of bar buckling.

The peak column base moment was 7,391 kN-m (5,452 kip-ft). This was the maximum overturning moment obtained in any of the tests, see Figure 8.40. The peak shear force was 812 kN (182.5 kip); the second largest shear force obtained in any of the tests. The lateral shear force and displacement response is shown in Figure 8.41.

Longitudinal strains, in terms of peak tensile demand, are shown in Figure 8.42. Unfortunately, only one gauge was reliable at each location in Figure 8.42(c), so buckling onset cannot be confirmed in this bar with these sensors. Transverse strain demands were similar to the prior test with the largest demands occurring at 0.6 m (24 in.); see Figure 8.43

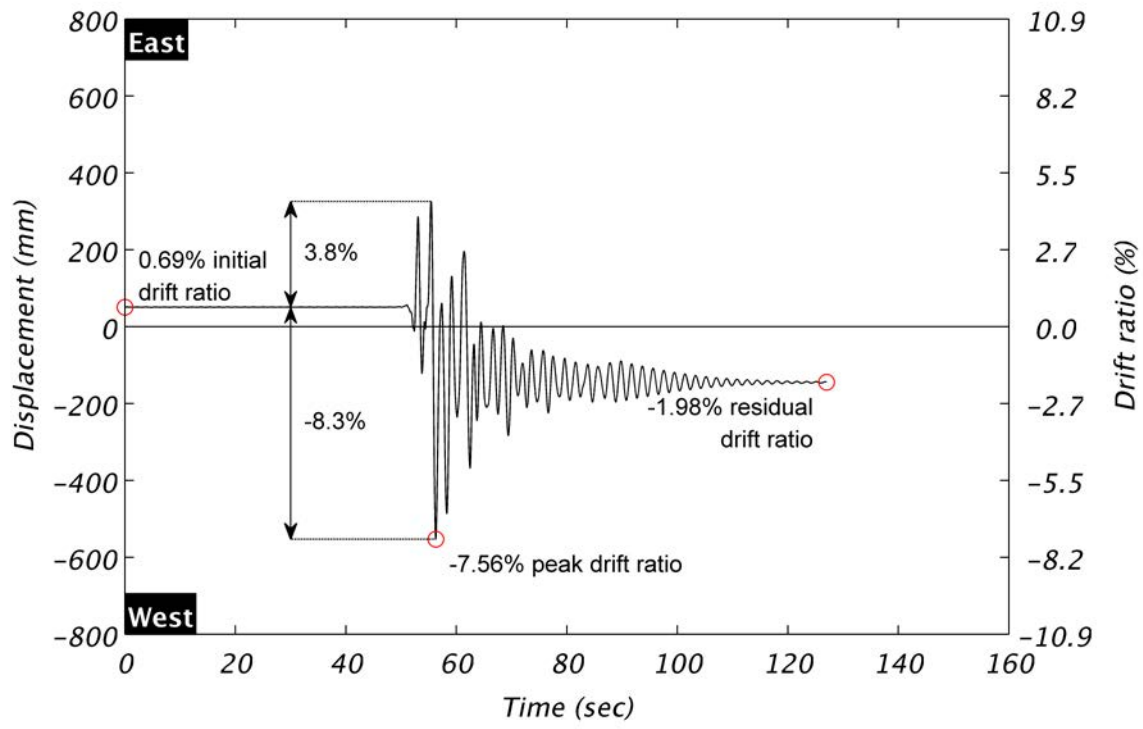


Figure 8.38 Column displacement during EQ7.

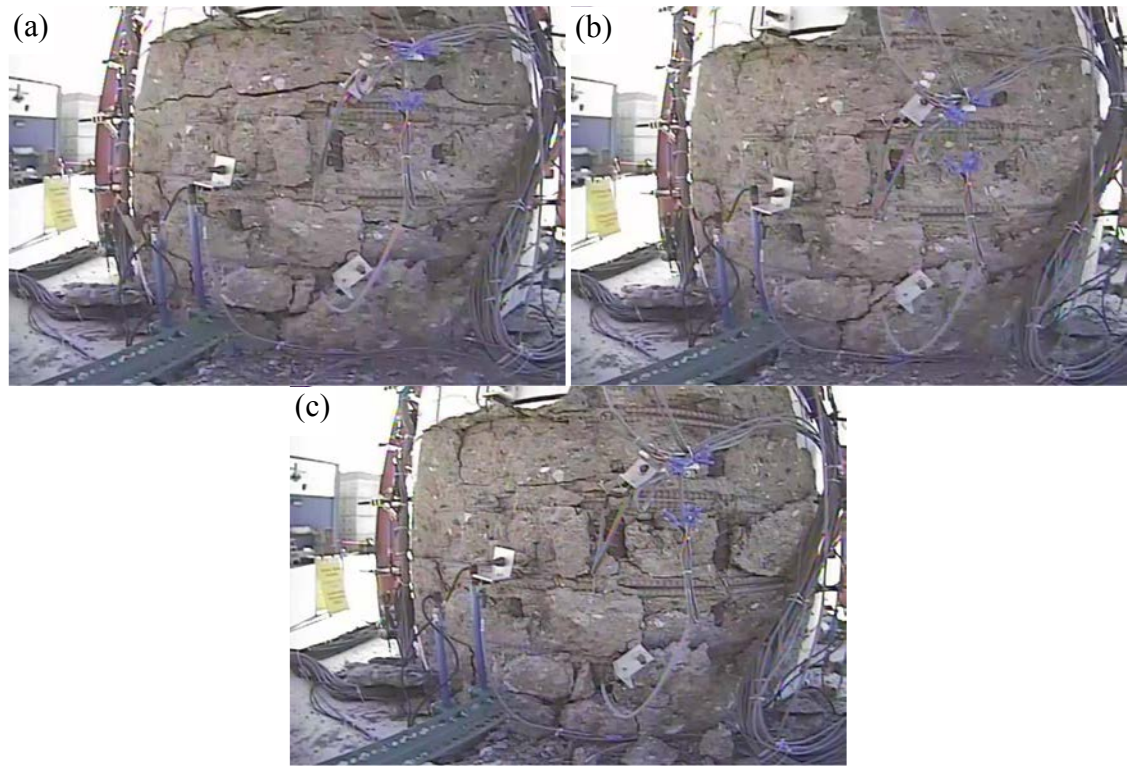


Figure 8.39 Column base East face during EQ7 at (a) peak West displacement, (b) peak East displacement, and (c) post-test.

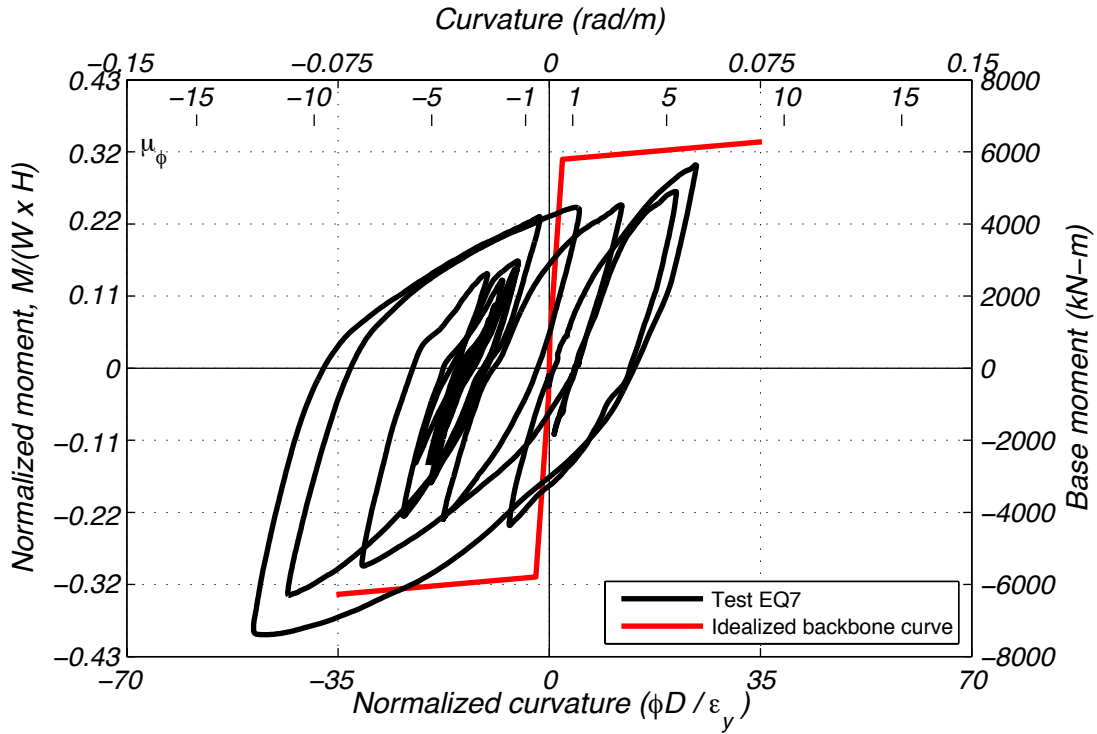


Figure 8.40 Column response during EQ7 in terms of base moment and curvature.

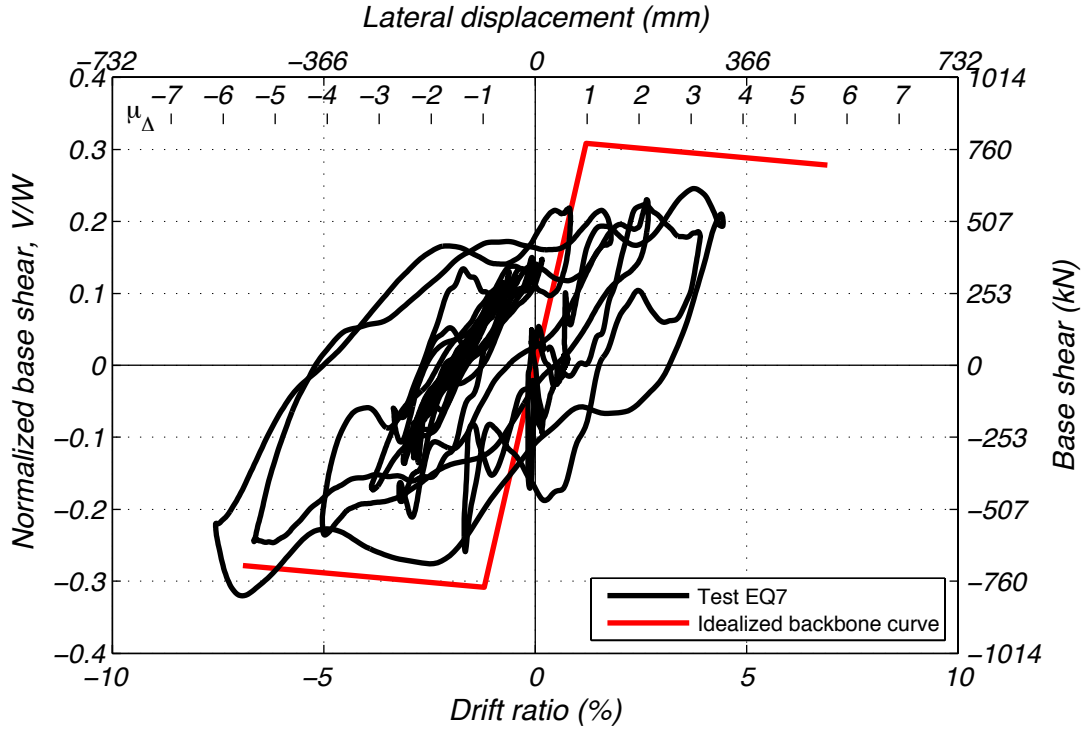


Figure 8.41 Column response during EQ7 in terms of base shear and drift ratio.

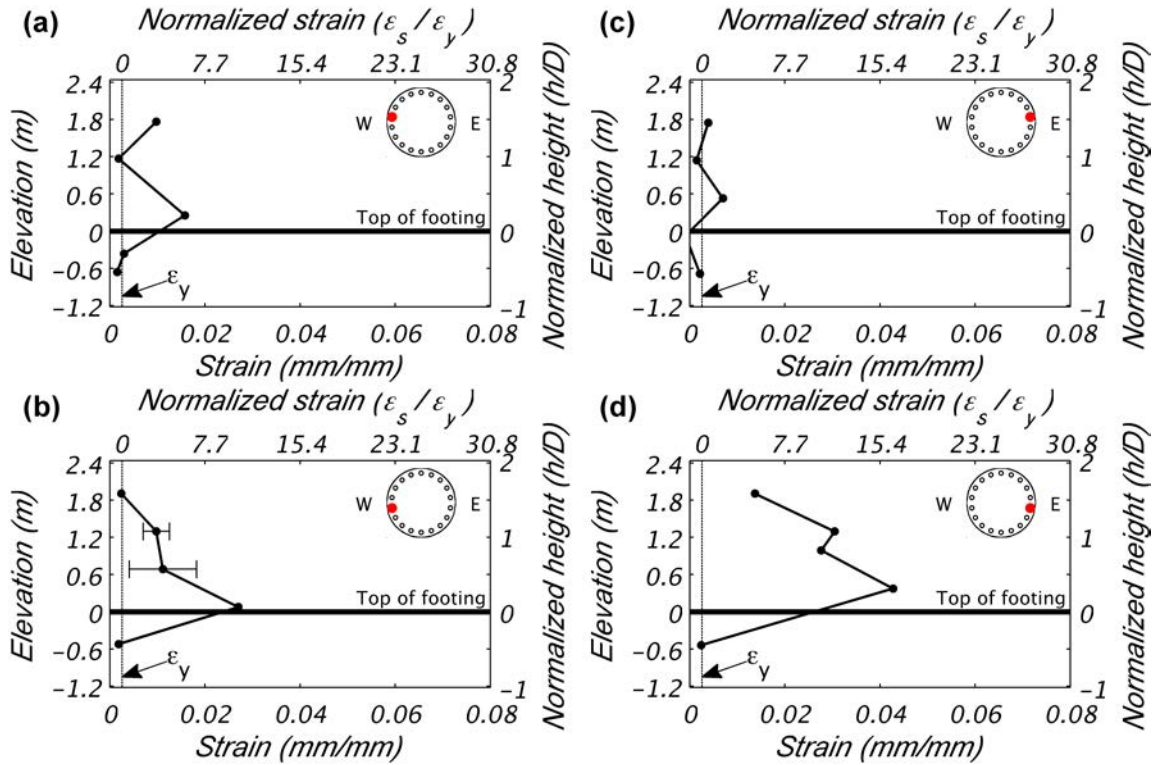


Figure 8.42 Longitudinal reinforcement tensile strain demand during EQ7.

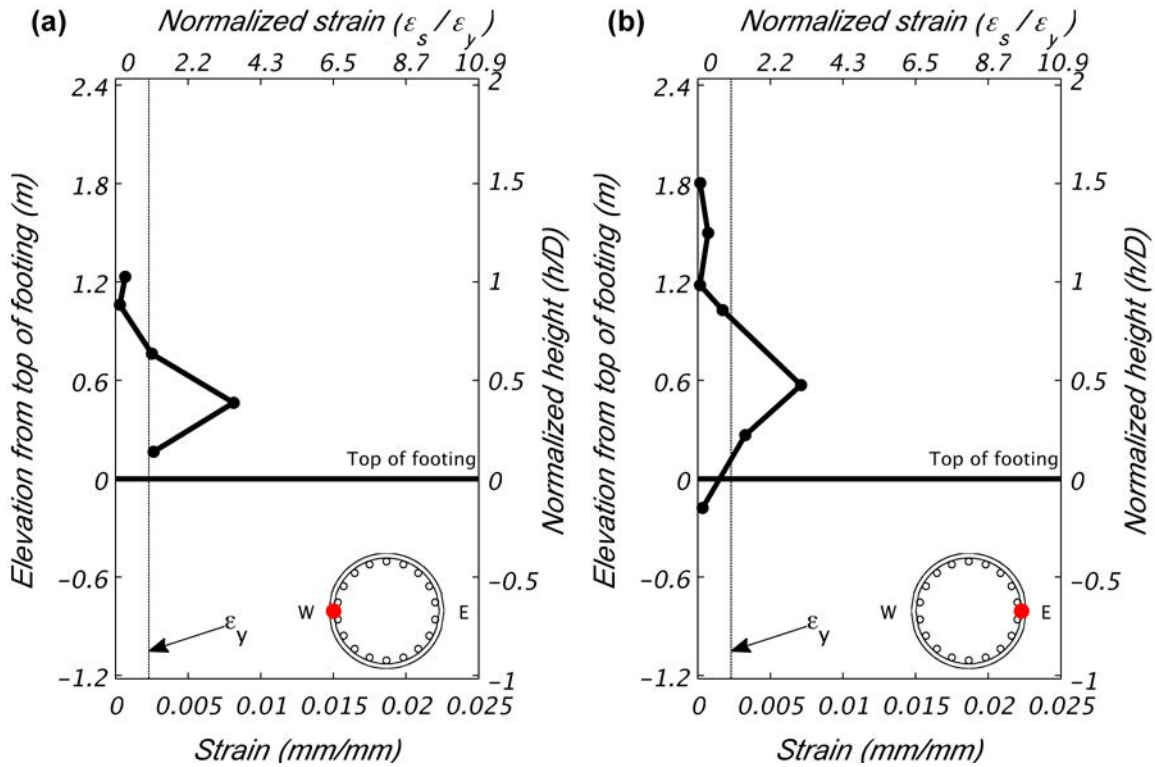


Figure 8.43 Transverse hoop reinforcement tensile strain demand during EQ7.

8.8 TEST EQ8

With the robustness observed in the prior test and drift demands still shy of the 10% limit, the prior signal was repeated and amplified. A scale factor of -1.2 was used with the original Takatori record. This imposed a displacement ductility of 6.73 at 606 mm (23.85 in.) of column displacement. The corresponding drift ratio was 8.28%. The residual displacement was 97 mm (3.83 in.) at the top of the column. This normalizes to 1.33% residual drift ratio and was slightly lower than the prior residual drift ratio of 1.98%. The displacement time history is shown in Figure 8.44. Figure 8.45 (a) and (b) show the East face of the column base at peak displacement in the West and East directions, respectively.

A post-test view of the East face of the column base is shown in Figure 8.45 (c). In this figure, the two exposed longitudinal reinforcing bars on the right side of the column centerline have fractured. The fractures and buckled shapes are apparent in this figure. This was the first damage beyond concrete cracking and spalling induced in the test specimen.

The peak column base moment was 7,164 kN-m (5,284 kip-ft), see Figure 8.46. Reduced capacity in the reloading cycle beyond a normalized curvature of +35.0 is not due to rebar fracture. Flexural demands put these bars in compression during these cycles, and fractures occurred after this sequence near zero curvature. The peak shear force was 742 kN (166.8 kip), see Figure 8.47.

Longitudinal strain demands are shown in Figure 8.48. One of the fractured bars was instrumented with strain gauges, see Figure 8.48(c), but tensile demands on this bar occurred early in the loading sequence during negative curvature demands. Tensile strain demands on the diametrically opposite bar were the largest yet recorded and occurred at the column-to-footing interface, see Figure 8.48(b). In this test peak transverse strain demands were similar to prior tests, see Figure 8.49. On both column faces, strain gauges on the hoop where maximum stain had previously been measured were no longer providing viable readings. Eleven of the twenty transverse gauges were reliable at this level of testing.

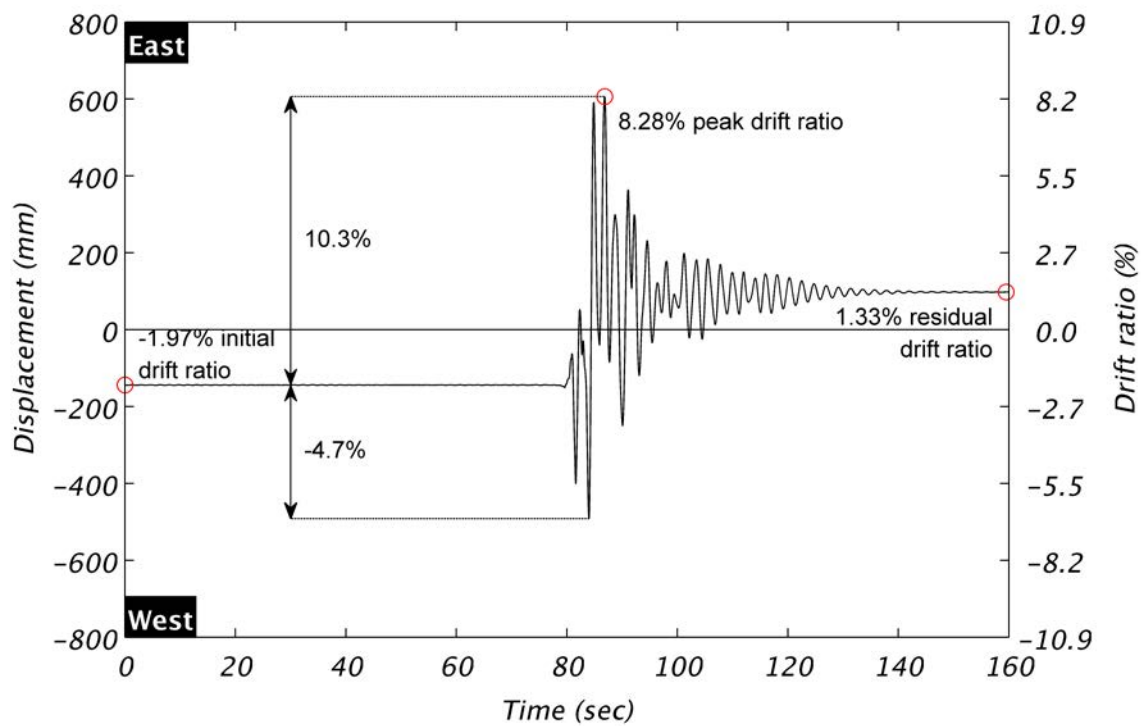


Figure 8.44 Column displacement during EQ8.

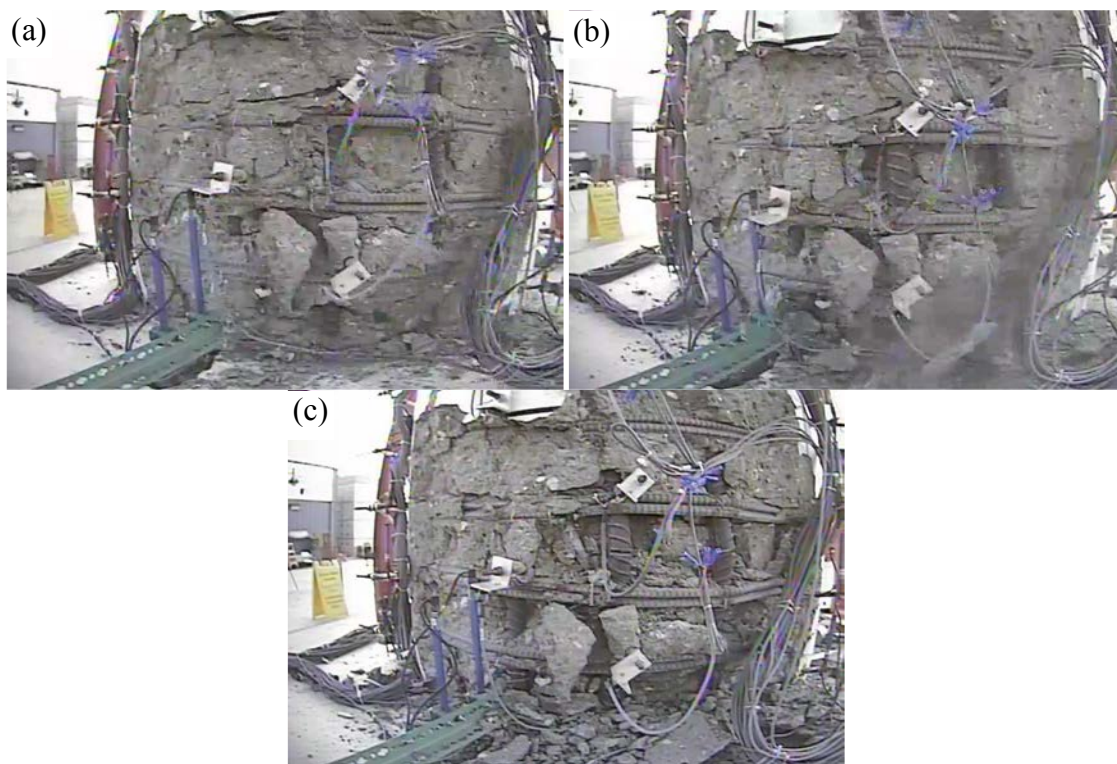


Figure 8.45 Column base East face during EQ8 at (a) peak West displacement, (b) peak East displacement, and (c) post-test.

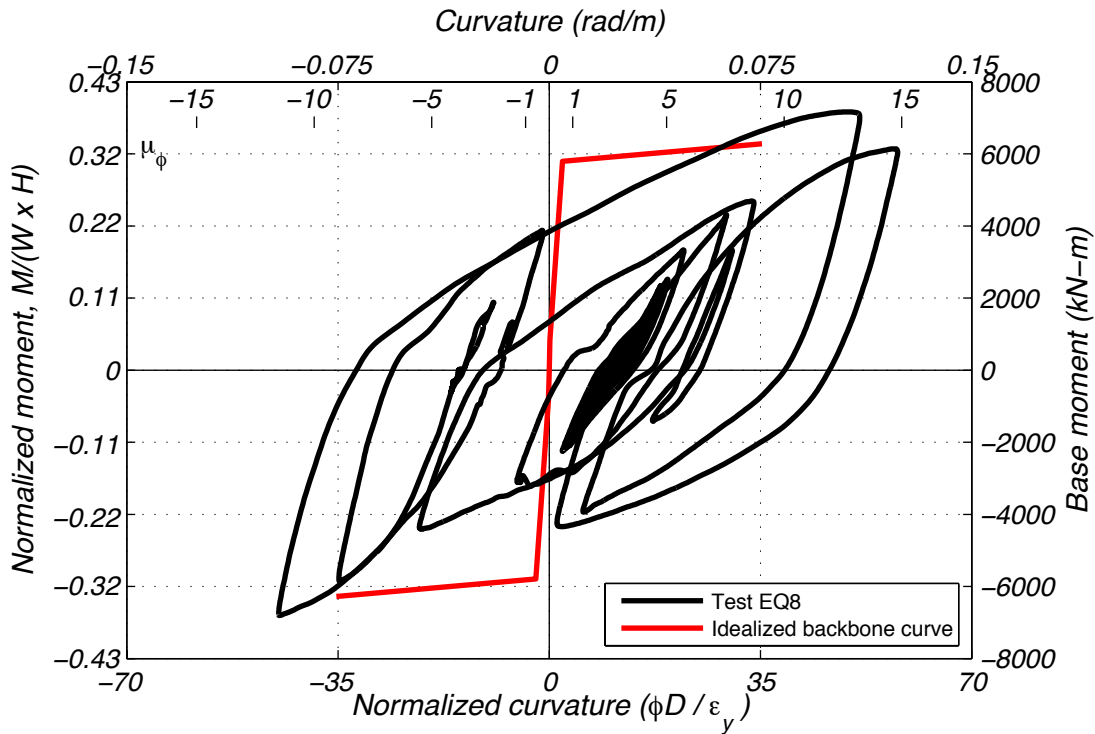


Figure 8.46 Column response during EQ8 in terms of base moment and curvature.

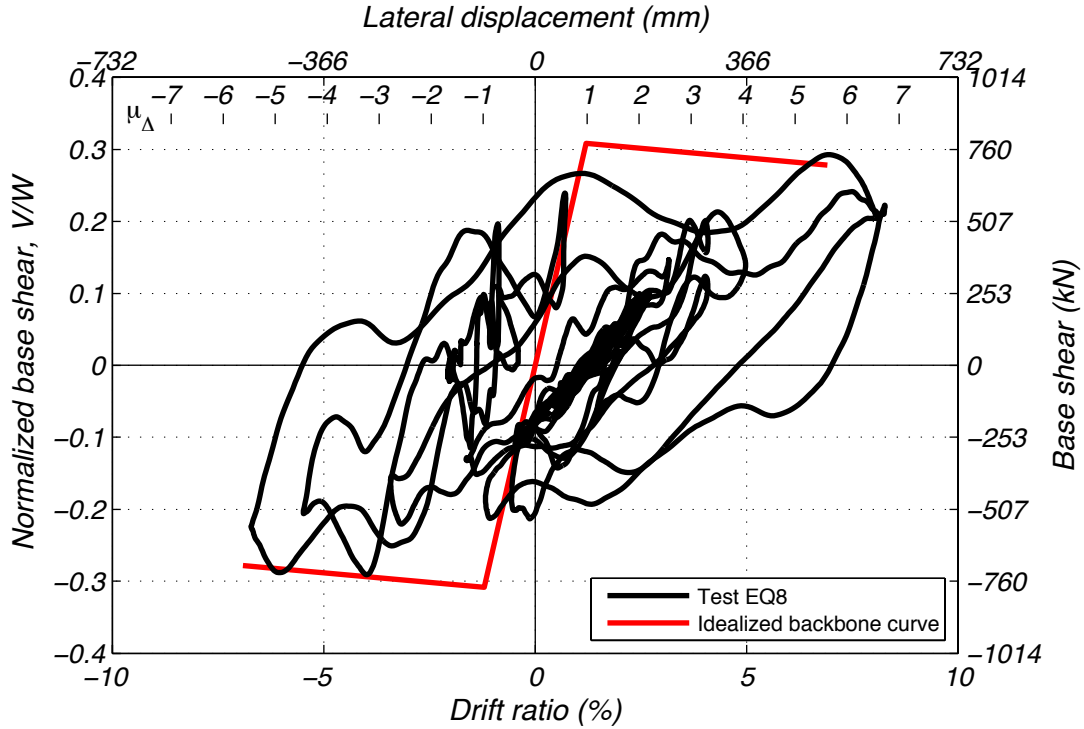


Figure 8.47 Column response during EQ8 in terms of base shear and drift ratio.

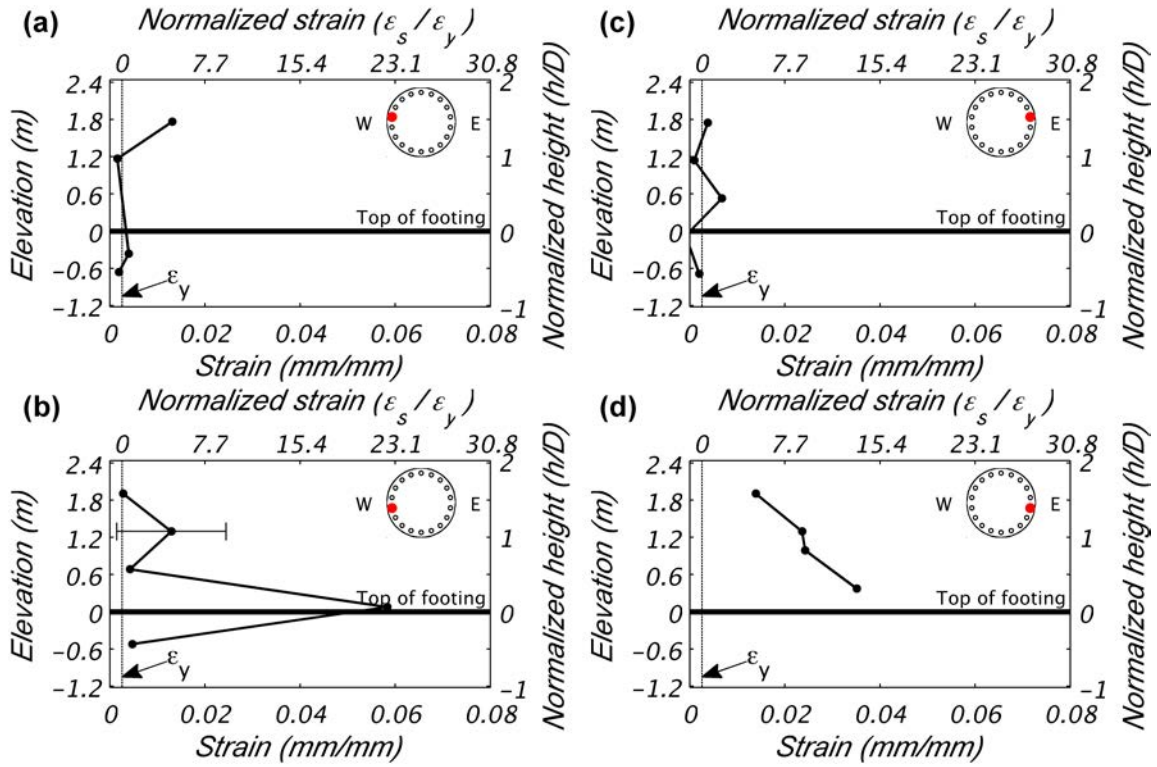


Figure 8.48 Longitudinal reinforcement tensile strain demand during EQ8.

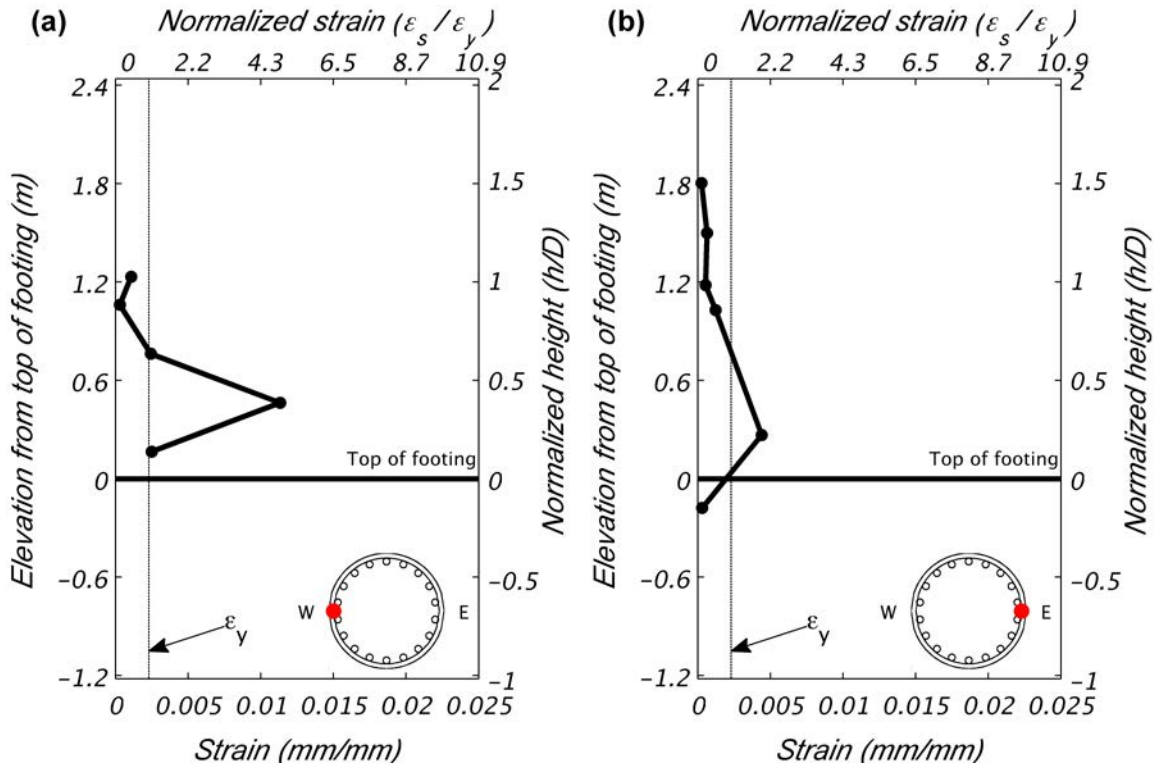


Figure 8.49 Transverse hoop reinforcement tensile strain demand during EQ8.

8.9 TEST EQ9

Reversing the polarity of the previous test, a scale factor of +1.2 was used with the original Takatori record for test EQ9. Despite the reversed polarity the column accumulated further residual displacement to the East, see Figure 8.50. Early in the time history, a third longitudinal reinforcing bar fractured on the East face of the column. A post-test view of the East face of the column base is shown in Figure 8.51 (c), but the new fracture is not apparent. Two reinforcing bars fractured on the West face during this test. This is evident as a drop in moment capacity at about 0.11 rad/m (0.0028 rad/in) in the moment-curvature relationship of Figure 8.52.

The peak column displacement was 635 mm (25.01 in.) corresponding to a drift ratio of 8.69%. The displacement ductility achieved was 7.06. A residual displacement of 225 mm (8.85 in.), or 3.07% residual drift ratio, remained post-test. These values are indicated in the displacement time history of Figure 8.50. Figure 8.51 (a) and (b) show the East face of the column base at peak displacement in the West and East directions, respectively.

The peak column base moment was 6,155 kN-m (4,540 kip-ft). This is 83% of the peak moment achieved in test EQ7. Stiffness degradation is apparent in the moment-curvature response, see Figure 8.52. The peak shear force of 755 kN (169.7 kip) was largely a product of the mass moment of inertia of the top mass that induces an inflection point at approximately 75% of the column height. The consequence is a relatively low overturning moment demand, approximately 4,000 kN-m (2,950 kip-ft), that produces the peak shear force. The lateral shear force-displacement response is shown in Figure 8.53.

Only thirteen of sixty-four longitudinal strain gauges remained intact for this test. These are shown in Figure 8.54, but the bar in Figure 8.54 (c) fractured in the prior test and the bars in (a) and (d) fractured during this test. The largest longitudinal strain, 6.4%, recorded during any test was obtained in a bar on the West face just above the footing, see Figure 8.54 (b). Transverse strain demands remained consistent with demands imposed in the prior five tests, see Figure 8.55.

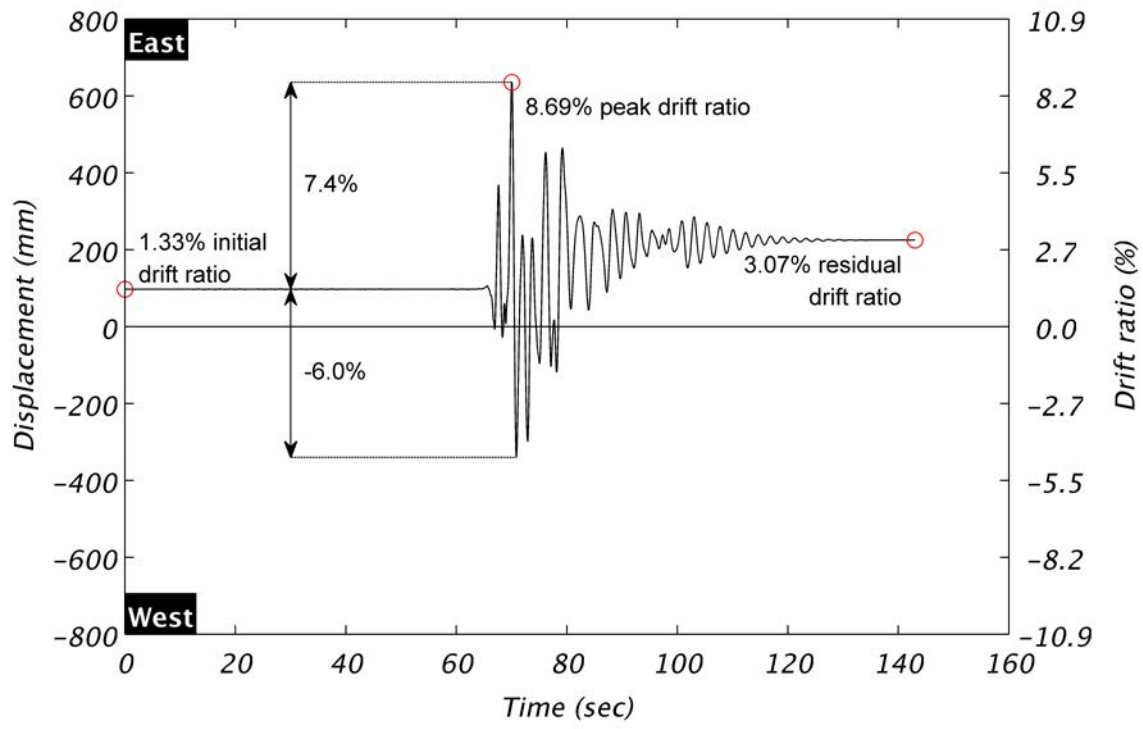


Figure 8.50 Column displacement during EQ9.

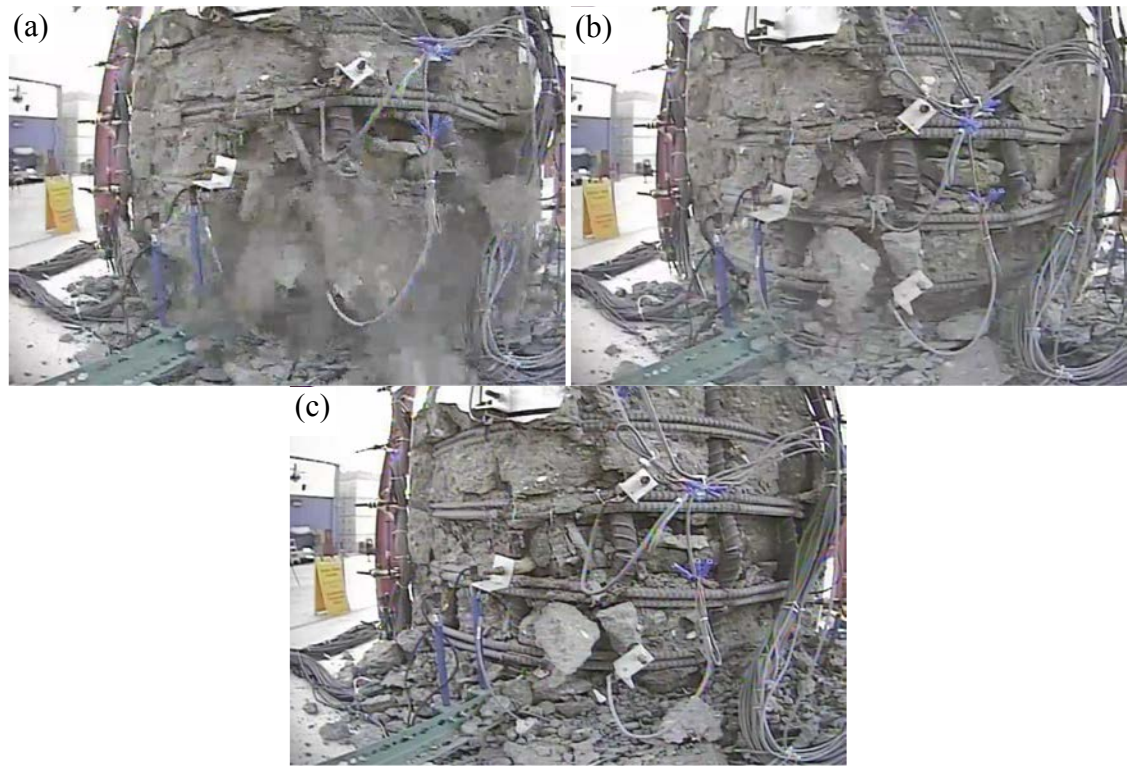


Figure 8.51 Column base East face during EQ9 at (a) peak West displacement, (b) peak East displacement, and (c) post-test.

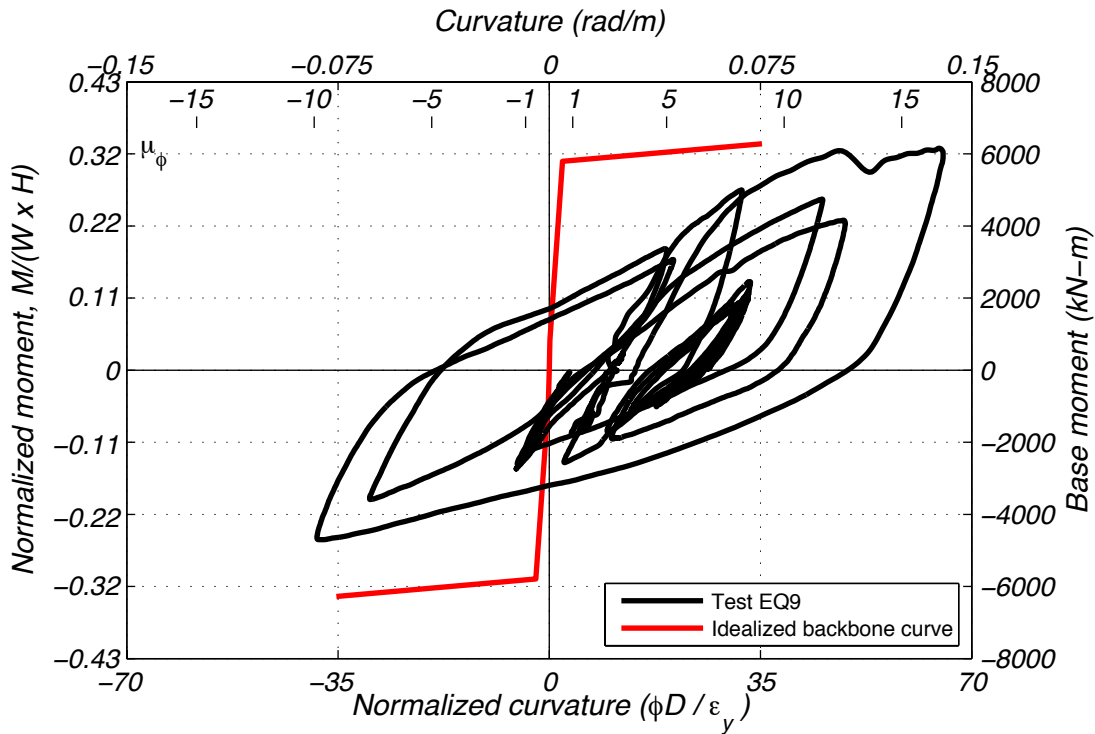


Figure 8.52 Column response during EQ9 in terms of base moment and curvature.

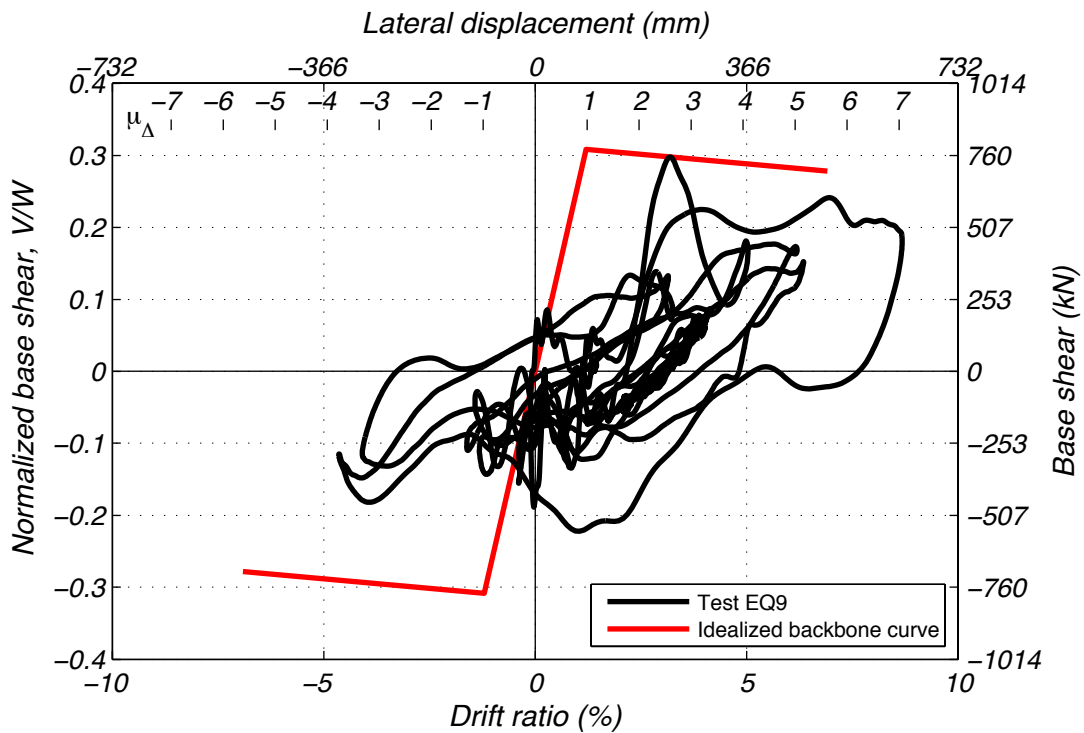


Figure 8.53 Column response during EQ9 in terms of base shear and drift ratio.

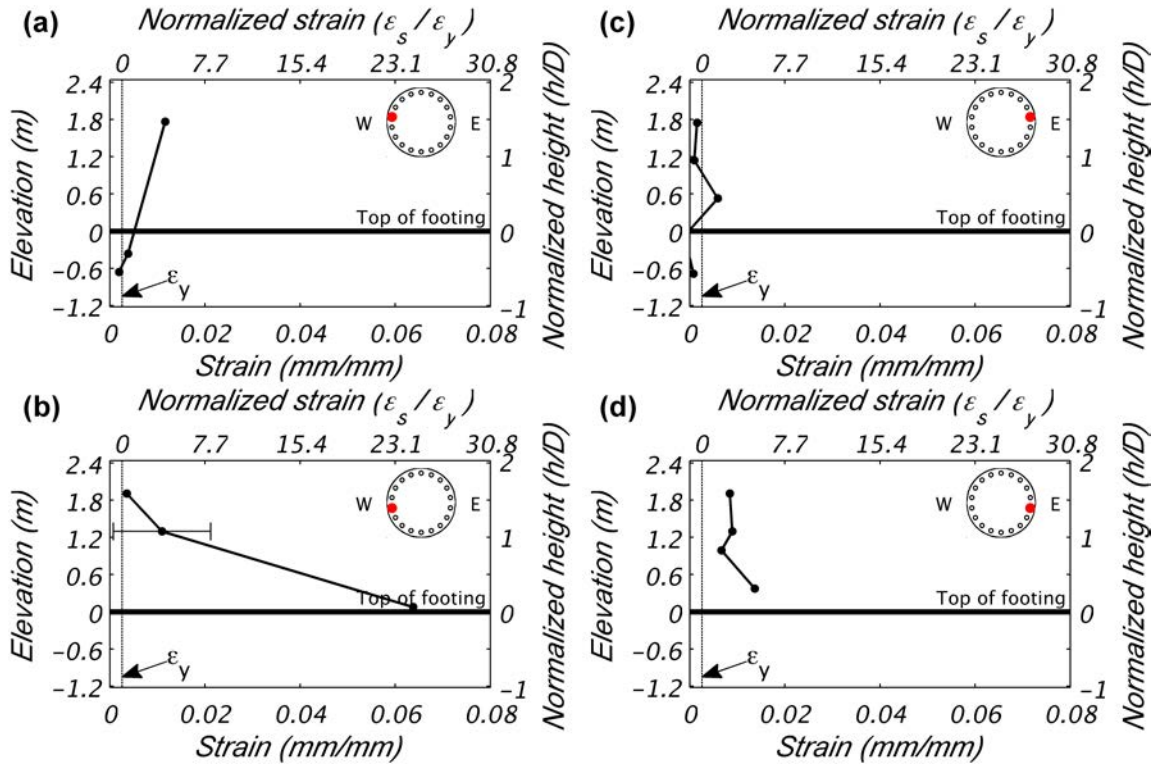


Figure 8.54 Longitudinal reinforcement tensile strain demand during EQ9.

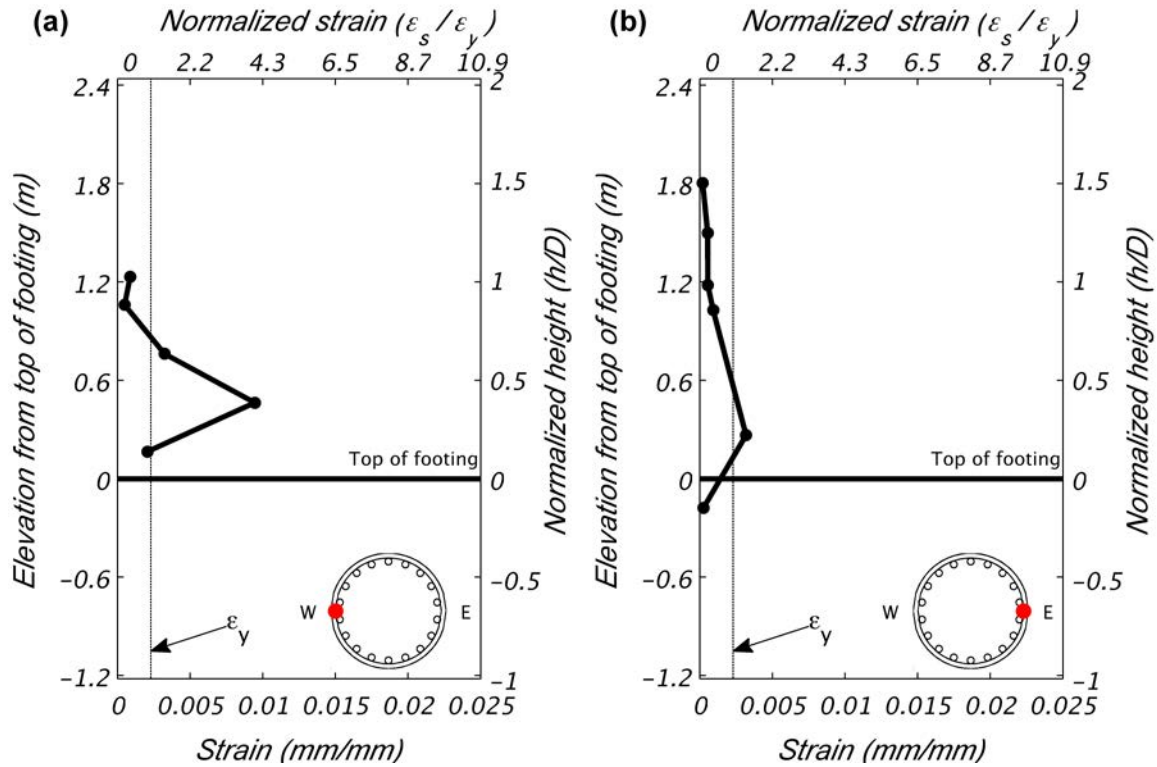


Figure 8.55 Transverse hoop reinforcement tensile strain demand during EQ9.

8.10 TEST EQ10

Prior earthquake simulation tests resulted in a reduced column capacity caused by the fracture of five longitudinal bars, buckling of others, and crushing of the concrete core. Continued testing at this point was aimed at pushing the column to the imposed drift limit of 10%. For this purpose, the same scale factor of 1.2 was utilized with the Takatori record consistent with the prior test. A sixth longitudinal reinforcing bar fractured during this test. This was the fourth bar to fracture on the East face of the column. However, the superstructure mass impacted the East safety column before this fracture occurred. During impact, the column displaced 757 mm (29.79 in.). The drift ratio at impact was 8.69. The displacement time history is shown in Figure 8.56.

Figure 8.57 (a) and (b) show the East face of the column base at peak displacement in the West and East directions, respectively. A post-test view of the East face of the column base is shown in Figure 8.57 (c). Vertical offset of the transverse hoops caused by the buckled longitudinal reinforcement is evident in this figure, but transverse reinforcement did not fracture. Exposed longitudinal reinforcement was hot to the touch post-test. Cracks in the top of the footing surrounding the column were present post-test. Their onset was not identifiable due to debris, but they extended 0.61 m (24 in.) from the column face.

The derived moment and shear force are heavily influenced by the impact due to their calculation from inertial forces, see Figure 8.58 and Figure 8.59 respectively. Figure 8.58 shows the overturning moment-curvature response, but calculated curvature was not corrected for the influence of curvature rod movement within the crushed concrete core. Hoop dislocation caused by buckled longitudinal reinforcement disturbed vertical LVDT measurements as evident in videos footage of the North and South faces.

Longitudinal strain gauge readings in Figure 8.60 contain results from three bars that fractured in prior tests. Figure 8.60 (b) contains the only bar that was not visually identified as having fractured previously. Transverse strain demands, see Figure 8.61, were lower than prior tests. This is likely attributed to reduced shear capacity, prior fractures of buckled longitudinal bars, and concrete core crushing.

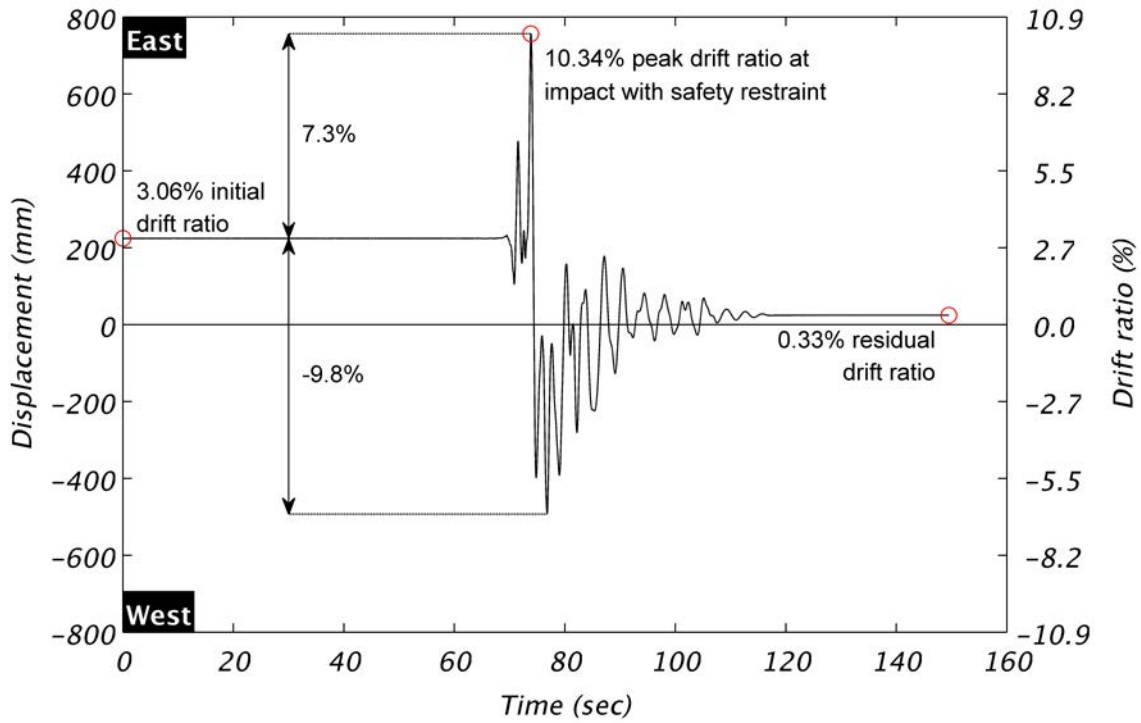


Figure 8.56 Column displacement during EQ10.

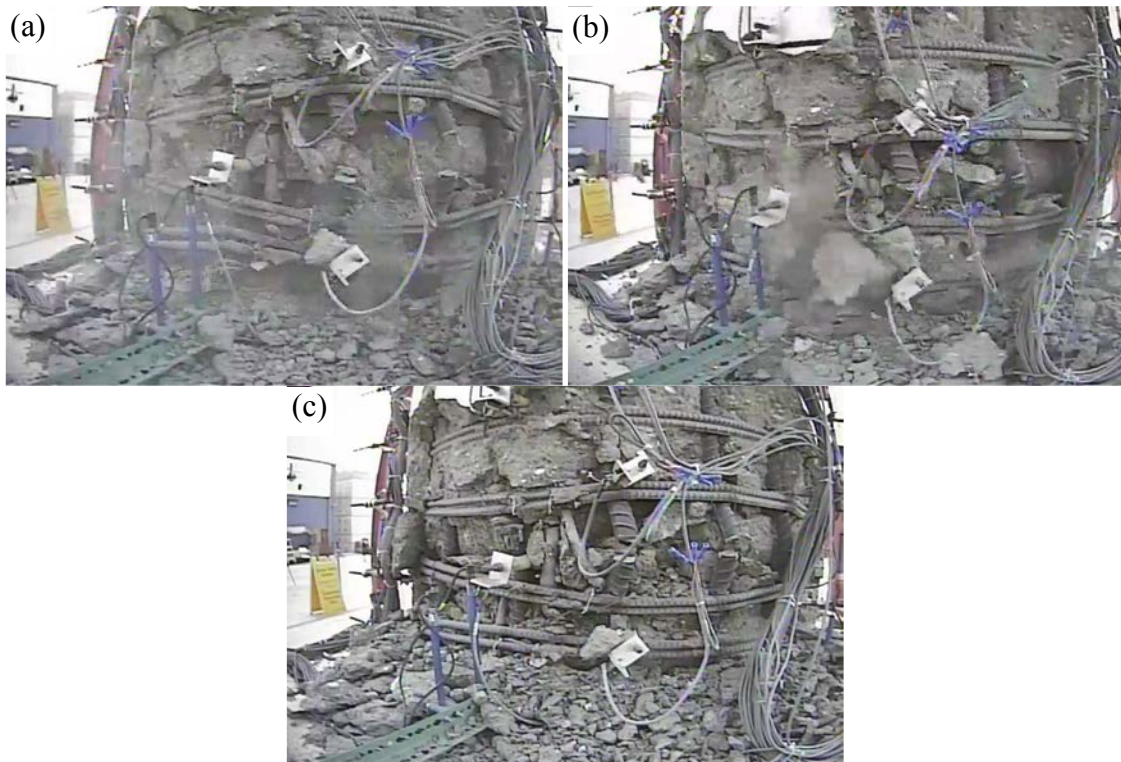


Figure 8.57 Column base East face during EQ10 at (a) peak West displacement, (b) peak East displacement, and (c) post-test.

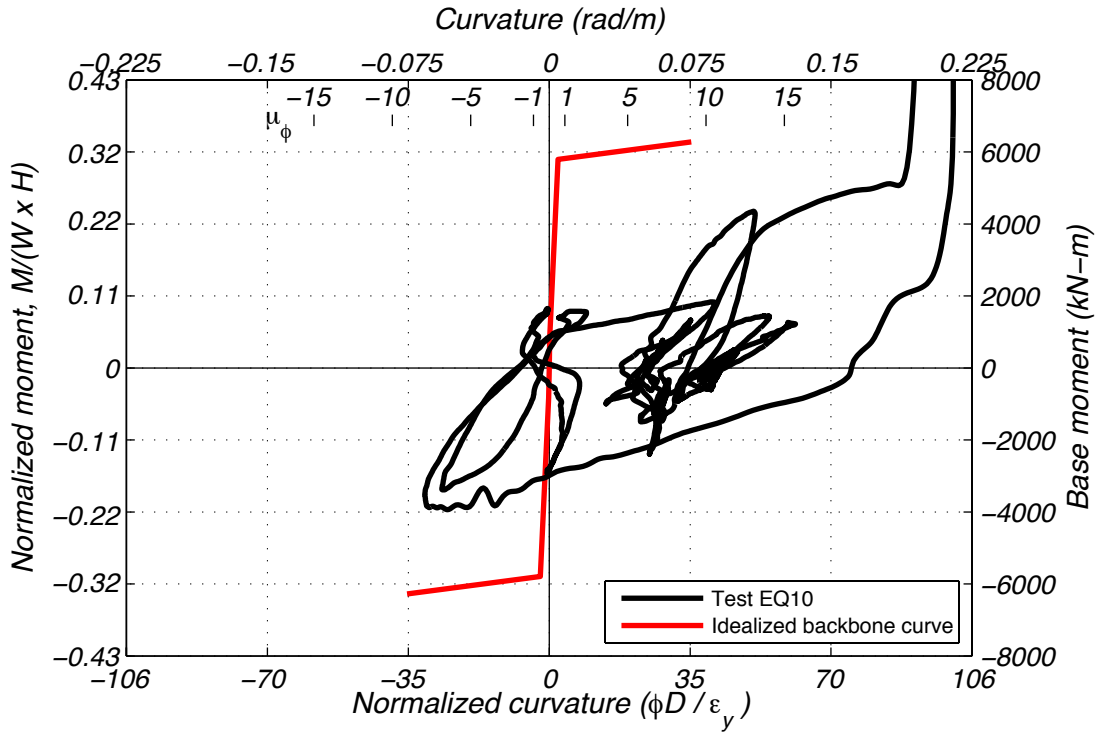


Figure 8.58 Column response during EQ10 in terms of base moment and curvature.

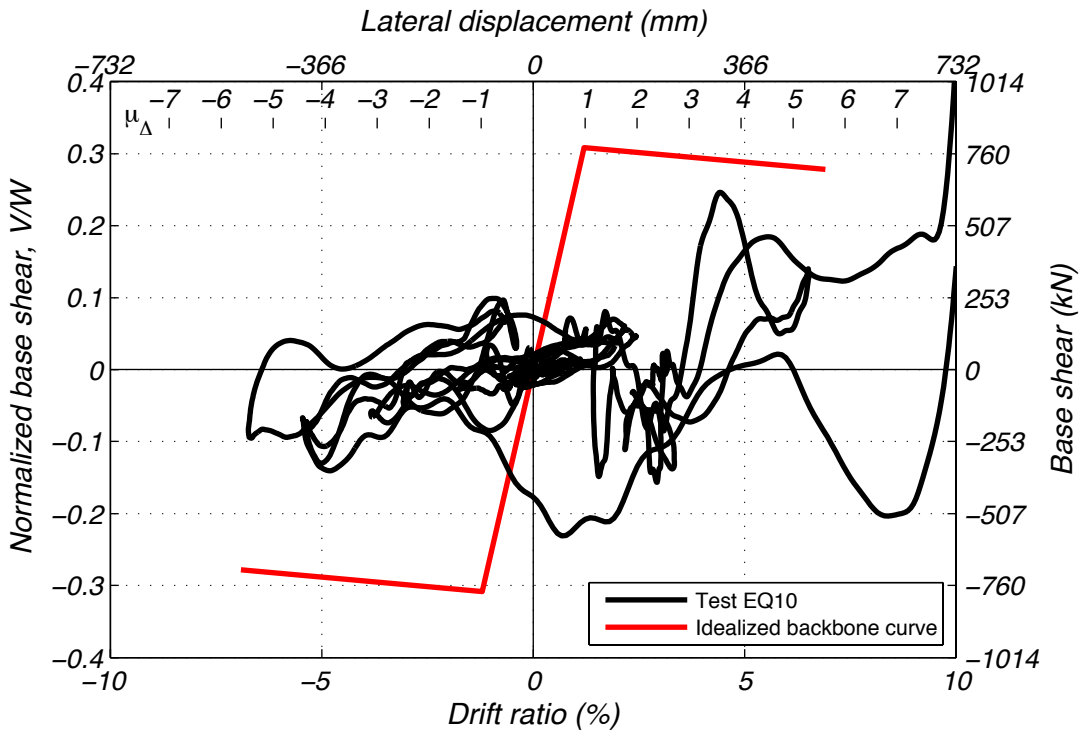


Figure 8.59 Column response during EQ10 in terms of base shear and drift ratio.

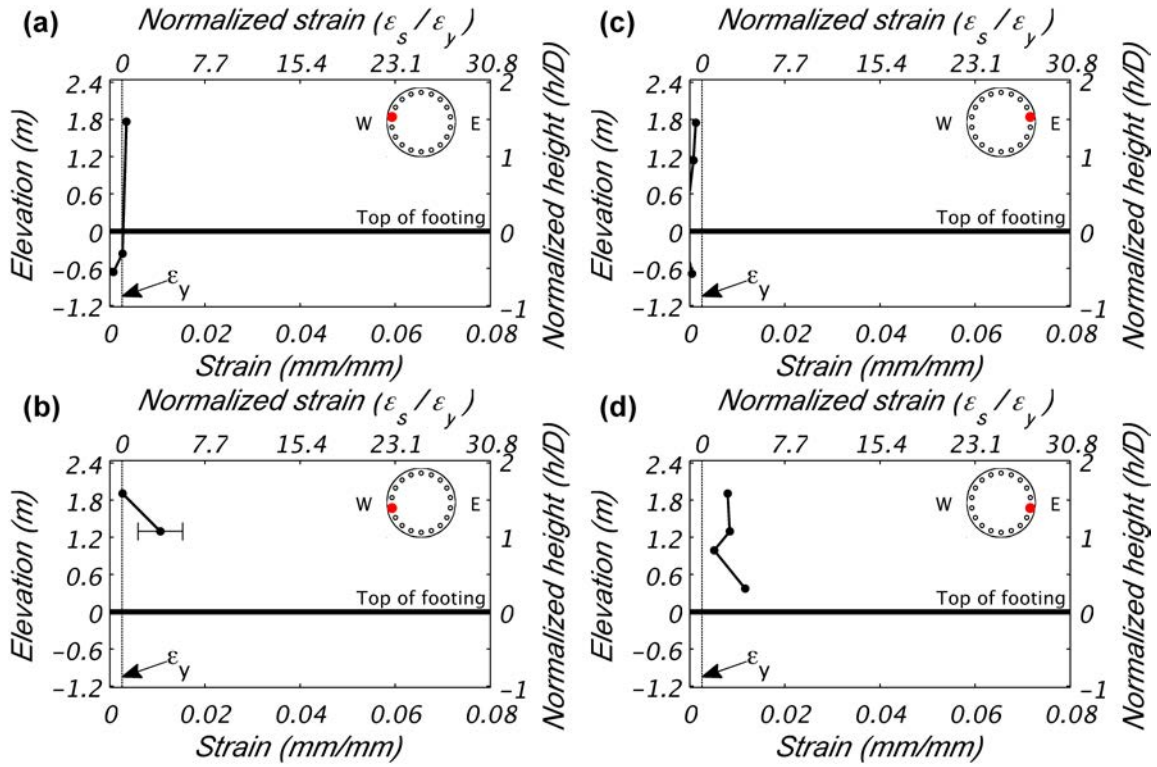


Figure 8.60 Longitudinal reinforcement strain demand during EQ10.

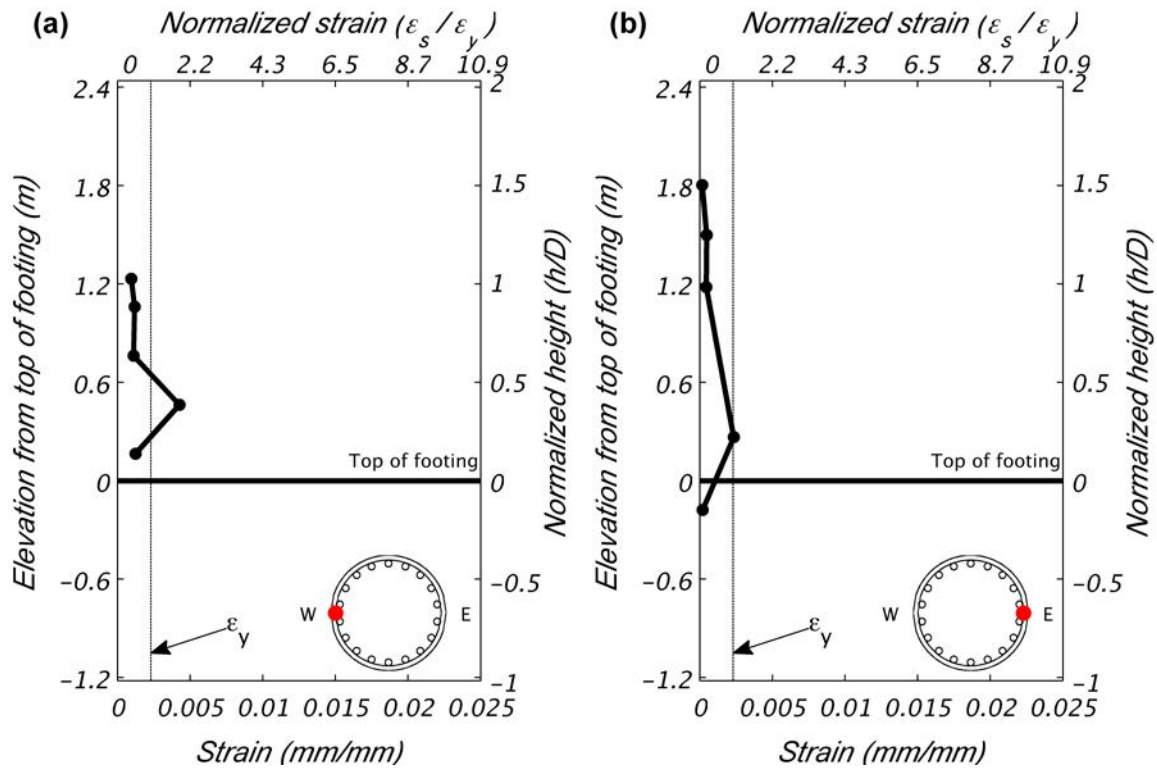


Figure 8.61 Transverse hoop reinforcement strain demand during EQ10.

9 Summary and Conclusions

9.1 SUMMARY

Ten earthquake simulations were conducted on a full-scale bridge column built to current Caltrans design specifications. The column exhibited ductile behavior and achieved a maximum displacement ductility of 7.06, where the experimental yield displacement was calculated as 90 mm (3.54 in.). Table 9.1 contains a summary of response quantities from each of the tests.

Table 9.1 Peak response quantities.

Test	Displacement ductility	Peak drift ratio (%)	Peak longitudinal strain (mm/mm)	Peak moment (MN-m)	Peak shear (kN)	Peak curvature (rad/km)
EQ1	0.69	0.85	0.0022	3.95	500	6.8
EQ2	1.48	1.82	0.0132	5.90	699	15.6
EQ3	4.01	4.93	0.0298	6.59	888	60.8
EQ4	1.89	2.33	0.0144	3.75	401	25.1
EQ5	6.32	7.78	0.0466	7.24	811	105.3
EQ6	5.44	6.69	0.0423	6.50	771	91.6
EQ7	6.15	7.56	0.0428	7.39	812	104.9
EQ8	6.73	8.28	0.0584	7.16	742	123.3
EQ9	7.06	8.69	0.0638	6.16	755	139.6
EQ10*	8.41	10.34	0.0116	-	-	214.2

* Impacted the East safety column at peak displacement.

Test EQ1 demonstrated the column's elastic behavior. Test EQ2 initiated nonlinear response with limited ductility demands. Design level demands were imposed by test EQ3 with a displacement ductility of 4.0. Concrete spalling was the extent of visible damage, and peak longitudinal strains were less than 3%. Damage was repairable and the residual drift ratio was less than 0.9%. Test EQ4 represented an aftershock, which resulted in linear column response.

Tests EQ5 represented a loading scenario beyond design level, followed by a repeat of the design level event in EQ6. Structural integrity remained after the intended protocol with concrete spalling as the extent of damage. Remaining tests were added successively with the aim of inducing failure. Test EQ7 triggered bar buckling and generated the largest overturning moment of any test. Two longitudinal bar fractures occurred in EQ8, which was the fifth consecutive test to impose drift ratio demands greater than 6.5%. Bar fracture corresponded with onset of concrete core crushing. Test EQ9 induced bar fracture in three additional longitudinal bars and caused further core crushing. Moment capacity reduced to 83% of the maximum obtained in EQ7. Subsequent testing brought the specimen to near collapse and impact with the safety restraint. This prompted the conclusion of the test program. Just before impact, the moment capacity was reduced to 69% of the maximum obtained during EQ7.

Figure 9.1 illustrates the peak and residual drift ratios achieved during testing. The largest residual drift ratio was 3.1% after EQ9. A residual drift ratio of 0.9% remained after the design level scenario of EQ3. Repeated demands beyond the design level demonstrate the durability of the seismic details provided. Contributions from the modes of deformation were governed by flexure, see Figure 9.2. This accounted for 70% or more of the measured column tip displacement in nearly all tests. The secondary contribution of approximately 15% was due to fixed end rotation and was consistent throughout testing. A minor contribution due to shear deformation was computed as 5% or less in all tests.

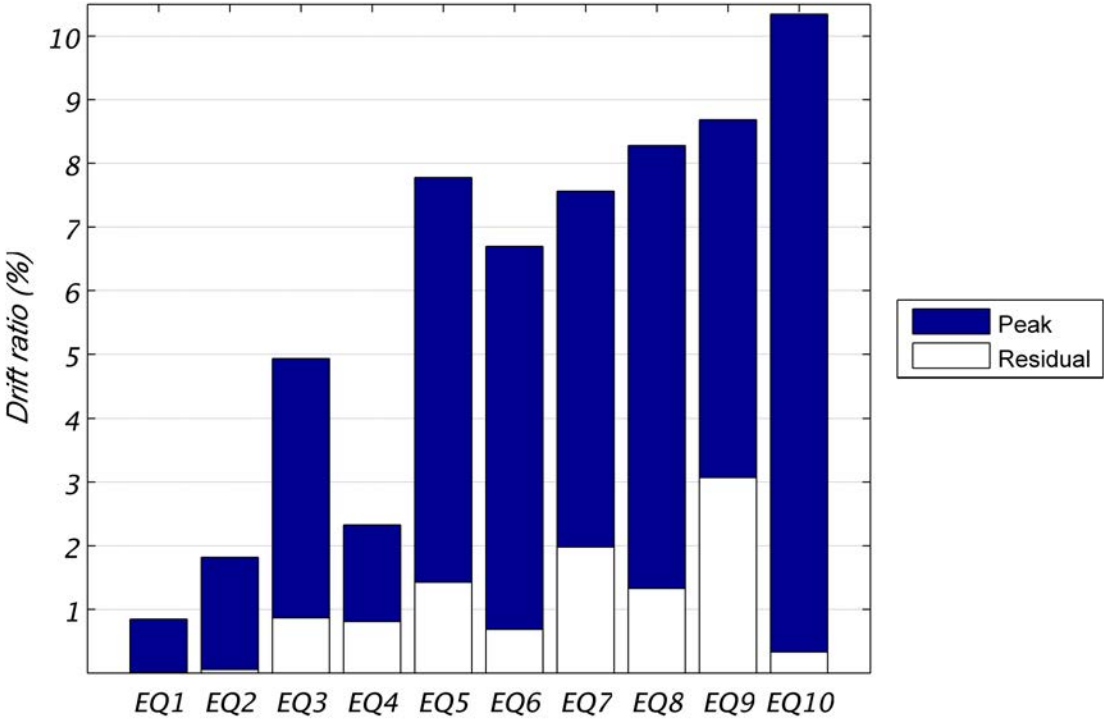


Figure 9.1 Drift ratios achieved during tests.

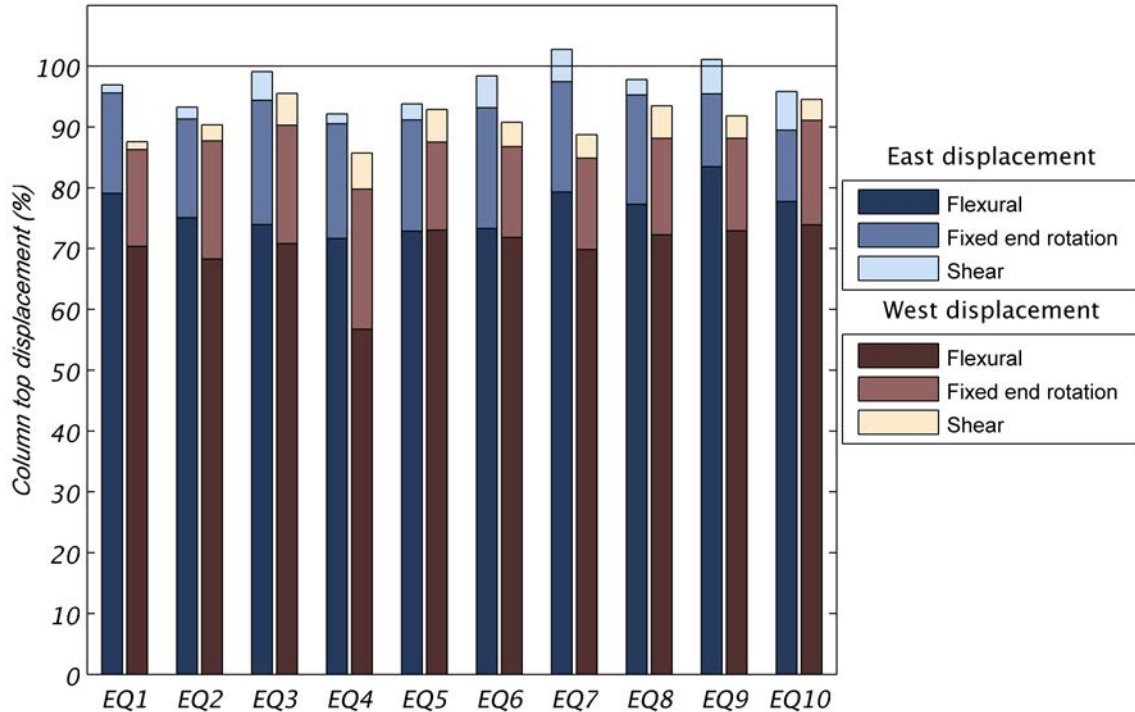


Figure 9.2 Displacement components at peak displacements.

The progressive damage is shown chronologically Figure 9.3 as the post-test state of the column's East face. The images show the column base up to 0.61 m (24 in.) or $\frac{1}{2}$ column diameter. After the design level earthquake only cracks are evident in Figure 9.3 (c), but spalling initiated on the opposite face. The damage state at this level was cosmetic and easily repairable. This was the same scenario after a simulated aftershock, and onset of bar buckling did not occur until a third test at or beyond the design level.

Damage occurred in a concentrated plastic hinge at the base of the column. The response was flexurally dominant and shear capacity was maintained throughout testing. Column cracks extended the accessible height of the column by testing completion. However, concrete spalling, longitudinal bar buckling, and longitudinal bar fracture were located within 1.22-m (4-ft), or one column diameter, of the base of the column. Footing cracks were evident in the top of the footing after test EQ10 due to cone pullout from strain penetration.

After testing, all of the visible longitudinal bars exhibited buckling deformation. Four longitudinal bars on the East face of the column fractured. Three longitudinal bars on the West face fractured and an additional two bars developed cracks which did not propagate through the bar diameter. During demolition, the longitudinal bars were cut from the specimen for inspection. Photos of the extracted bars are arranged radially from their location in the column in Figure 9.4. Thirteen of the eighteen bars were buckled. The typical buckled shape was 300 mm (12 in.) or twice the hoop spacing.

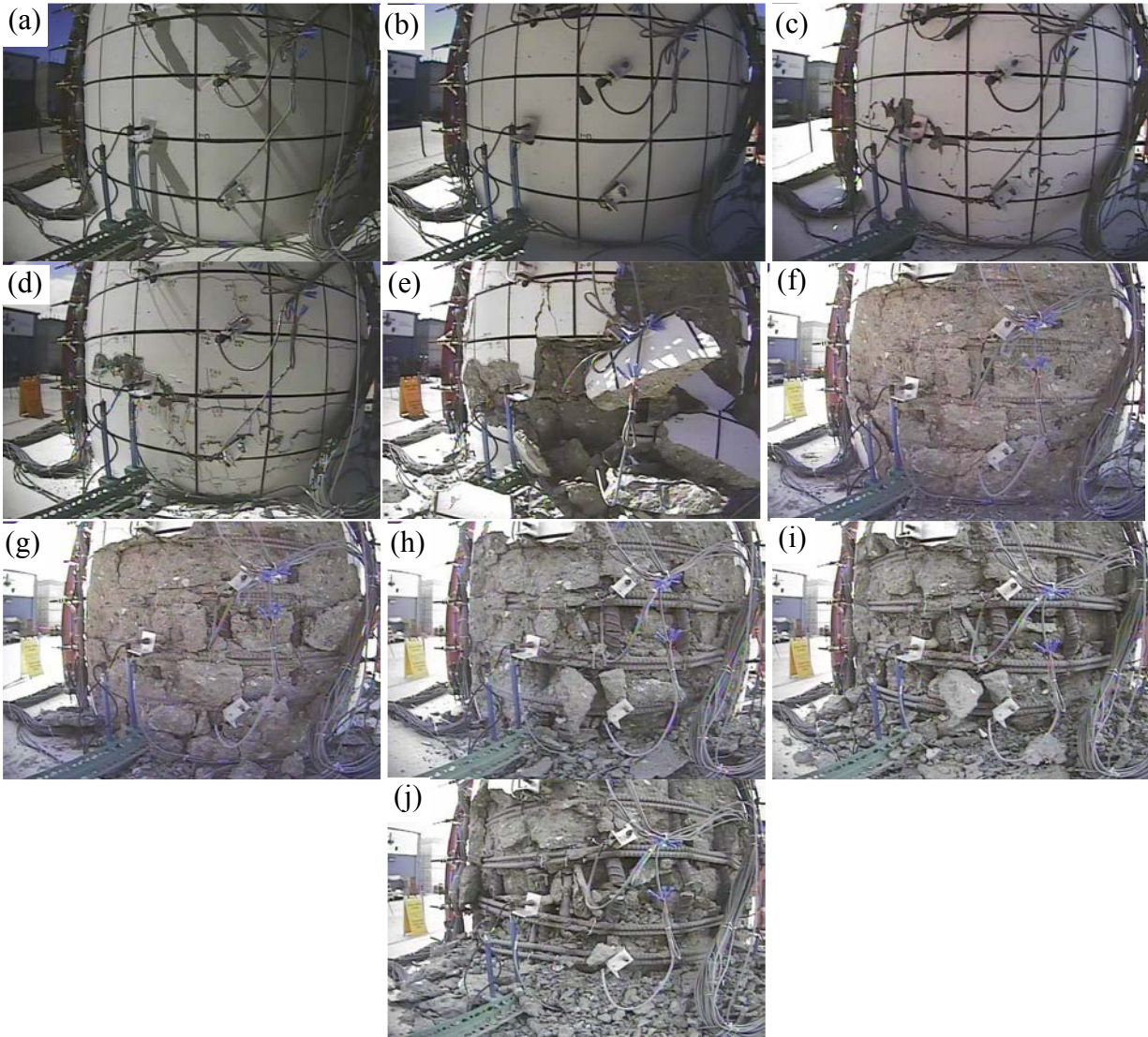


Figure 9.3 Column base East face post test (a) EQ1, (b) EQ2, (c) EQ3, (d) EQ4, (e) EQ5, (f) EQ6, (g) EQ7, (h) EQ8, (i) EQ9, and (j) EQ10

A necking phenomenon was not apparent in the fractured bars, which is evidence of fracture initiated by a compressive crack due to buckling. However, some of the buckling deformation was induced after bar fracture when fractured ends came in contact with each other during a compression cycle. The peak longitudinal strain measured by strain gauges was 6.4% during EQ9.

Of the seven fractured bars, the occurrence of six were identified from videos; two on the West face during EQ8, one on West face and two on the East face during EQ9, and one on the East face during EQ10. The last fracture on the West face may have occurred near impact with the safety restraint during EQ10, but there are no other cues in the videos or data.

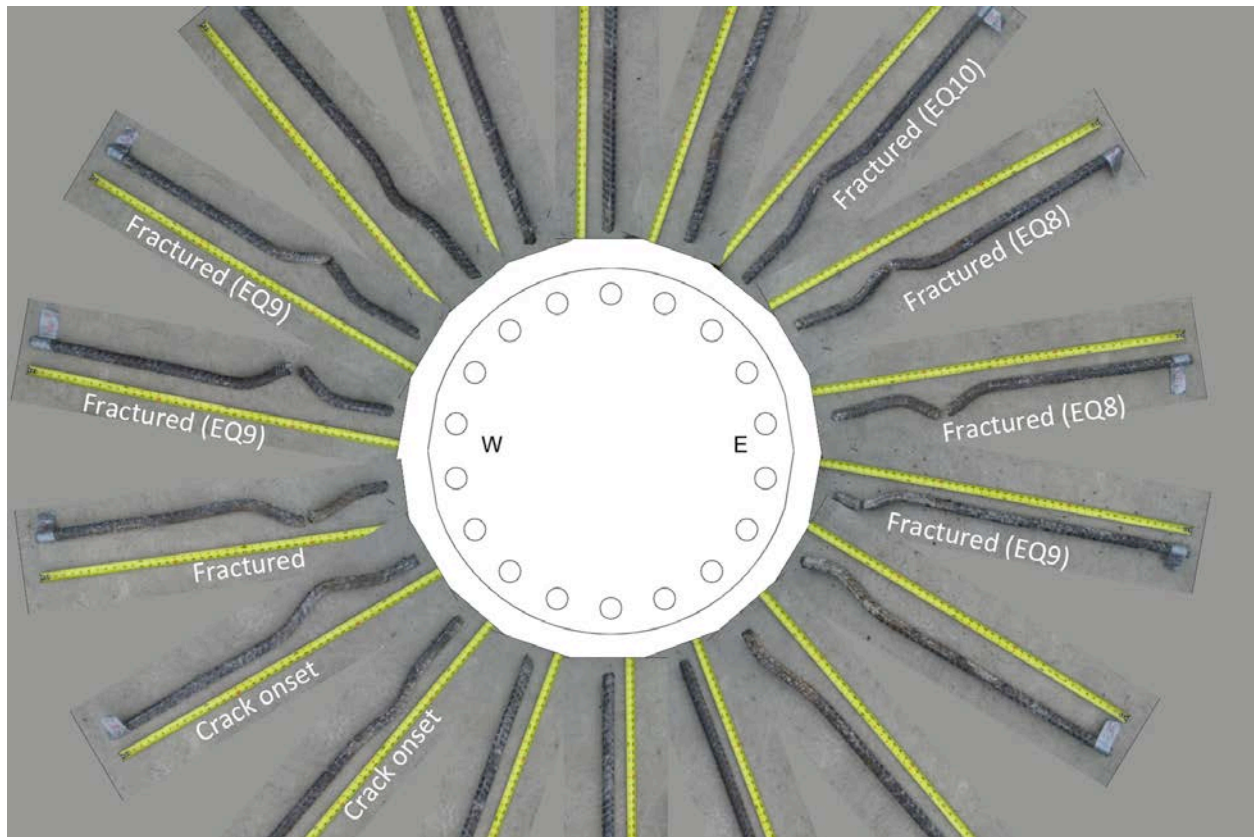


Figure 9.4 Extracted longitudinal reinforcement.

Transverse hoops did not fracture despite the nonlinear demands imposed. Redundancy provided by bundled hoops may have been beneficial and kept transverse strains low, but strain gauges were not installed on the bundled pairs. Only one gauge was installed per bundle, so the redundancy provided cannot be quantified. The maximum strain in any test, measured during EQ5, was 2.5% and the maximum strain demand in all other tests was less than 1.2%. Demands imposed on the hoops from shear transfer and concrete dilation were within the strain capacity of the hoops.

Vertical offset of the transverse hoops caused by the buckled longitudinal reinforcement is evident in Figure 9.5. Buckling is clearly seen in this figure as occurring across multiple spacings of transverse reinforcement. The region of the column requiring enhanced lateral confinement per section 7.6.3 of the Seismic Design Criteria [Caltrans 2006a] was 1.5 times the column diameter for this test setup, but no change in reinforcement detailing was made up the column height. This plastic hinge region, L_{pr} , is indicated in Figure 9.5 and extends 0.61 m (24 in.) or $\frac{1}{2} D$ above the extent of spalling.



Figure 9.5 South face of the column post-test.

9.2 CONCLUSIONS

The 1.22-m (4-ft) diameter column was the largest column tested in the U.S. under dynamic loading conditions. Significant nonlinear response was induced during the uni-axial shake table tests. Durability of the structure and conformity to the design philosophy were demonstrated by repeated cycles beyond the design level with strength degradation only after rebar fractures (EQ8). Ductile behavior was observed with a plastic hinge forming at the base of the cantilevered column. The concentrated hinge developed concrete spalling of up to one column diameter from its base. This was within the code specified region for enhanced confinement of 1.5 column diameters.

Concrete spalling initiated during the simulated design level earthquake (EQ3). This damage was cosmetic and repairable. For classification as an ordinary bridge, the seismic performance criteria were exceeded; Damage was limited and collapse was not imminent. A residual drift ratio of 0.9%, however, is significant. This is dependent on the loading history, and not an implication of design, but deserves consideration. Difficulty repairing bridges in Japan after the 1995 Kobe earthquake led the Japan Road Association [2002] to adopt seismic design guidelines that limit residual drift ratios to 1%. For this reason and because the seismic hazard was defined as a 975 year return period rather than at the functional and safety seismic hazards, it is difficult to assess if this column would have satisfied the performance criteria for classification as an important bridge. Seismic performance was exceptional for an ordinary bridge classification.

As anticipated, a higher mode contribution from the mass moment of inertia of the superstructure block is evident in base shear response. This contribution is present in real bridges not just an artifact of the test setup. Its effect should be considered in design where analytical modeling or dynamic amplification factors can be used as a remedy.

Longitudinal reinforcement buckled during later stages of testing (EQ7), but the provisions for anti-buckling restraint in the Seismic Design Criteria [Caltrans 2006a] were successful at the design level. However, transverse hoops were spaced 25% closer than the maximum allowed; specified spacing was 0.15 m (6 in.) versus 0.20 m (8 in.) maximum allowed. The reduced spacing may have played a role in the buckling onset, but an alternate loading sequence would have had a more pronounced influence. Seismic design guidelines anticipate the prevention of buckling between layers of transverse reinforcement [Caltrans 2006a], but the observed mode was across adjacent layers.

By the conclusion of testing, some crushing of the core concrete occurred at the exterior. However, this was limited the core remained largely intact. A flow of core concrete spilling through the cage, as observed by Kawashima et al. [2009], did not occur.

Test objectives to produce and monitor nonlinear lateral demands at targeted deformations were achieved. Targeted deformations were induced at and beyond the design level, thus achieving the objective of validating current design practices. While validation holds only for the case investigated, the design philosophy and methodology appear sound. Scale effects can be assessed once published results on a replica model have been made available. Based on a blind prediction competition of this test specimen, analysis methods require further development to gain sufficient confidence in the reliable prediction of response quantities across platforms.

REFERENCES

- Abolhassan, A., Bertero, V.V., Bolt, B.A., Mahin, S.A., Moehle, J.P., and Seed, R.B. (1989). "Preliminary report on the seismological and engineering aspects of the October 17, 1989 Santa Cruz (Loma Prieta) Earthquake." Earthquake Engineering Research Center, Report No. UCB/EERC-89/14.
- ACI 318 (2005). Building Code Requirements for Structural Concrete and Commentary, American Concrete Institute, Farmington Hills, MI.
- ASTM A615 (2009). Standard Specification for Deformed and Plain Carbon-Steel Bars for Concrete Reinforcement, American Society for Testing and Materials International, West Conshohocken, PA.
- ASTM A706 (2009). Standard Specification for Low-Alloy Steel Deformed and Plain Bars for Concrete Reinforcement, American Society for Testing and Materials International, West Conshohocken, PA.
- Caltrans, (2010a). "20-1 Seismic Design Methodology." California Department of Transportation. Memo to Designers, 20-1.
- Caltrans, (2010b). Caltrans ARS Online. http://dap3.dot.ca.gov/shake_stable/.
- Caltrans (2006a). Seismic Design Criteria, California Department of Transportation, Sacramento, CA.
- Caltrans (2006b). Standard Specifications, California Department of Transportation, Sacramento, CA.
- Caltrans, (2004). Bridge Design Specifications, California Department of Transportation, Sacramento, CA.
- Carr, A.J. (2002). "Ruaumoko, Volume 2: User Manual for the 2-dimensional version, Ruaumoko2D." Department of Civil Engineering, University of Canterbury, Christchurch, New Zealand.
- Carrea, F. (2010). "Shake-table test on a full-scale bridge reinforced concrete column." Tesi di Laurea, Dipartimento di Ingegneria Civile, Ambientale e dei Materiali, Università Bologna, Bologna, Italy.
- Douglas, B.M. and Buckle, I.G. (1985). "Field response studies of two highway bridges subject to simulated earthquake loads." Proceedings of the second joint U.S. – Japan workshop on performance and strengthening of bridge structures and the research needs, San Francisco, California, pp. 203-208.
- Eberhard, M.O., MacLardy, J.A., Marsh, M.L., and Hjartarson, G. (1993). "Lateral-load response of a reinforced concrete bridge." Washington State Department of Transportation, Olympia, Washington.
- FEMA-273 (1997). NEHRP Guidelines for the Seismic Rehabilitation of Buildings, Federal Emergency Management Agency, Washington, D.C.
- Gilani, A.S., Chavez, J.W., and Fenves, G.L. (1996). "Field testing of bridge design and retrofit concepts." UCB/EERC-95/14, Earthquake Engineering Research Center, University of California, Berkeley.
- Housner, G.W., et al. (1994). *The continuing challenge – The Northridge Earthquake of January 17, 1994*, (Report to Director, California Department of Transportation), Sacramento, California.
- JRA (2002). Specifications for highway bridges, Part V, Seismic Design. Japan Road Association. Japan Road Association, Tokyo.
- Kawashima, K., et al. (2009). "Shake table experiment on RC bridge columns using E-Defense." 41st Panel on Wind and Seismic Effects, UJNR, Public Works Research Institute, Tsukuba Science City, Japan.
- Kawashima, K. (1995). "Impact of the Hanshin/Awaji, Japan, earthquake on seismic design and seismic strengthening of highway bridges." Federal Highway Administration (FHWA), Proceedings of the National Seismic Conference on Bridges and Highways, San Diego, CA.
- Kuebitz, K.C. (2002). *Development and calibration of Columna, a Windows-based moment-curvature program for columns of arbitrary cross-section*. M.S. thesis, Department of Structural Engineering, University of California, San Diego, La Jolla, California.
- NEES (2011). "NEES Project Warehouse – Large-Scale Validation of Seismic Performance of Bridge Columns." <<https://nees.org/warehouse/project/987/>> (December 2011).

- NEES (2010). "NEES @ UC San Diego – Shake Table Specifications." <<http://nees.ucsd.edu/facilities/shake-table.shtml>> (October, 2010).
- Mellon, S. (1988). *Highway bridge damage, Whittier earthquake, October 1, 1987*. California Department of Transportation, Seismic report / Post earthquake investigation team.
- Penzien, J. and Clough, R.W. (1971). "Observations on the damages of highway bridge structures, San Fernando, California, earthquake February 9th, 1971." Sacramento, CA.
- PEER (2007). "PEER Strong Motion Database: Introduction." <<http://peer.berkeley.edu/smcat/>> (July, 2010).
- Sasaki, T. and Kawashima, K. (2009). "Scale effect on the shear strength of reinforced concrete columns with termination of main reinforcements." 3rd International Conference on Advances in Experimental Structural Engineering, San Francisco, CA Paper 2009-10.
- Shen, J.J., Yen, W.H., and O'Fallon, J. (2006). "FHWA recommendations for seismic performance testing of bridge piers." Proceedings of the Fourth International Workshop on Seismic Design and Retrofit of Transportation Facilities, San Francisco, California.
- Stone, W.C. and Cheok, G.S. (1989). *Inelastic behavior of full-scale bridge columns subjected to cyclic loading*. Report No. NIST/BSS-166. National Institute of Standards and Technology. U.S. Department of Commerce, Gaithersburg, Maryland.
- Marquez, T.M. (2010). "Seismic design methodology." California Department of Transportation, Memo to designers, No. 20-1, pp. 1-15.
- Nakashima, M., Kawashima, K., Ukon, H., and Kajiwara, k. (2008). "Shake Table Experimental Project on the Seismic Performance of Bridges using E-Defense." 14 WCEE, Beijing, China, Paper No. S17-02-010.
- Unjoh, S., Nakatani, S., Tamura, K., Fukui, J., and Hoshikuma, J. (2002). "2002 Seismic design specifications for highway bridges." National Institute of Standards and Technology, NIST Special Publication 987, pp. 231-240.

Appendix A: Instrumentation Layout

Instrumentation plans included in this appendix identify the Cartesian coordinates of each sensor deployed. The origin of the coordinate system was taken as the centroid of the column at the column-to-footing interface. From the origin, positive is taken as East, North, and up. Other sensor metadata include the channel name, data acquisition system, gauge length if applicable, and sensor orientation. The data acquisition system corresponds to the Node to which the sensor was wired. There were six nodes, numbered 1, 2, 4, 5, 7, and 8, that recorded data. Electronic versions of these drawings are available in the project's archive at NEEShub [NEES 2011]. Sensor coordinates are also available there in tabulated format in the sensor plans.

Figures A.1 through A.4 contain locations for longitudinal and transverse strain gauges. Figures A.5 through A.10 contain locations of the various LVDT configurations. Figures A.11 through A.12 primarily contain locations for string potentiometers. Figures A.13 through A.16 contain accelerometer locations on the shake table, footing, column, and mass block. Figures A.17 contains locations of sensors on the inclined safety columns and the bond slip LVDTs at the column-to-footing interface.

TEST DATES: 9/20/2010 - 9/21/2010

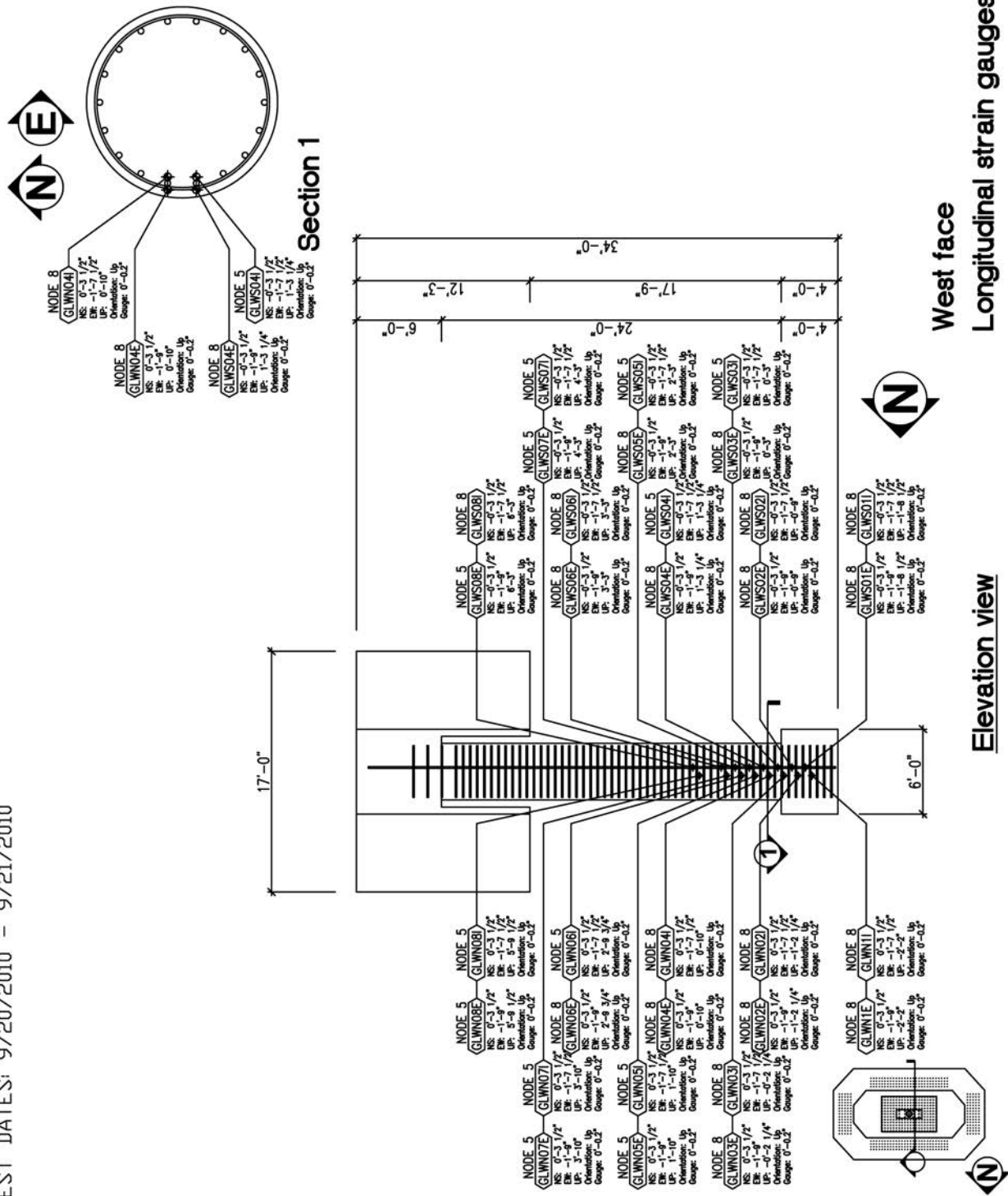


Figure A.2 Longitudinal strain gauge locations on the West face of the column.

TEST DATES: 9/20/2010 - 9/21/2010

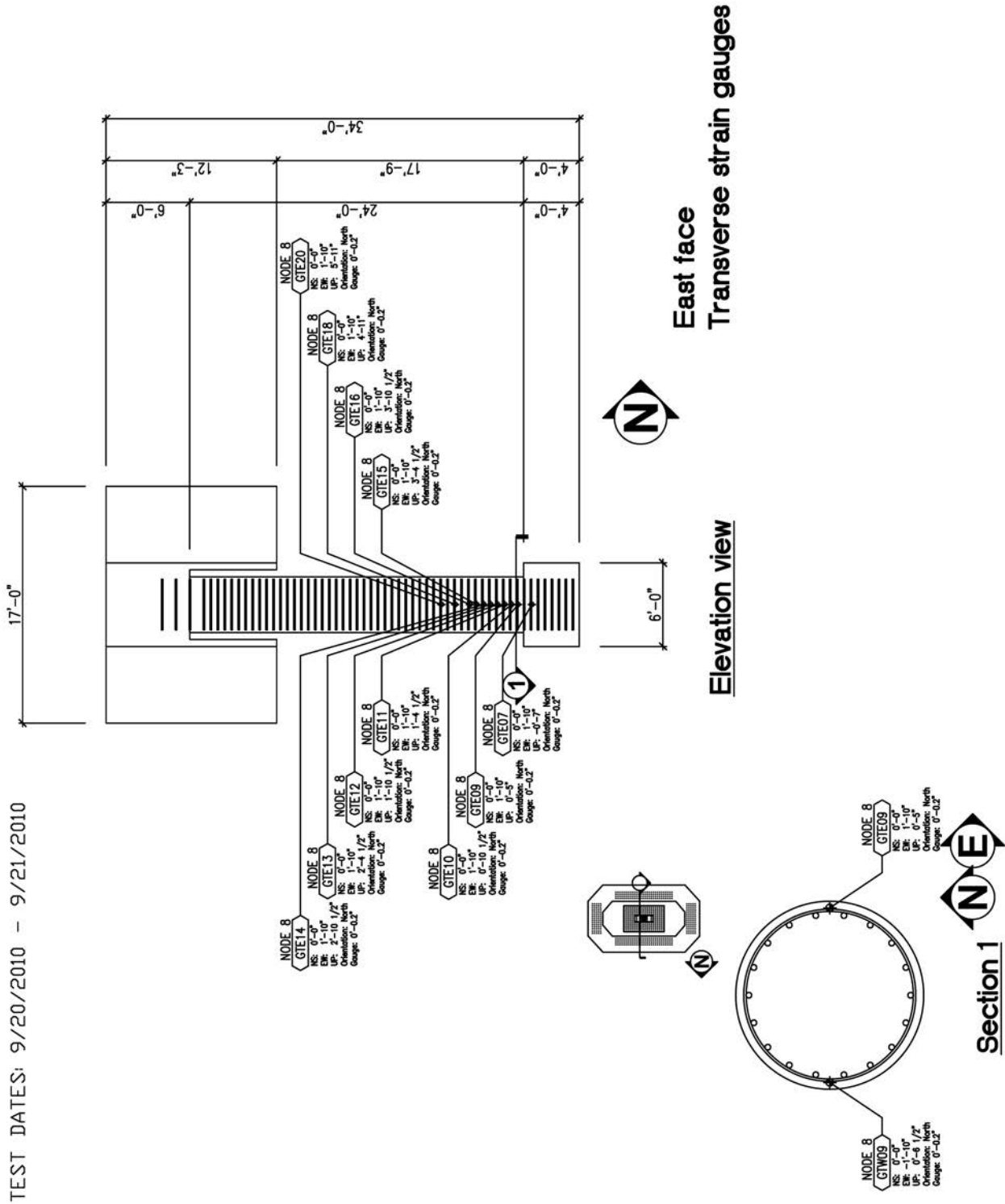


Figure A.3 Transverse strain gauge locations on the East face of the column.

TEST DATES: 9/20/2010 - 9/21/2010

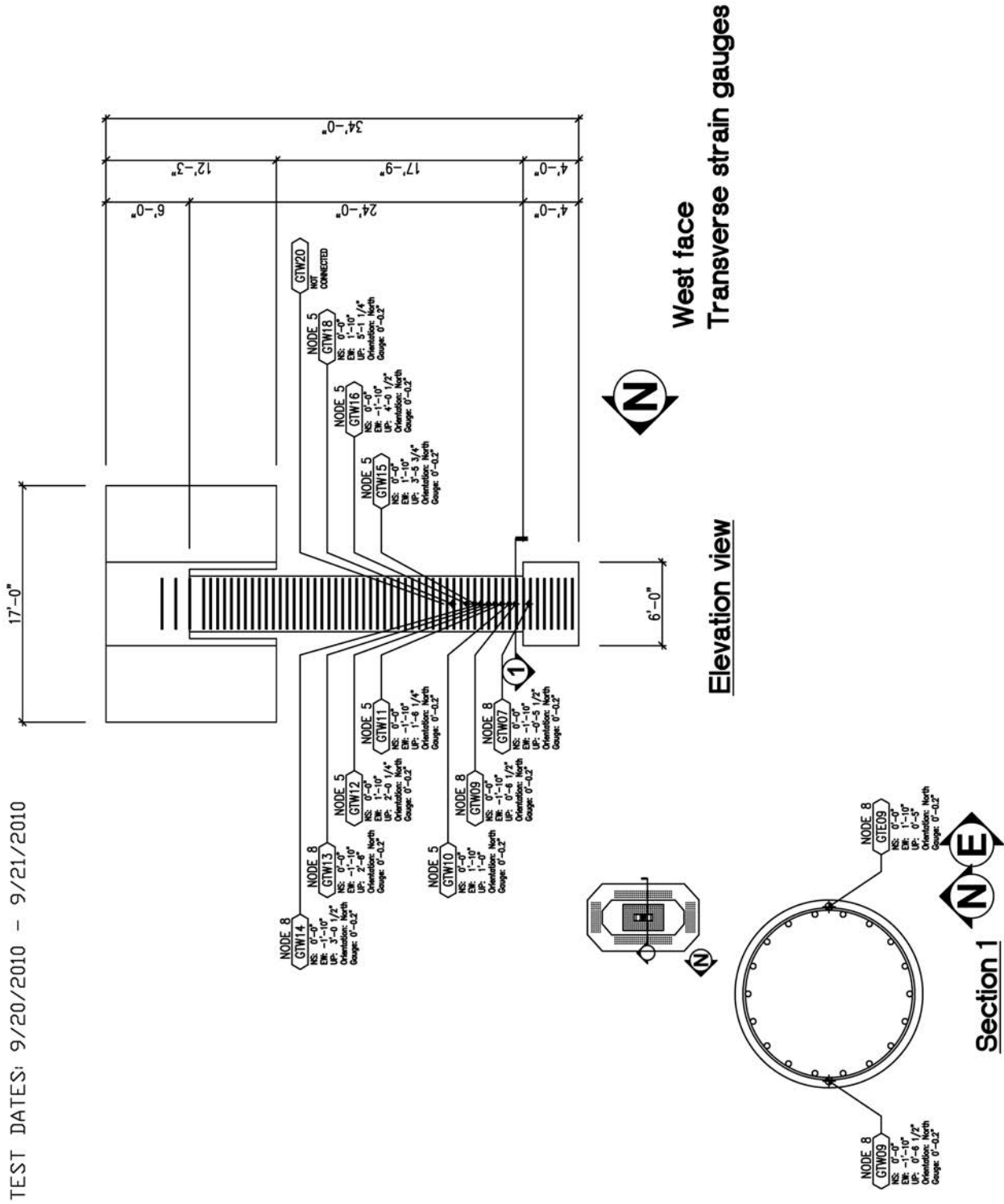


Figure A.4 Transverse strain gauge locations on the West face of the column.

A.2 LINEAR VOLTAGE DISPLACEMENT TRANSDUCERS

TEST DATES: 9/20/2010 – 9/21/2010

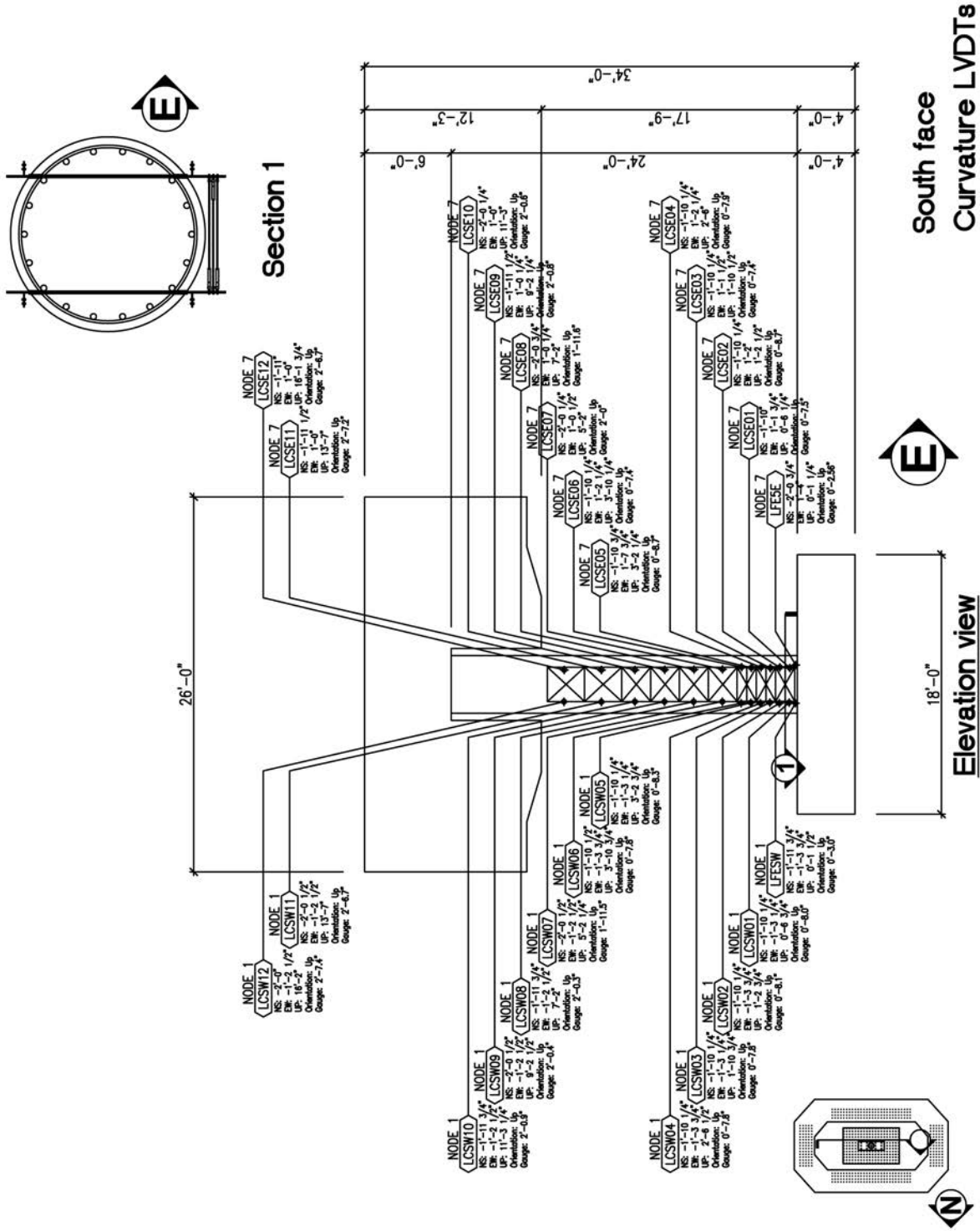


Figure A.5 Curvature and fixed-end rotation LVDT locations on the South face of the column.

TEST DATES: 9/20/2010 - 9/21/2010

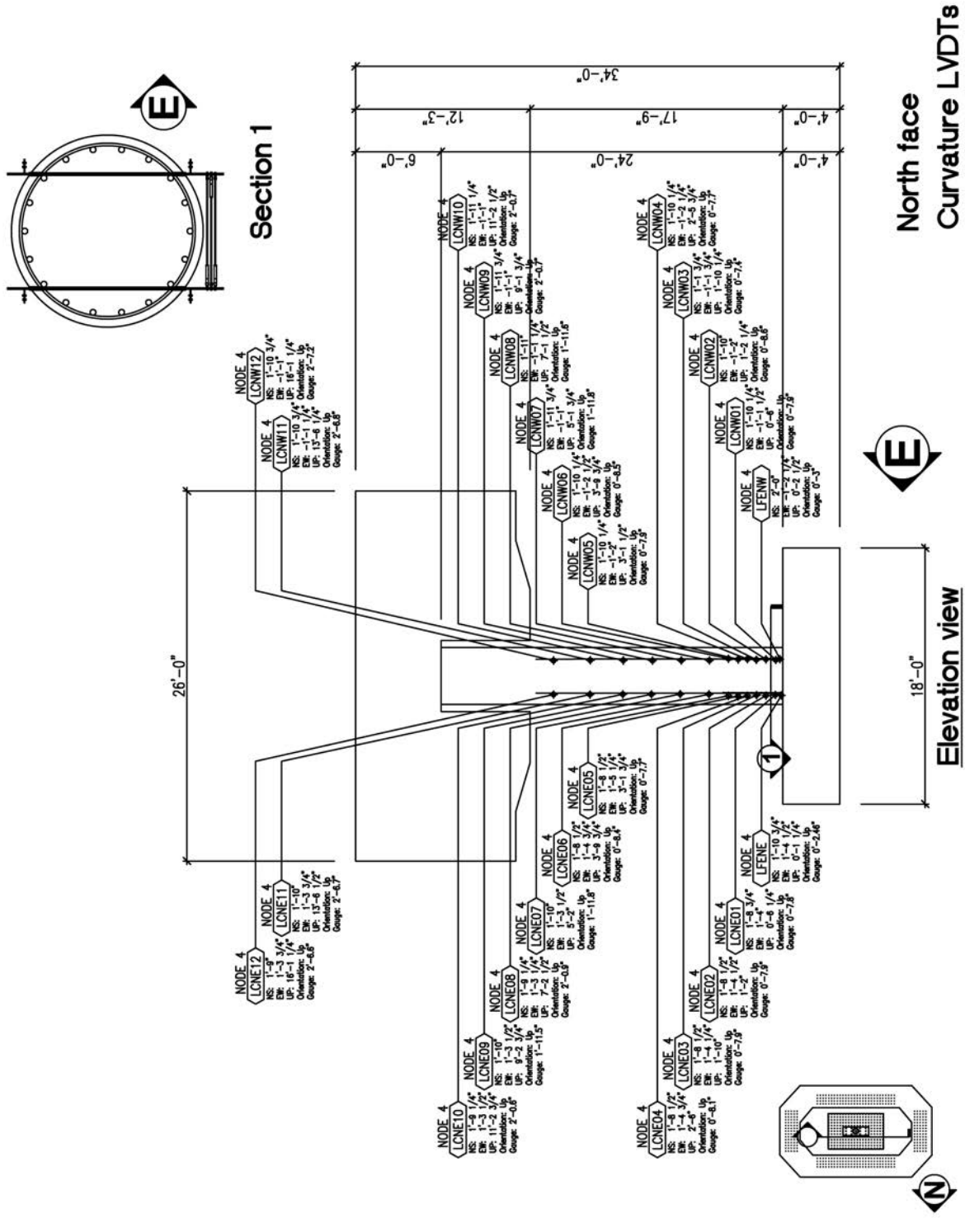


Figure A.6 Curvature and fixed-end rotation LVDT locations on the North face of the column.

TEST DATES: 9/20/2010 - 9/21/2010

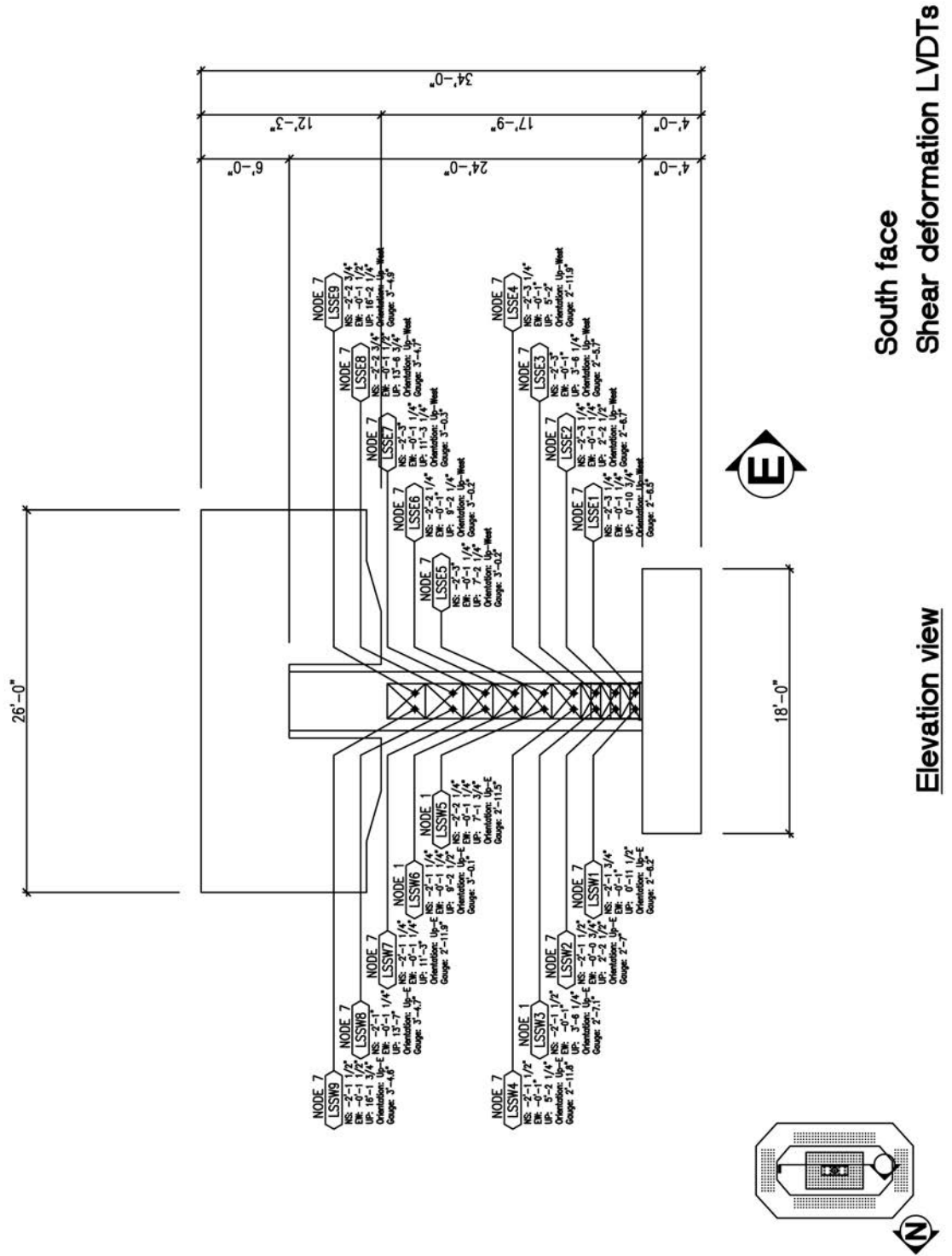


Figure A.7 Inclined shear LVDT locations on the South face of the column.

TEST DATES: 9/20/2010 - 9/21/2010

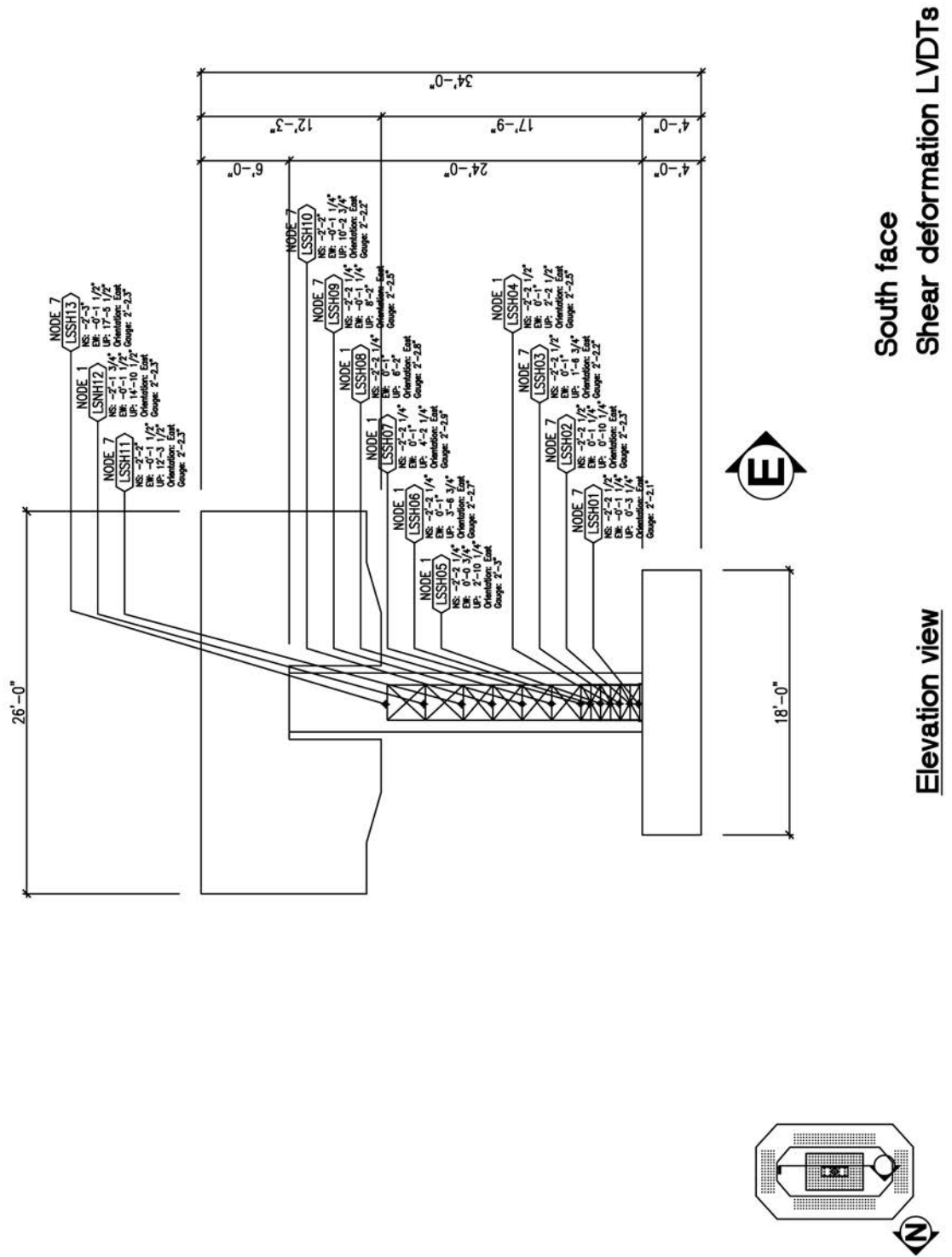


Figure A.8 Horizontal shear LVDT locations on the South face of the column.

TEST DATES: 9/20/2010 – 9/21/2010

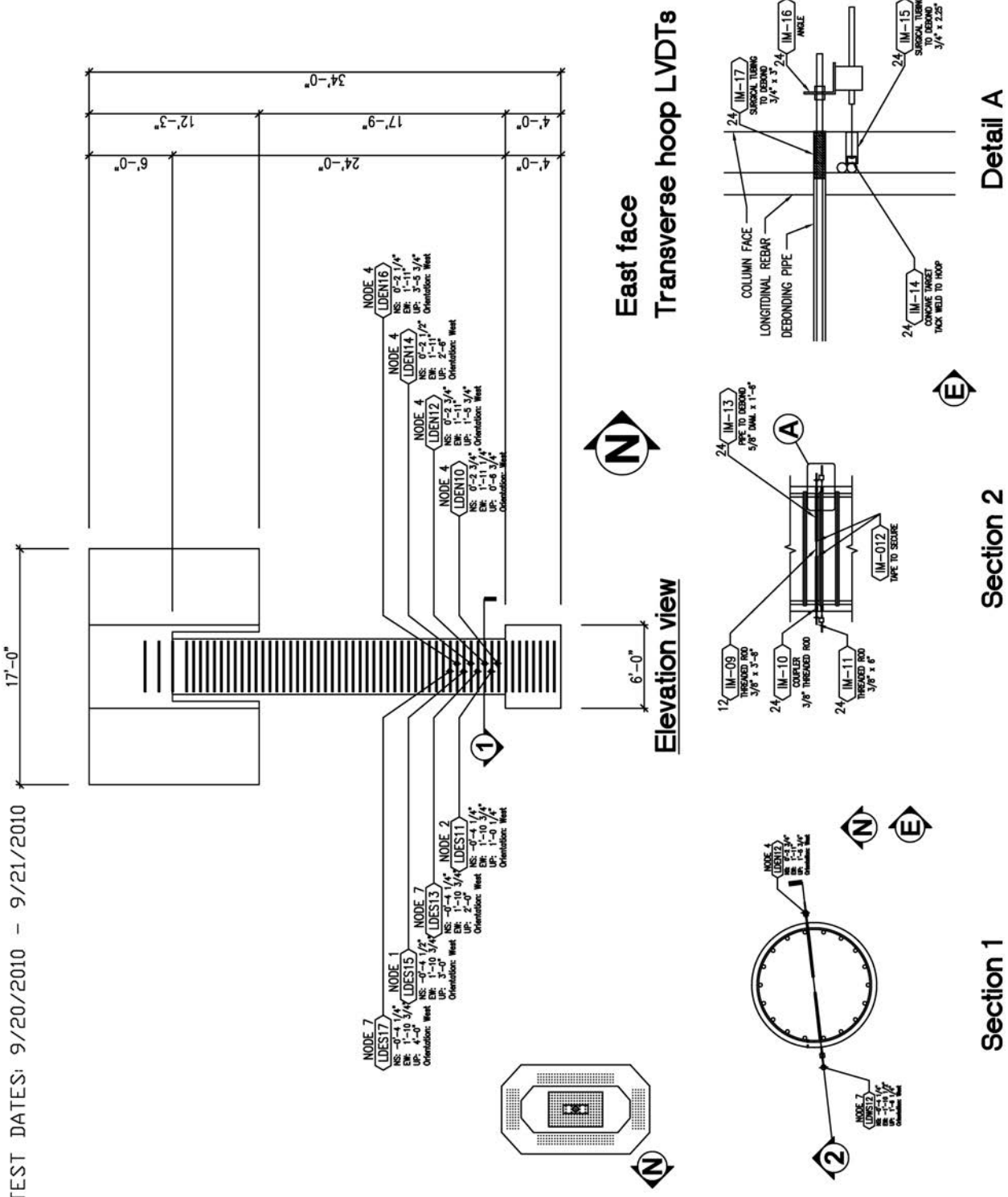


Figure A.9 Transverse hoop LVDT locations on the East face of the column.

TEST DATES: 9/20/2010 - 9/21/2010

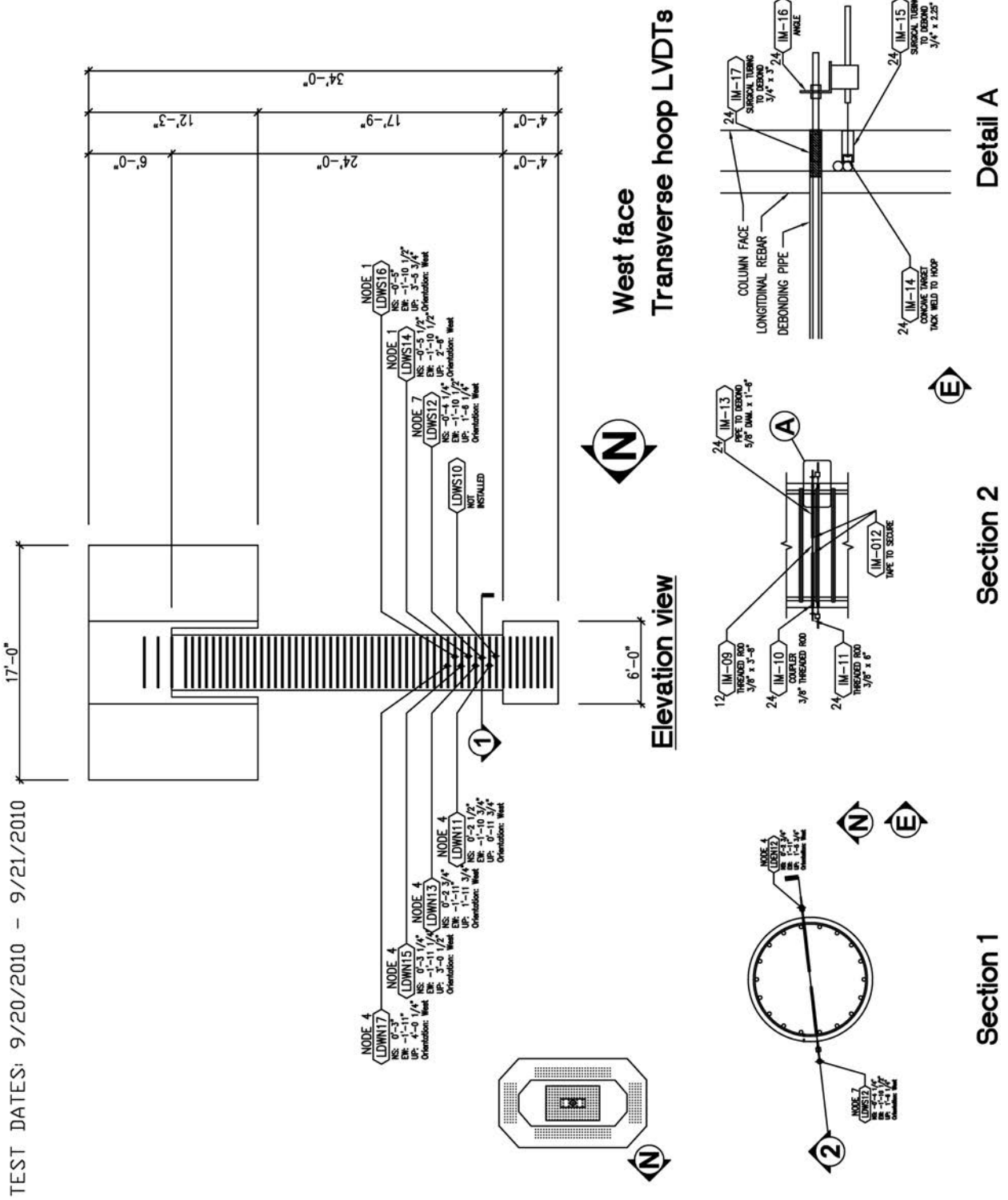


Figure A.10 Transverse hoop LVDT locations on the West face of the column.

TEST DATES: 9/20/2010 - 9/21/2010

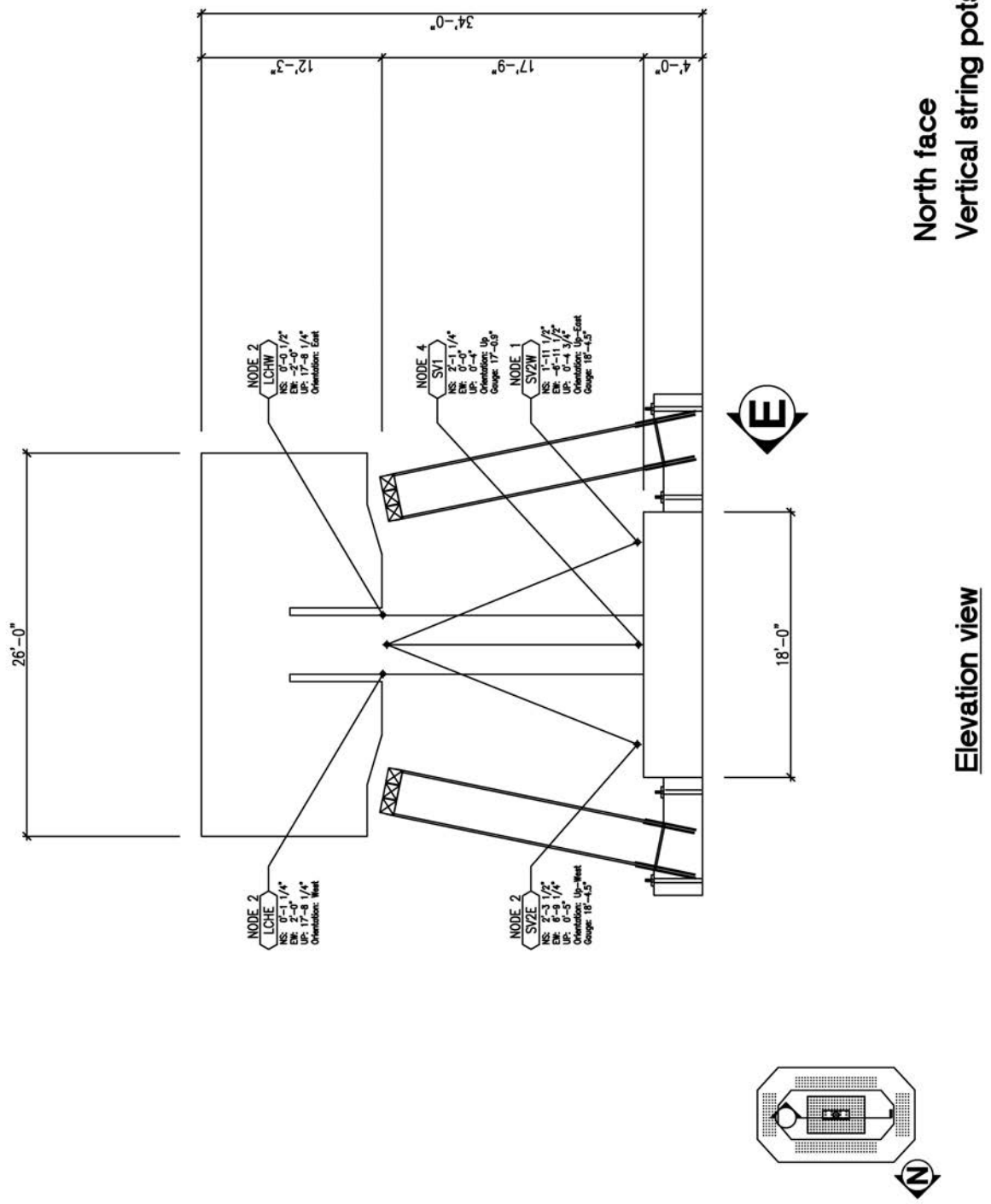
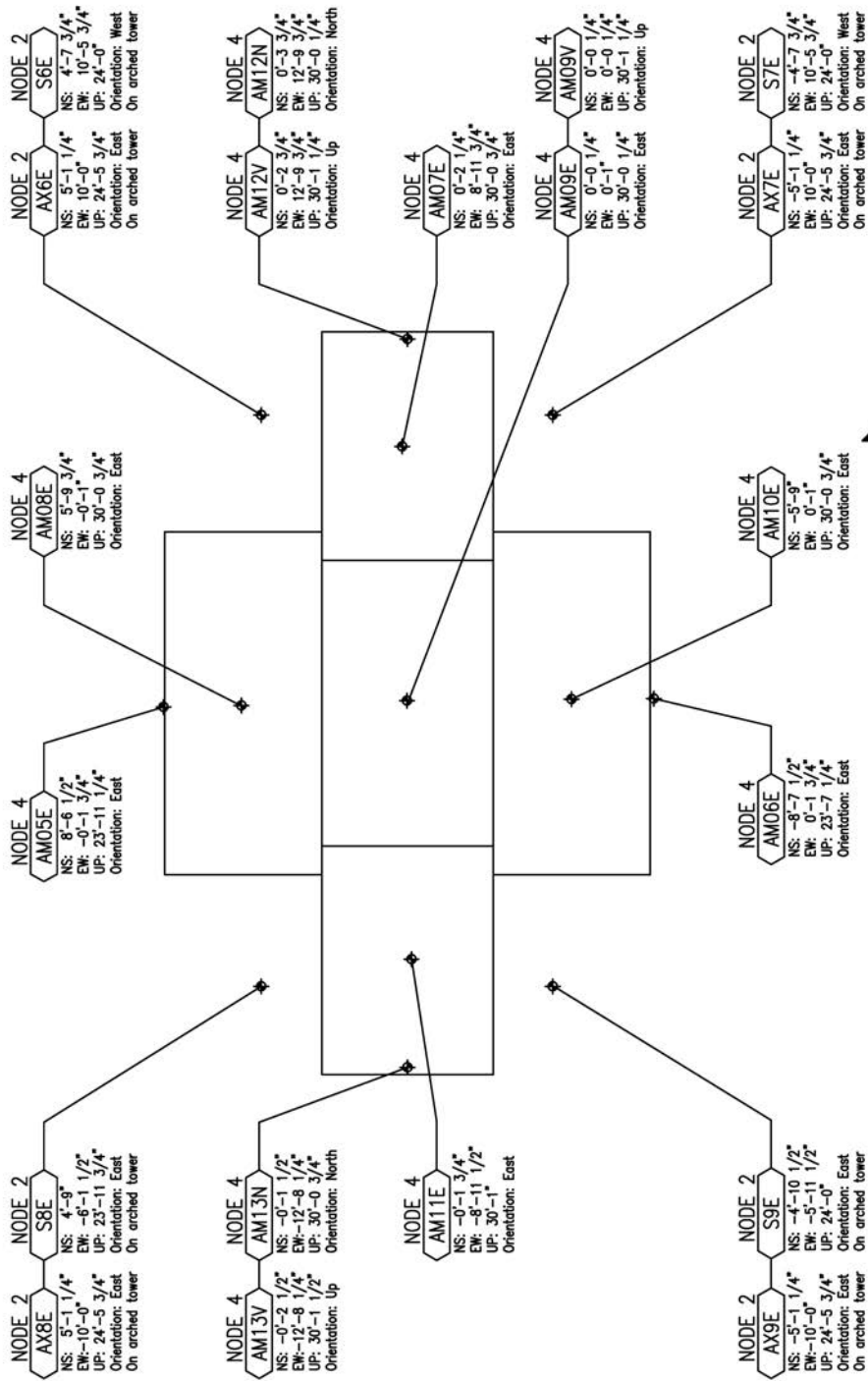


Figure A.12 Inclined spring potentiometer and column-to-top mass LVDT locations.

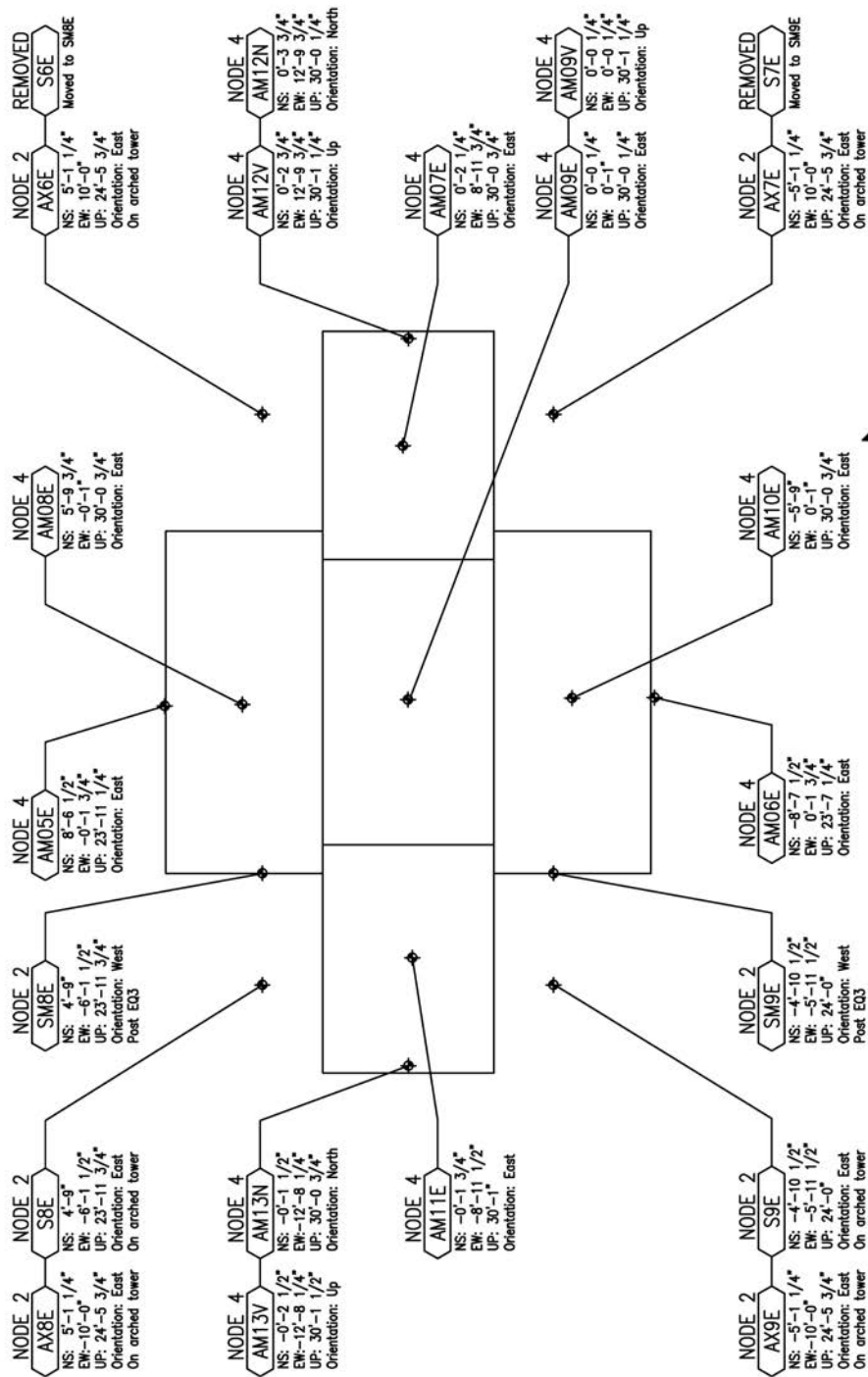
TEST DATE: 9/20/2010



Superstructure mass
Accelerometer layout

Plan view

TEST DATE: 9/21/2010



Superstructure mass
Accelerometer layout

Plan view

Figure A.16 Mass block accelerometer and wire pot locations for tests on 9/21/2010.

A.5 INCLINED SAFETY COLUMN INSTRUMENTATION AND BOND-SLIP LVDTs

TEST DATES: 9/20/2010 - 9/21/2010

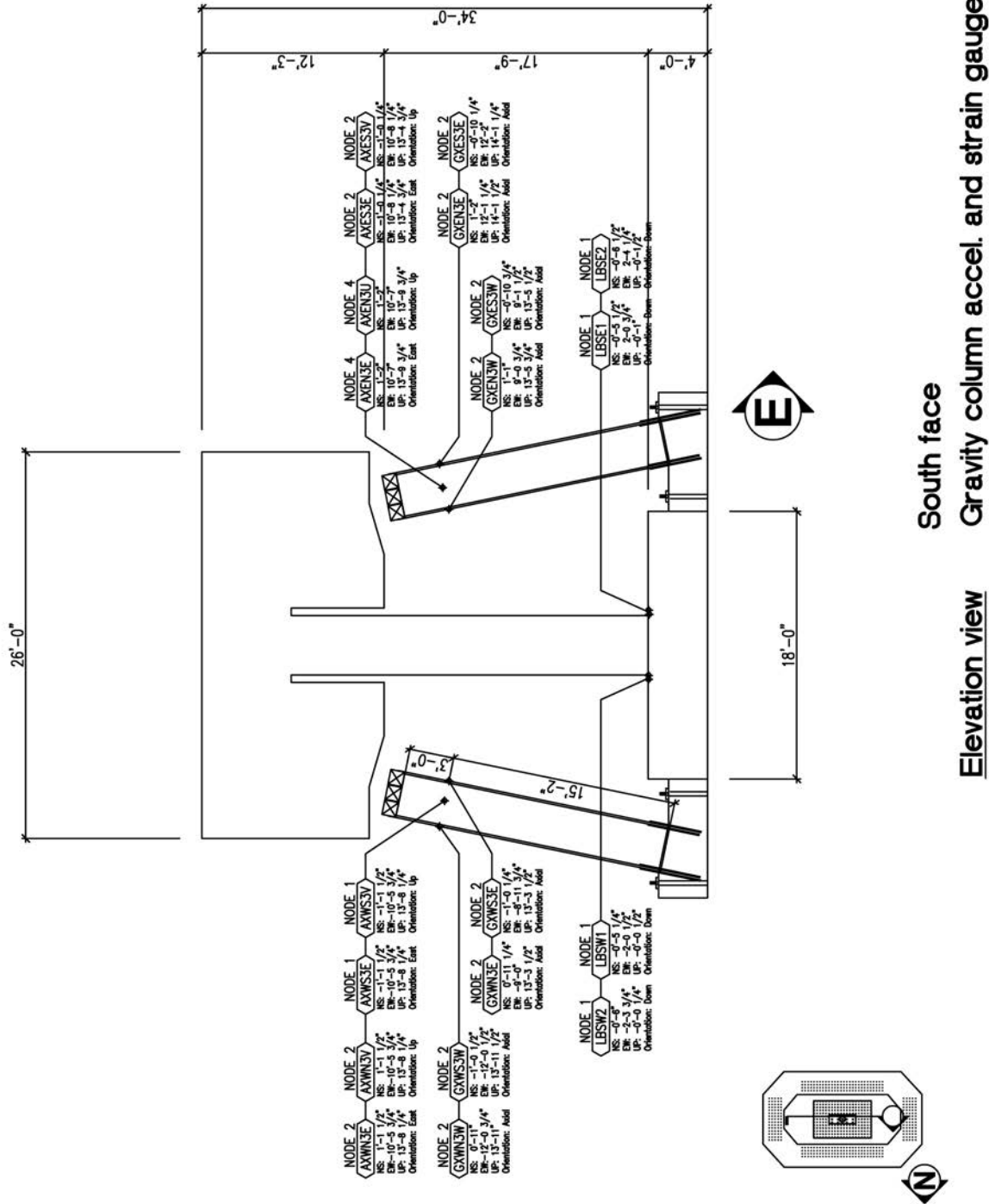


Figure A.17 Bond-slip LVDT locations and instrumentation locations on the inclined safety restraints.

